

PLASMA ASTROPHYSICS

Marian Karlický

Astronomical Institute,
Academy of Sciences of the Czech Republic

Chapter 1

Basic concepts and equations

Plasma means a partially or completely ionized gas, which is electrically neutral as a whole, and which consists of electrons, ions and neutral atoms. Furthermore the plasma, in the sense used here, is characterized by so called collective behavior of its particles. This aspect is used to be expressed by the following conditions:

a) The mean force of near interactions is much less than that of distant collective interactions of particles

$$F_{near} \ll F_{dist},$$

b) the number of particles in the so called Debye sphere is large

$$\frac{1}{n\lambda_D^3} \ll 1,$$

where n is the plasma particle density and λ_D is the Debye length,

c) the thermal kinetic energy KE is much greater than potential energy PE

$$KE \gg PE, \quad \frac{3}{2}k_B T \gg \frac{e^2}{4\pi\epsilon_0\lambda_D}.$$

It means that the plasma is a sufficiently diluted and hot gas, which characteristic length L is much greater than the Debye length ($L \gg \lambda_D$).

Debye shielding

Let us assume a charge q_0 at zero point of the reference system at $\mathbf{r}_0 = 0$. The potential of this charge in free space is

$$\varphi_0(\mathbf{r}) = \frac{q_0}{4\pi\epsilon_0 |\mathbf{r}|}, \quad (1.1)$$

where ϵ_0 is the permittivity of the free space.

Now, let us consider a test charge q_0 surrounded by a neutral plasma (electrons with the electron density n_e and temperature T_e and heavy protons of the same density $n_e = n_p$). Then the potential φ can be determined from Poisson equation

$$\nabla^2\varphi(\mathbf{r}) = -\frac{q_0}{\epsilon_0}\delta(\mathbf{r}) + \frac{e}{\epsilon_0} \langle \rho_e \rangle, \quad (1.2)$$

where the mean charge density is

$$\langle \rho_e \rangle = n_e \exp\left(\frac{e\varphi}{k_B T_e}\right) - n_p. \quad (1.3)$$

Here k_B is the Boltzmann constant, and for electrons the Maxwell-Boltzmann statistics ($\sim \exp(-q\varphi/(k_B T))$) is used. As mentioned above, in a plasma the kinetic energy of electrons is much greater than their potential energy, and that is why the exponential function can be expanded in a Taylor series and only two first terms can be used. Thus, the charge density in the form of $\langle \rho_e \rangle \approx n_e e \varphi / (k_B T_e)$ can be put into Poisson equation which can be written as

$$-\nabla^2 \varphi_0(r) + \frac{n_e e^2 \varphi(r)}{\epsilon_0 k_B T_e} = \frac{q_0}{\epsilon_0} \delta(\mathbf{r}). \quad (1.4)$$

Solving this equation in polar coordinates (i.e. $\nabla^2 \rightarrow \frac{\partial^2}{\partial r^2} + \frac{2}{r} \frac{\partial}{\partial r}$) the solution is

$$\varphi_0(\mathbf{r}) = \frac{q_0}{4\pi\epsilon_0 r} \exp\left(-\frac{r}{\lambda_D}\right), \quad (1.5)$$

where

$$\lambda_D \equiv \sqrt{\left(\frac{\epsilon_0 k_B T}{n_e e^2}\right)}, \quad (1.6)$$

is the Debye radius. As seen the electric field at distances $L \geq \lambda_D$ is effectively shielded.

Plasma oscillations

In a quasi-neutral electron-ion plasma a relative displacement of electrons in comparison with ions causes the electric field:

$$E = \frac{n_e e \xi}{\epsilon_0}, \quad (1.7)$$

where ξ is the displacement. Then the Newton force equation gives the equation for oscillations of electrons

$$m_e \frac{d^2}{dt^2} \xi = -eE = -\frac{n_e}{\epsilon_0} e^2 \xi, \quad (1.8)$$

(where m_e is the electron mass) with the characteristic frequency called electron plasma frequency

$$\omega_{pe}^2 = \frac{n_e e^2}{\epsilon_0 m_e}. \quad (1.9)$$

Similarly, we can define the proton plasma frequency as

$$\omega_{pp}^2 = \frac{n_p e^2}{\epsilon_0 m_p}, \quad (1.10)$$

where m_p is the proton mass, and so on.

Equations describing plasma processes

a) Kinetic description

Plasma is fully described by a distribution function $f(\mathbf{r}, \mathbf{v}, t)$. The distribution gives the number of particles which are present in a unit volume of the 6-dimensional phase space located in coordinates \mathbf{r}, \mathbf{v} at time t . The distribution function is a solution of the **Boltzmann equation**

$$\frac{\partial f(\mathbf{r}, \mathbf{v}, t)}{\partial t} + \mathbf{v} \cdot \nabla f(\mathbf{r}, \mathbf{v}, t) + \frac{\mathbf{F}}{m} \cdot \frac{\partial f(\mathbf{r}, \mathbf{v}, t)}{\partial \mathbf{v}} = \left(\frac{\partial f(\mathbf{r}, \mathbf{v}, t)}{\partial t} \right)_{coll}, \quad (1.11)$$

where m is the particle mass, \mathbf{F} is the general force, and in our case usually in the form

$$\mathbf{F} = q(\mathbf{E} + \mathbf{v} \times \mathbf{B}), \quad (1.12)$$

where \mathbf{E} and \mathbf{B} are the electric field and magnetic induction.

The term on the right side of the equation (1.11) expresses effects of particle collisions.

Because plasma can have many different components (electrons, protons, neutrals, ions of different chemical elements), the Boltzmann equation should be solved for every single plasma component and the interactions between components should appear in the collisional terms on the right side of the individual Boltzmann equations. But, for many tasks some simplifications are made, and e.g. only the Boltzmann equation for electrons is solved.

Furthermore, if the collisional term is very low (e.g. if the plasma frequency is much greater than the collision one; $\omega_{pe} \gg \nu_c$) then such a plasma is called collisionless and for its description the **Vlasov equation** is used

$$\frac{\partial f(\mathbf{r}, \mathbf{v}, t)}{\partial t} + \mathbf{v} \cdot \nabla f(\mathbf{r}, \mathbf{v}, t) + \frac{\mathbf{F}}{m} \cdot \frac{\partial f(\mathbf{r}, \mathbf{v}, t)}{\partial \mathbf{v}} = 0, \quad (1.13)$$

For a full set of equations describing a plasma behaviour the **Maxwell equations** need to be added

$$\nabla \times \mathbf{E} = -\frac{\partial \mathbf{B}}{\partial t} \quad \nabla \cdot \mathbf{E} = \frac{1}{\epsilon_0} \rho_e \quad (1.14)$$

$$\nabla \times \mathbf{B} = \mu_0 \mathbf{j} + \frac{1}{c^2} \frac{\partial \mathbf{E}}{\partial t} \quad \nabla \cdot \mathbf{B} = 0$$

where \mathbf{j} is the electric current density and ρ_e is the charge density, which can be expressed as follows

$$\mathbf{j} = \sum_{\alpha} e_{\alpha} \int \mathbf{v} f_{\alpha} d^3 v, \quad (1.15)$$

$$\rho_e = \sum_{\alpha} e_{\alpha} \int f_{\alpha} d^3 v, \quad (1.16)$$

where the index α corresponds to individual plasma components.

Fokker-Planck equation

If the particle collisions are dominant then an evolution of the particle distribution function is described by the Fokker-Planck equation. Let $P(\mathbf{v}, \Delta \mathbf{v})$ be the probability that a test particle changes its velocity \mathbf{v} to $\mathbf{v} + \Delta \mathbf{v}$ in the time interval Δt . Provided that the particle number is conserved, the velocity distribution at time t can be written as

$$f(\mathbf{v}, t) = \int f(\mathbf{v} - \Delta \mathbf{v}, t - \Delta t) P(\mathbf{v} - \Delta \mathbf{v}, \Delta \mathbf{v}) d^3 \Delta \mathbf{v}. \quad (1.17)$$

Noting that for small-angle deflections $|\Delta v| \ll v$, the product fP in Equation (1.17) can be expanded into a Taylor series,

$$f(\mathbf{v}, t) = \int (fP - \Delta t \left[\frac{\partial f}{\partial t} \right] P - \Delta \mathbf{v} [\nabla_{\mathbf{v}} f P] + \frac{1}{2} \Delta v_i \Delta v_j \left[\frac{\partial}{\partial v_i} \frac{\partial}{\partial v_j} f P \right] + \dots) d^3 \Delta \mathbf{v}. \quad (1.18)$$

The Einstein convection has been introduced that the sums over the indices i and j have to be used if they appear together in the numerator and denominator, or as subscripts and superscripts. Since the probability that some transition takes place is unity, P is normalized to

$$\int P d^3 \Delta v = 1. \quad (1.19)$$

We define the average velocity change per time interval Δt :

$$\int \Delta \mathbf{v} P d^3 \Delta v \equiv \langle \Delta \mathbf{v} \rangle, \quad (1.20)$$

$$\int \Delta v_i \Delta v_j P d^3 \Delta v \equiv \langle \Delta v_i \Delta v_j \rangle. \quad (1.21)$$

Exchanging integration and differentiation, the integral in Eq. (1.18) can be evaluated. The first term in the integrant cancels with the left hand side of the equation. The remaining terms form the important Fokker-Planck equation,

$$\left(\frac{\partial f(\mathbf{v}, t)}{\partial t} \right)_{coll} = \frac{\partial^2}{\partial v_i \partial v_j} \left(f \frac{\langle \Delta v_i \Delta v_j \rangle}{2\Delta t} \right) - \frac{\partial}{\partial v_i} \left(f \frac{\langle \Delta v_i \rangle}{\Delta t} \right). \quad (1.22)$$

The possibility of neglecting the higher-order terms in the expansion (1.18) is a property of inverse-square law particles having multiple collisions. Equation (1.22) shows that the motion of particles in velocity space then can be visualized as a diffusion process. Its right hand side describes the temporal change of a distribution of test particles by multiple, small-angle collision processes. It corresponds to the right hand side of the Boltzmann equation (1.11). The first term in Equation (1.22) represents the three-dimensional diffusion of the test particle in velocity space; the second term is a friction, slowing down the test particle and moving it radially toward the origin of velocity space.

b) Magnetohydrodynamic description

For many tasks in astrophysical plasmas the kinetic approach is too complex, in reality we do not need to know distribution functions of plasma particles. In these cases the description using the macroscopic quantities as e.g. the mean plasma velocity and so on is sufficient. Mathematically it means that the integration of kinetic equations in velocity space is justifiable. Thus, the equations with the macroscopic quantities (called the magnetohydrodynamic equations, MHD equations for short) can be obtained as the moments of the Boltzmann equation [BKE]:

$$\int [BKE] d^3 v, \quad (1.23)$$

$$\int m \mathbf{v} [BKE] d^3 v, \quad (1.24)$$

$$\int \frac{1}{2} m v^2 [BKE] d^3 v. \quad (1.25)$$

Example of derivation of the first moment - first MHD equation

Let us integrate the first moment

$$\frac{\partial}{\partial t} \int f d^3 v + \frac{\partial}{\partial \mathbf{r}} \int \mathbf{v} f d^3 v + \frac{q}{m} \int (\mathbf{E} + \mathbf{v} \times \mathbf{B}) \frac{\partial f}{\partial \mathbf{v}} d^3 v = \int \left(\frac{\partial f}{\partial t} \right)_{coll} d^3 v, \quad (1.26)$$

where $\nabla \cdot \mathbf{v} = 0$ was used in the second term. Due to the particle number conservation the integral of the collisional term is zero. Furthermore, using the Gauss theorem and per partes integration, the force term can be expressed as

$$\int (\mathbf{E} + \mathbf{v} \times \mathbf{B}) \frac{\partial f}{\partial \mathbf{v}} d^3v = \mathbf{E} \int f d\mathbf{S}_{\mathbf{v}} - \int f \frac{\partial (\mathbf{v} \times \mathbf{B})_j}{\partial v_j} d^3v, \quad (1.27)$$

where $d\mathbf{S}_{\mathbf{v}}$ is the surface element in the velocity space. The first part is zero because $f \rightarrow 0$ for $|v| \rightarrow \infty$, and the second one is zero because the $(\mathbf{v} \times \mathbf{B})_j$ do not consist of v_j . Thus, the relation (1.26) can be written as

$$\frac{\partial}{\partial t} \int f d^3v + \frac{\partial}{\partial \mathbf{r}} \int \mathbf{v} f d^3v, \quad (1.28)$$

or

$$\frac{\partial \rho}{\partial t} + \text{div } \rho \mathbf{u} = 0, \quad (1.29)$$

where the density is $\rho = \int f d^3v$ and the mean plasma velocity $\mathbf{u} = \int \mathbf{v} f d^3v / \int f d^3v$. This last equation is known as the continuity equation or the mass conservation equation.

MHD equations

Mass conservation:

$$\frac{d\rho}{dt} \equiv \frac{\partial \rho}{\partial t} + \mathbf{v} \cdot \nabla \rho = -\rho \nabla \cdot \mathbf{v}, \quad (1.30)$$

where d/dt is the convective derivative.

Momentum conservation:

$$\rho \frac{d\mathbf{v}}{dt} = -\nabla p + \mathbf{j} \times \mathbf{B} + \nabla \cdot \mathbf{S} + \mathbf{F}_g, \quad (1.31)$$

where p is the plasma pressure, \mathbf{j} is the current density, \mathbf{B} is the magnetic induction, \mathbf{S} is the viscous stress tensor, and \mathbf{F}_g is the gravitation force.

Internal energy conservation:

$$\rho \frac{de}{dt} + p \nabla \cdot \mathbf{v} = \nabla \cdot (\kappa \cdot \nabla T) + (\eta_e \cdot \mathbf{j}) \cdot \mathbf{j} + Q_\nu - Q_T, \quad (1.32)$$

where

$$e = \frac{p}{(\gamma - 1)\rho}$$

is the internal energy per unit mass, κ is the thermal conductivity tensor, T is the temperature, Q_ν is the heating by viscous dissipation, γ is the ratio of specific heats, and $Q_T = \rho^2 Q(T)$ is the radiative energy loss, $Q(T)$ is a function describing the temperature variation of the radiative loss in the optically thin approximation.

Faraday's equation:

$$\nabla \times \mathbf{E} = -\frac{\partial \mathbf{B}}{\partial t}. \quad (1.33)$$

Ampère's law:

$$\nabla \times \mathbf{B} = \mu \mathbf{j}. \quad (1.34)$$

In comparison with Maxwell equations the displacement current term ($\sim \partial \mathbf{E} / \partial t$) is negligible in the MHD approximation.

Gauss's law:

$$\nabla \cdot \mathbf{B} = 0. \quad (1.35)$$

Ohm's law:

$$\mathbf{E}' = \mathbf{E} + \mathbf{v} \times \mathbf{B} = \eta_e \cdot \mathbf{j}. \quad (1.36)$$

Here $\mathbf{E}' = \mathbf{E} + \mathbf{v} \times \mathbf{B}$ gives the Lorentz transformation from the electric field (\mathbf{E}) in a laboratory frame of reference to the electric field (\mathbf{E}') in a frame moving with the plasma. This Ohm's law states that it is the electric field (\mathbf{E}') in the moving frame which is proportional to the current.

Equation of state:

$$p = R\rho T = nk_B T, \quad (1.37)$$

where R is the universal gas constant, n is the particle density, and k_B is Boltzmann's constant. The density can be expressed as

$$\rho = n\bar{m},$$

where \bar{m} is the mean particle mass. For a hydrogen plasma the pressure becomes

$$p = 2n_e k_B T$$

and the plasma density is

$$\rho \approx n_e m_p,$$

where m_p is the proton mass.

The above system of MHD equations constitutes a set of 16 coupled equations for 15 unknown variables (\mathbf{v} , \mathbf{B} , \mathbf{j} , \mathbf{E} , ρ , p , and T). It seems that the system is over-determined. However, from Faraday's law follows that if we take a divergence-free initial state, Gauss's law follows from Faraday's equation ($\partial/\partial t(\nabla \cdot \mathbf{B}) = -\nabla \cdot (\nabla \times \mathbf{E}) = 0$). In this sense Gauss's law is not necessary.

Induction equation

If we put $\mathbf{E} = -\mathbf{v} \times \mathbf{B} + \eta_e \mathbf{j}$ from Ohm's law and $\mathbf{j} = \nabla \times \mathbf{B} / \mu_0$ (where μ_0 is the magnetic permeability of free space) from Ampère's law into Faraday's law we can write

$$\frac{\partial \mathbf{B}}{\partial t} = \nabla \times (\mathbf{v} \times \mathbf{B}) - \frac{\eta_e}{\mu_0} \nabla \times (\nabla \times \mathbf{B}). \quad (1.38)$$

Now, using the vector formula

$$\nabla \times \nabla \times \mathbf{B} = \nabla(\nabla \cdot \mathbf{B}) - \nabla^2 \mathbf{B}$$

and Gauss's law the induction equation can be written as

$$\frac{\partial \mathbf{B}}{\partial t} = \nabla \times (\mathbf{v} \times \mathbf{B}) + \eta \nabla^2 \mathbf{B}, \quad (1.39)$$

where $\eta = \eta_e / \mu_0$ is the magnetic diffusivity.

Approximations of the induction equation

Now, let us compare terms on the right side of the induction equation by defining so called magnetic Reynolds number:

$$R_m = \frac{\nabla \times (\mathbf{v} \times \mathbf{B})}{\eta \nabla^2 \mathbf{B}} \approx \frac{\frac{v_0 B_0}{L_0}}{\frac{\eta B_0}{L_0^2}} = \frac{L_0 v_0}{\eta}, \quad (1.40)$$

where v_0 is the characteristic plasma velocity and L_0 is the characteristic length scale.

As can be seen, two extreme regime of the induction equation can be considered. For processes with small characteristic velocities, i.e. $v_0 \rightarrow 0$ and $R_m \rightarrow 0$, the induction equations gives a form of the diffusion equation

$$\frac{\partial \mathbf{B}}{\partial t} = \eta \nabla^2 \mathbf{B}. \quad (1.41)$$

On the other hand, in a collisionless plasma with $\eta_e = 0$, i.e. for $R_m \gg 1$, the induction equation becomes

$$\frac{\partial \mathbf{B}}{\partial t} = \nabla \times (\mathbf{v} \times \mathbf{B}). \quad (1.42)$$

Chapter 2

Magnetic field structures

The \mathbf{B} and \mathbf{j} descriptions of plasma processes

Considering Ampere's law

$$\nabla \times \mathbf{B} = \mu \mathbf{j}. \quad (2.1)$$

it looks that the descriptions using the magnetic field \mathbf{B} or the electric current \mathbf{j} as basic variables are equivalent. But in reality only \mathbf{B} is directly measured on the Sun. Therefore, the description with \mathbf{B} is preferred in solar circumstances, and the electric current is a variable derived from the magnetic field.

Based on magnetic measurements at the photosphere the magnetic field in the corona can be extrapolated (see Fig. 2.1). In model situation the magnetic field was extrapolated even between two stars (see Fig. 2.2). Commonly used methods are so-called potential ($\mathbf{j} = 0$ everywhere above the photosphere) and linear force-free field extrapolations. But there are attempts to make so-called non-linear extrapolations. One a rough method is described in the file **non-extra.pdf**.

Reference:

Karlický, M.: 1997, Evolution of force-free electric currents in the solar atmosphere, *Astron. Astrophys.* 318, 289-292.

Basic structures

a) Gravitational stratification

A comparison of the sizes of terms in the equation of motion

$$\rho \frac{d\mathbf{v}}{dt} = -\nabla p + \mathbf{j} \times \mathbf{B} + \rho \mathbf{g}$$

shows that the inertial term on the left-hand side may be neglected when the flow speed is much smaller than both the sound speed $(\gamma p_0/\rho_0)^{1/2}$, the Alfvén speed $B_0/(\mu\rho_0)^{1/2}$ and the gravitational free-fall speed $(2gl_0)^{1/2}$ for a vertical scale-length l_0 . The result is a magnetohydrostatic balance

$$\mathbf{0} = -\nabla p + \mathbf{j} \times \mathbf{B} + \rho \mathbf{g} \quad (2.2)$$

between the pressure gradient, the Lorentz force and the gravitational force. The full set of equation is given by adding

$$\mathbf{j} = \nabla \times \mathbf{B}/\mu \quad (2.3)$$

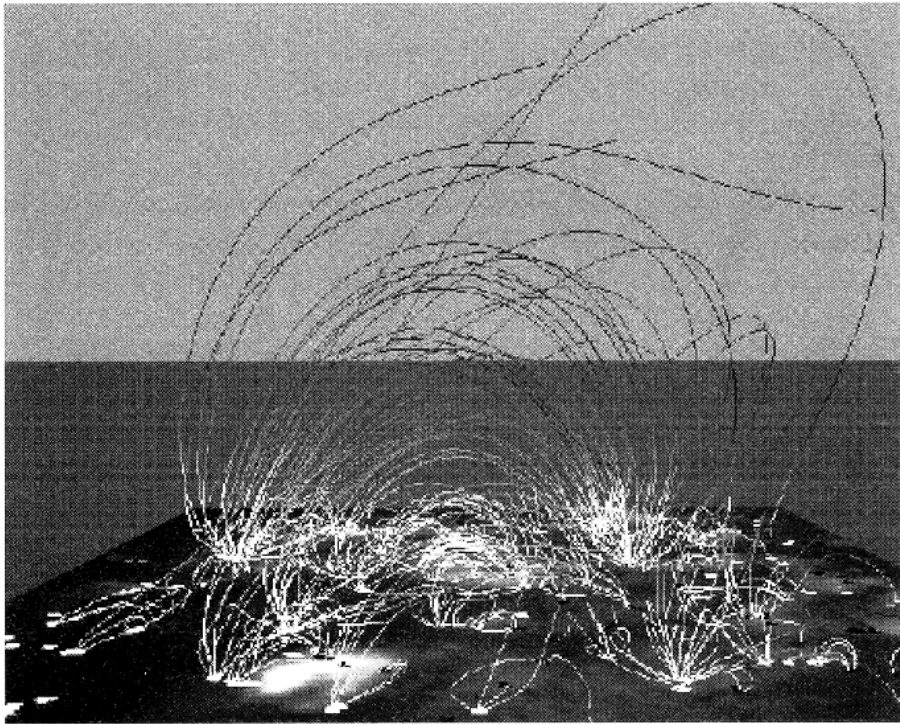


Fig. 2.1: The so-called 'magnetic carpet' showing observed photospheric magnetic field and extrapolated overlying magnetic field lines.

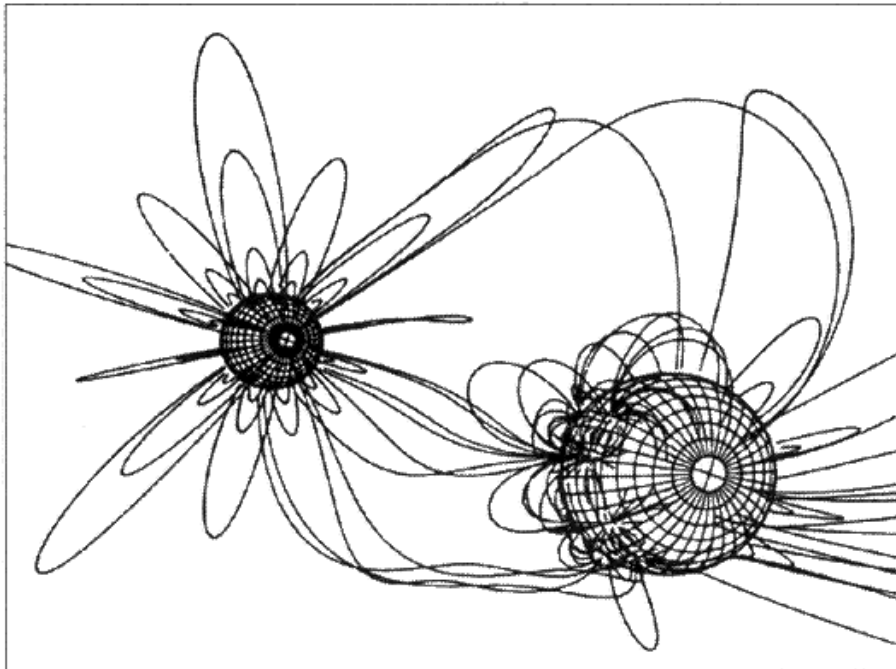


Fig. 2.2: Model magnetic field for an RS CVn binary system in which the two stars are tidally locked into rapid synchronous rotation.

$$\nabla \mathbf{B} = 0, \quad (2.4)$$

$$\rho = \frac{mp}{k_B T}. \quad (2.5)$$

If gravity acts along the negative z -axis and s measures the distance along magnetic field lines inclined at the angle θ to the vertical, the component of Eq. (2.2) parallel to \mathbf{B} is

$$0 = -\frac{dp}{ds} - \rho g \cos \theta. \quad (2.6)$$

Since $\delta s \cos \theta = \delta z$ this becomes

$$0 = -\frac{dp}{dz} - \rho g, \quad (2.7)$$

where p and ρ are functions of z along a particular field line. After substituting for ρ from Eq.(2.5) in Eq. (2.7) and integrating, we find

$$p = p_0 \exp - \int_0^z \frac{1}{\Lambda(z)} dz, \quad (2.8)$$

where p_0 is the base pressure (at $z = 0$) which may vary from one field line to another; also

$$\Lambda(z) = \frac{k_B T(z)}{mg} \quad (2.9)$$

is the pressure scale-height, which represents the vertical distance over which the pressure falls by a factor e .

For the particular case when the temperature is uniform along a field line (due to, for instance, the dominance of thermal conduction), Λ is constant and Eq. (2.8) reduces to

$$p = p_0 e^{-z/\Lambda}. \quad (2.10)$$

c) Structure of magnetic flux tubes

Consider a cylindrically symmetric flux tube whose magnetic field components

$$(0, B_\phi(R), B_z(R)) \quad (2.11)$$

in cylindrical polar coordinates are functions of R alone. The field lines are then helical and lie on cylindrical surfaces, as indicated in Fig. 2.3, while the electric current components are, from Eq. (2.3)

$$\left(0, -\frac{1}{\mu} \frac{dB_z}{dR}, \frac{1}{\mu R} \frac{d}{dR}(RB_\phi) \right). \quad (2.12)$$

Under the neglect of gravity the force-balance equation then reduces to (see the matrix with rows: (i,j,k),2.12,2.11)

$$\frac{dp}{dR} + \frac{d}{dR} \left(\frac{B_\phi^2 + B_z^2}{2\mu} \right) + \frac{B_\phi^2}{\mu R} = 0, \quad (2.13)$$

the second term representing the magnetic pressure and the third term the magnetic tension due to the azimuthal component (B_ϕ) that encircles the axis.

On each cylindrical surface the field lines have a constant inclination, but this may vary from one radius to another. The field lines are given by

$$\frac{Rd\phi}{B_\phi} = \frac{dz}{B_z}, \quad (2.14)$$

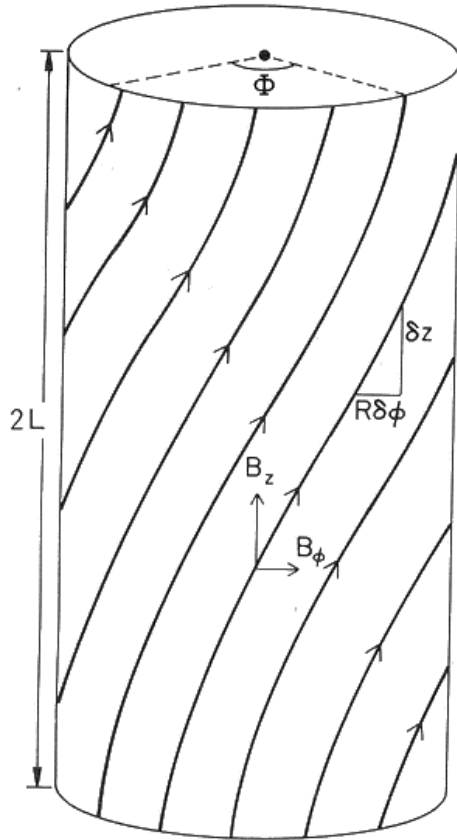


Fig. 2.3: The notation for a cylindrically symmetric flux tube of length $2L$.

and the amount by which a given line is twisted in going from one end of the tube (length $2L$) to the other is

$$\Phi = \int d\phi = \int_0^{2L} \frac{B_\phi}{RB_z} dz, \quad (2.15)$$

or

$$\Phi(R) = \frac{2LB_\phi(R)}{RB_z(R)}, \quad (2.16)$$

($4\pi L/\Phi$ is called sometimes the pitch of the field and gives the axial length of a field line that encircles the axis once, i.e. for $\Phi = 2\pi$ this length is $2L$).

Purely axial field

When no azimuthal component (B_ϕ) is present, Eq. (2.13) reduces to

$$\frac{d}{dR} \left(p + \frac{B^2}{2\mu} \right) = 0, \quad (2.17)$$

with solution $p + B^2/(2\mu) = \text{constant}$, so that the total pressure (gas plus magnetic) is conserved.

Purely azimuthal field

When the axial component vanishes, equation Eq. (2.13) becomes

$$\frac{dp}{dR} + \frac{d}{dR} \left(\frac{B_\phi^2}{2\mu} \right) + \frac{B_\phi^2}{\mu R} = 0, \quad (2.18)$$

where, according to Eq. (2.3), B_ϕ is related to the current by (2.12)

$$j_z = \frac{1}{\mu R} \frac{d}{dR} (RB_\phi). \quad (2.19)$$

If, in particular, the current flows with uniform total value I within a cylinder of radius a , an integration of Eq. (2.19) yields

$$\begin{aligned} \mu \int j_z \mathbf{dS} &= \int \nabla \times \mathbf{B} d\mathbf{S}, \\ \mu I \frac{R^2}{a^2} &= 2\pi R B_\phi(R), \\ B_\phi &= \frac{\mu I R}{2\pi a^2}, \quad R < a, \\ B_\phi &= \frac{\mu I}{2\pi R}, \quad R > a, \end{aligned} \quad (2.20)$$

assuming B_ϕ to be finite and continuous. The corresponding plasma pressure results from integrating Eq. (2.18). Assuming that it takes the value p_∞ outside the current column, we find

$$\begin{aligned} \frac{dp}{dR} &= -\frac{d}{dR} \left(\frac{1}{2\mu} \frac{\mu^2 I^2 R^2}{4\pi^2 a^4} \right) - \frac{1}{\mu R} \frac{\mu^2 I^2 R^2}{4\pi^2 a^4} \Big|_a^R, \\ p &= p_\infty + \frac{1}{4} \mu (I/(\pi a^2))^2 (a^2 - R^2), \quad R < a, \\ p &= p_\infty, \quad R > a. \end{aligned} \quad (2.21)$$

The magnetic field lines are shown in Fig. 2.4. Within the cylinder of radius a B_ϕ increases linearly with R , while the gas pressure decreases, so that the outwards gas pressure is balanced by inwards magnetic pressure and tension forces. Outside the cylinder the pressure is uniform and the magnetic field is potential, so that the outwards magnetic pressure and inwards tension balance one another.

In the laboratory, a plasma configuration in which the current is axial and the magnetic field azimuthal is known as a linear pinch. A simple relation may be derived in this case between the current

$$I \equiv \int_0^{R_0} j_z 2\pi R dR \quad (2.22)$$

flowing through the plasma column (of radius R_0) and the number

$$N \equiv \int_0^{R_0} n 2\pi R dR \quad (2.23)$$

of particles per unit length of the column. Eq. (2.18) may first be multiplied by R^2 and integrated to give

$$R^2 dp = -dR \left(R^2 \frac{B_\phi}{\mu} \frac{dB_\phi}{dR} + \frac{B_\phi^2 R}{\mu} \right),$$

$$R^2 dp = -\frac{RB_\phi}{\mu}(RdB_\phi + B_\phi dR) = -\frac{RB_\phi}{\mu}d(RB_\phi),$$

$$\int_0^{R_0} R^2 dp = -\int_0^{R_0} RB_\phi/\mu d(RB_\phi). \quad (2.24)$$

Then, assuming that the plasma pressure vanishes at R_0 and the temperature ($T = p/(nk_B)$) is uniform across the column, an integration by parts of the left-hand side together with the use of Eq. (2.19) on the right-hand side yields the expression

$$\left| R^2 p \right|_0^{R_0} - \int_0^{R_0} 2Rp dR = -\left| \frac{(RB_\phi)^2}{2\mu} \right|_0^{R_0} = \frac{R_0^2 B_\phi^2}{2\mu},$$

$$\int_0^{R_0} 2Rn k_B T dR = \frac{k_B T N}{\pi},$$

$$I = \int_0^{R_0} 2\pi R \frac{1}{\mu R} \frac{d(RB_\phi)}{dR} dR = \int_0^{R_0} \frac{2\pi}{\mu} d(RB_\phi) = \frac{2\pi}{\mu} R_0 B_\phi,$$

$$I^2 = (8\pi/\mu)k_B T N, \quad (2.25)$$

known as Bennett's relation.

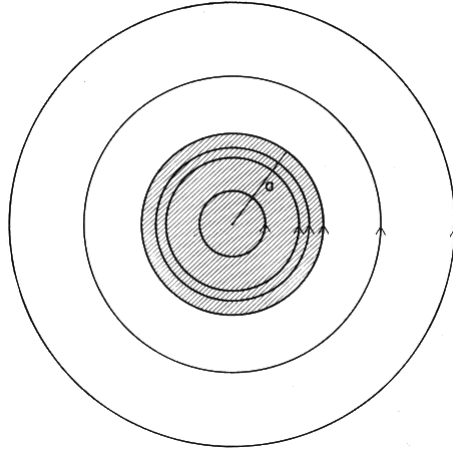


Fig. 2.4: The purely azimuthal magnetic field lines in a section across a column of uniform current and radius a .

Force-free fields

I. Linear field

In the absence of pressure, Eq.(2.13) reduces to

$$\frac{d}{dR} \left(\frac{B_\phi^2 + B_z^2}{2\mu} \right) + \frac{B_\phi^2}{\mu R} = 0. \quad (2.26)$$

Here, either B_ϕ or B_z may be prescribed and the other deduced. For the so-called 'constant- α ' field one assumes that $\mu\mathbf{j} = \alpha\mathbf{B}$, where α is uniform. After using Eq. (2.3), the ϕ -component of this becomes

$$\mu j_\phi = \alpha B_\phi, \quad -\frac{dB_z}{dR} = \alpha B_\phi. \quad (2.27)$$

Finally, an elimination of B_ϕ between Eqs. (2.26) and (2.27) yields Bessel's equation whose solution subject to $B_z = B_0$ and $dB_z/dR = 0$ at $R = 0$ is

$$\frac{d}{dR} \left(\frac{1}{2\mu\alpha^2} \left(\frac{dB_z}{dR} \right)^2 + \frac{1}{2\mu} B_z^2 \right) + \left(\frac{dB_z}{dR} \right)^2 \frac{1}{\mu R \alpha^2} = 0,$$

$$R^2 B_z'' + R B_z' + R^2 \alpha^2 B_z = 0, \quad \text{Bessel's equation}$$

$$B_\phi = B_0 J_1(\alpha R), \quad B_z = B_0 J_0(\alpha R), \quad (2.28)$$

where J_0, J_1 are Bessel functions.

II. Nonlinear fields

An easy way to generate solution to Eq. (2.26) is to choose

$$B^2 = f(R), \quad (2.29)$$

and then Eq. (2.26) gives

$$B_\phi^2 = -\frac{1}{2} R \frac{df}{dR} \quad (2.30)$$

and

$$B_z^2 = B^2 - B_\phi^2. \quad (2.31)$$

The restrictions that B_ϕ^2 and B_z^2 be positive imply that df/dR is negative and that f approaches zero slower than R^{-2} as $R \rightarrow \infty$. The limiting case $f = R^{-2}$ gives the purely azimuthal field $R^{-1}\phi$.

Another simple example of a force-free field is the 'uniform-twist' field, for which Φ is (given by Eq. (2.16)) is constant and the field components are

$$B_\phi = \frac{B_0 \Phi R / (2L)}{1 + \Phi^2 R^2 / (2L)^2}, \quad B_z = \frac{B_0}{1 + \Phi^2 R^2 / (2L)^2}. \quad (2.32)$$

They have the property that field lines at different radii are twisted through the same angle, so that the whole tube is twisted like a rigid body.

Basic topology of twisted magnetic configurations

Let us construct a simple magnetic loop as presented in Fig. 2.5. Such a configuration resembles to that in the solar atmosphere. The z -axis points in the vertical direction and the plane $z = 0$ represents the photosphere.

The whole magnetic field is obtained here by superimposing three components denoted by $\mathbf{B}_I, \mathbf{B}_q$ and \mathbf{B}_θ . The first component \mathbf{B}_I is the field created by a ring current I uniformly distributed

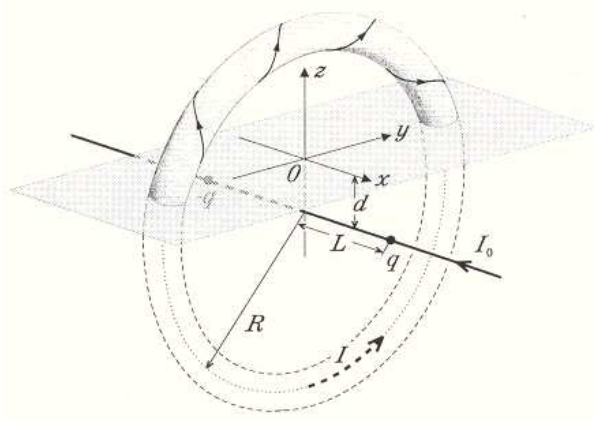


Fig. 2.5: The magnetic field under study is modelled by a force-free circular flux tube with the total current I , a pair of magnetic charges $-q, q$ and a line current I_0 . Below the photospheric plane $z = 0$ this configuration has no real physical meaning: it is used only to construct the proper magnetic field in corona.

over its circular cross section of radius a . The plane of symmetry of the ring coincides with the plane $x = 0$, while its axis of symmetry is parallel to the x -axis and submerged under the photosphere by a depth d , so that in corona only an arc of the ring with major radius R is present. The second component \mathbf{B}_q is created by the leading and following spots of the modelling active region, which are represented here by two charges $-q$ and q lying on the axis of symmetry of the ring from both sides of the plane $x = 0$ on the distance L . The third component \mathbf{B}_θ is created by a line current I_0 flowing exactly along the axis of symmetry of the ring. In this model, of course, only the field above the photospheric plane $z = 0$ has a real physical meaning, while the sub-photospheric currents and sources play an auxiliary role in constructing the configuration. One can ignore its sub-photospheric part and regard that the coronal force-free field is in fact determined by the vertical components of the field $\mathbf{B}_q + \mathbf{B}_I + \mathbf{B}_\theta$ and current density on the photosphere. The region occupied by the ring current is further assumed to be thin, so that the equilibrium of this current can be investigated by using appropriate asymptotic expansions in small parameters a/R and a/L . The external equilibrium here corresponds to the equilibrium of a ring current in an axisymmetric potential field. Due to the present axial symmetry, the respective equilibrium condition is the same for each element of the flux tube and, is reduced to the balance of only two forces: the Lorentz force \mathbf{F}_q caused by interaction of the current I with the field \mathbf{B}_q and the Lorentz self-force \mathbf{F}_I resulting from the curvature of the tube axis. Both forces act along the normal \mathbf{n} to thin axis and can be written as

$$\mathbf{F}_q = -\frac{2qLI\mathbf{n}}{(R^2 + L^2)^{3/2}}, \quad (2.33)$$

$$\mathbf{F}_I = \frac{\mu_0 I^2}{4\pi R} \left(\ln \frac{R}{a} + \ln 8 - 3/2 + l_i/2 \right) \mathbf{n}, \quad (2.34)$$

where l_i is the internal self-inductance per unit length of the tube ($l_i = 1/2$ in our case). From the force balance $\mathbf{F}_q + \mathbf{F}_I = 0$ we obtain the total equilibrium current

$$I = \frac{8\pi qLR(R^2 + L^2)^{-3/2}}{\mu_0 [\ln(8R/a) - 3/2 + l_i/2]}, \quad (2.35)$$

which flows in the corona.

Now, let us construct approximate analytical expressions for the magnetic field. We use the tubal system of coordinates (ρ, ϕ, θ) , ρ is the distance from the axis of the tube and ϕ is the angle between radius ρ and the plane symmetry $x = 0$, while θ measures the angular arc length of the tube from the positive direction of y -axis. Since the flux tube in our model is assumed to be thin in configuration with its radius of curvature R and the characteristic size L , the corresponding force-free condition in zero order approximation by small parameters a/R and a/L is the same as for the straight tube. So in the above tubal coordinates the force-free condition can be written at $0 < \rho \leq a$ as follows

$$\frac{\rho}{2} \frac{\partial}{\partial \rho} (B_{\phi in}^2 + B_{\theta in}^2) + B_{\phi in}^2 \approx 0, \quad (2.36)$$

where the azimuthal magnetic field component

$$B_{\phi in} \approx \frac{\mu_0 I \rho}{2\pi a^2} \quad (2.37)$$

corresponds to the uniformly distributed toroidal current I . These equations give the toroidal field inside the tube (when we put Eq. 2.37 into Eq. 2.36)

$$B_{\theta in} \approx \text{sign}(I_0) \left(B_{\theta R}^2 + \frac{\mu_0^2 I^2}{2\pi^2 a^4} (a^2 - \rho^2) \right)^{1/2}, \quad (2.38)$$

where the toroidal field on the surface of the tube

$$B_{\theta R} \approx \frac{\mu_0 I_0}{2\pi R} \quad (2.39)$$

is followed from the appropriate approximation of the external toroidal field

$$B_{\theta ex} = \frac{\mu_0 I_0}{2\pi} (y^2 + (z + d)^2)^{-1/2}, \quad (2.40)$$

which is produced by the sub-photospheric line current I_0 .

Both internal and external toroidal fields can be sewed by using the following formula:

$$\mathbf{B}_\theta = \frac{\mu_0 I_0}{2\pi} \left[\frac{1}{R^2} + \frac{2\chi(a - \rho)}{a^2} \frac{I^2}{I_0^2} \left(1 - \frac{\rho^2}{a^2} \right) \right]^{1/2} \theta + \frac{\mu_0 I_0}{2\pi} [y^2 + (z + d)^2]^{-1/2} - R^{-1} \theta, \quad (2.41)$$

where

$$\theta = \left(0, -\frac{z + d}{r_\perp}, \frac{y}{r_\perp} \right), \quad (2.42)$$

$$\rho = [x^2 + (r_\perp - R)^2]^{1/2}, \quad (2.43)$$

$$r_\perp = [y^2 + (z + d)^2]^{1/2}, \quad (2.44)$$

and $\chi(X)$ stands for the Heaviside function such that $\chi = 1$ if $X > 0$ and $\chi = 0$ otherwise. The equation describes the toroidal magnetic field inside the flux tube only in zero order approximation by small parameters a/R and a/L , which is sufficient for determination of the topology in our configuration.

Remark: Thus, outside the loop ($\chi = 0$)

$$\mathbf{B}_\theta = \frac{\mu_0 I_0}{2\pi} \left[\frac{1}{R} + [y^2 + (z+d)^2]^{-1/2} - R^{-1} \right] \theta,$$

$$\mathbf{B}_\theta = \frac{\mu_0 I_0}{2\pi} [y^2 + (z+d)^2]^{-1/2} \theta,$$

and inside the loop ($\chi = 1$)

$$\mathbf{B}_\theta = \frac{\mu_0 I_0}{2\pi} \left[\frac{1}{R^2} + \frac{2}{a^2} \frac{I^2}{I_0^2} \left(1 - \frac{\rho^2}{a^2}\right) \right]^{1/2} \theta,$$

$$\mathbf{B}_\theta = \frac{\mu_0 I_0}{2\pi} \left[\frac{1}{R^2} + \frac{2}{a^2} \frac{I^2}{4\pi^2 R^2 B_{\theta R}^2 / \mu_0^2} \left(1 - \frac{\rho^2}{a^2}\right) \right]^{1/2} \theta,$$

$$\mathbf{B}_\theta = [B_{\theta R}^2 + \frac{\mu_0^2 I^2}{2\pi^2 a^4} (a^2 - \rho^2)]^{1/2} \theta,$$

which corresponds to previous formulae.

We also determine with the same accuracy, the poloidal magnetic field everywhere in the coronal volume. Inside the flux tube Eq. (2.37) yields it with the desired accuracy, outside the tube it is approximately a superposition of the point sources field

$$\mathbf{B}_q = q \left(\frac{\mathbf{r}_+}{|\mathbf{r}_+|^3} - \frac{\mathbf{r}_-}{|\mathbf{r}_-|^3} \right), \quad (2.45)$$

$$\mathbf{r}_\pm = (x \mp L, y, z + d), \quad (2.46)$$

and of the field \mathbf{B}_{Iex} produced by the line current I in the ring of radius R . In order to derive \mathbf{B}_{Iex} and the proper sewing function \mathbf{B}_I , it is helpful to represent the magnetic field in terms of the vector potential, which due to the symmetry of our configuration about x -axis can be reduced to only one non-vanishing θ -component $A_I(r_\perp, x)$, so that

$$\mathbf{B}_I = \nabla \times (A_I \theta) = -\frac{\partial A_I}{\partial x} \frac{\mathbf{r}_\perp}{r_\perp} + \left(\frac{\partial A_I}{\partial r_\perp} + \frac{A_I}{r_\perp} \right) \mathbf{x}. \quad (2.47)$$

Remark: Generally,

$$\mathbf{B} = B_\theta \theta + B_{r_\perp} \frac{\mathbf{r}_\perp}{r_\perp} + B_x \mathbf{x}.$$

Due to cylindrical symmetry

$$\mathbf{B}_I = B_{r_\perp} \frac{\mathbf{r}_\perp}{r_\perp} + B_x \mathbf{x},$$

and thus \mathbf{B}_I can be express as

$$\mathbf{B}_I = \nabla \times (A_I \theta).$$

Coordinate vectors are:

$$\frac{\mathbf{r}_\perp}{r_\perp} = \left(0, \frac{y}{r_\perp}, \frac{z+d}{r_\perp} \right), \quad \theta = \left(0, -\frac{z+d}{r_\perp}, \frac{y}{r_\perp} \right), \quad \mathbf{x} = (x, 0, 0). \quad (2.48)$$

Then using standard vector operation $\nabla \times (A_I \theta)$ in cylindrical coordinates we obtain the above mentioned Eq. (2.47).

From here and equation (2.37) one can derive A_I inside the tube

$$A_{Iin} \approx \frac{\mu_0 I}{2\pi} \left(const - \frac{\rho^2}{2a^2} \right). \quad (2.49)$$

$$\mathbf{B}_{Iin} \approx \frac{\mu_0 I}{2\pi} \left(-\frac{2x}{2a^2} \frac{\mathbf{r}_\perp}{r_\perp} - \frac{2(r_\perp - R)}{2a^2} \mathbf{x} \right), \quad const \text{ so } A_I/r_\perp \rightarrow 0,$$

$$|\mathbf{B}_{Iin}| = \frac{\mu_0 I}{2\pi a^2} (x^2 + (r_\perp - R)^2)^{1/2}.$$

Outside the flux tube, A_I is well approximated by the potential of the ring determined as: Generally we can write

$$A_{Iex} \approx \frac{\mu_0 IR}{4\pi} \int_0^{2\pi} \frac{\cos \theta' d\theta'}{(R^2 + r_D^2 - 2Rr_D \sin \theta \cos \theta')^{1/2}}, \quad (2.50)$$

where R is the radius of the ring current, r_D is the distance from the centrum of the ring to the position, where the vector potential is calculated. Thus, $r_D = \sqrt{r_\perp^2 + x^2}$ and $r_D \sin \theta = r_\perp$. Then we may write

$$A_{Iex} \approx \frac{\mu_0 IR}{4\pi(R^2 + r_\perp^2 + x^2)^{1/2}} \int_0^{2\pi} \frac{\cos \theta' d\theta'}{(1 - v \cos \theta')^{1/2}}, \quad (2.51)$$

where

$$v = \frac{2r_\perp R}{R^2 + r_\perp^2 + x^2}. \quad (2.52)$$

The above integral can be expressed in terms of the complete elliptic integrals of the first and second kinds, $K(k)$ and $E(k)$, as follows: First, in denominator of Eq. 2.51 we add $2Rr_\perp - 2Rr_\perp$

$$A_{Iex} \approx \frac{\mu_0 IR}{4\pi(R^2 + r_\perp^2 + x^2 + 2Rr_\perp)^{1/2}} \int_0^{2\pi} \frac{\cos \theta' d\theta'}{\left(1 - \frac{2 \cdot 2Rr_\perp}{R^2 + r_\perp^2 + x^2 + 2Rr_\perp} \frac{1 + \cos \theta'}{2}\right)^{1/2}},$$

Then we designate

$$k^2 = \frac{4Rr_\perp}{R^2 + r_\perp^2 + x^2 + 2Rr_\perp},$$

and use

$$\cos^2 \frac{\theta}{2} = \frac{1 + \cos \theta'}{2},$$

and $\theta/2 = H$, so the vector potential is

$$A_{Iex} \approx \frac{\mu_0 IR}{4\pi(R^2 + r_\perp^2 + x^2 + 2Rr_\perp)^{1/2}} \int_0^{\pi/2} \frac{4 \cos 2H dH}{(1 - k^2 \cos^2 H)^{1/2}},$$

where the multiplication factor 4 in integration is due to a change of integration limits. Now, using $\cos 2H = \cos^2 H - \sin^2 H$ and definitions of the complete elliptical integrals

$$\begin{aligned} K &= \int_0^{\pi/2} \frac{d\alpha}{\sqrt{1 - k^2 \sin^2 \alpha}}, \\ E &= \int_0^{\pi/2} \sqrt{1 - k^2 \sin^2 \alpha} d\alpha, \end{aligned} \quad (2.53)$$

we have

$$A_{Iex} \approx \frac{\mu_0 IR}{4\pi(R^2 + r_\perp^2 + x^2 + 2Rr_\perp)^{1/2}} 4 \left(\frac{1}{k^2}(K - E) - \frac{1}{k^2}(E - (1 - k^2)K) \right),$$

(in integrations we can replace $\sqrt{1 - k^2 \sin^2 \alpha}$ by $\sqrt{1 - k^2 \cos^2 \alpha}$), and after a simple manipulation the final formula for the vector potential is

$$A_{Iex}(x, r_\perp) \approx \frac{\mu_0 I}{2\pi} \sqrt{\frac{R}{r_\perp}} \mathcal{A}(k), \quad (2.54)$$

in which

$$\mathcal{A}(k) \equiv k^{-1}[(2 - k^2)K(k) - 2E(k)] \quad (2.55)$$

and

$$k \equiv 2\sqrt{\frac{r_\perp R}{(r_\perp + R)^2 + x^2}}. \quad (2.56)$$

There is a small mismatch at $\rho = a$ between A_{Iex} and A_{Iin} , which can be eliminated by using, instead of A_{Iin} , the following expression:

$$\bar{A}_{Iin} \approx \frac{\mu_0 I}{2\pi} \sqrt{\frac{R}{r_\perp}} [\mathcal{A}(k_a) + \mathcal{A}'(k_a)(k - k_a)], \quad (2.57)$$

where

$$\mathcal{A}'(k) \equiv \frac{d}{dk} \mathcal{A}(k) = \frac{(2 - k^2)E(k) - 2(1 - k^2)K(k)}{k^2(1 - k^2)} \quad (2.58)$$

and

$$K' = \frac{(E/(1 - k^2) - K)}{k}, \quad E' = \frac{E - K}{k},$$

and

$$k_a = 2\sqrt{\frac{r_\perp R}{4r_\perp R + a^2}} \quad (2.59)$$

is the value such that $k = k_a$ at $\rho = a$ and always $k_a < 1$, so $\mathcal{A}(k_a)$ and $\mathcal{A}'(k_a)$ are regular functions of r_\perp . One can show that in zero order approximation by a/R Eq. (2.57) reduces to Eq. (2.49), while \bar{A}_{Iin} and A_{Iex} at $\rho = a$ are equal to each other together with their first derivatives, so the corresponding sewing function is

$$\mathcal{A}_I = \chi(a - \rho)\bar{A}_{Iin} + \chi(\rho - a)A_{Iex}. \quad (2.60)$$

By using this and Eq. (2.47) one can derive now an explicit formula for B_I and so for the whole magnetic field.

References

- Priest, E.R.: 1982, Solar Magnetohydrodynamics, D. Reidel Publ. Comp., Dordrecht, Holland.
Titov, V.S., Demoulin, P.: 1999, Astron. Astrophys. 351, 707.

Chapter 3

Magnetic field reconnection

Diffusion in the current sheet

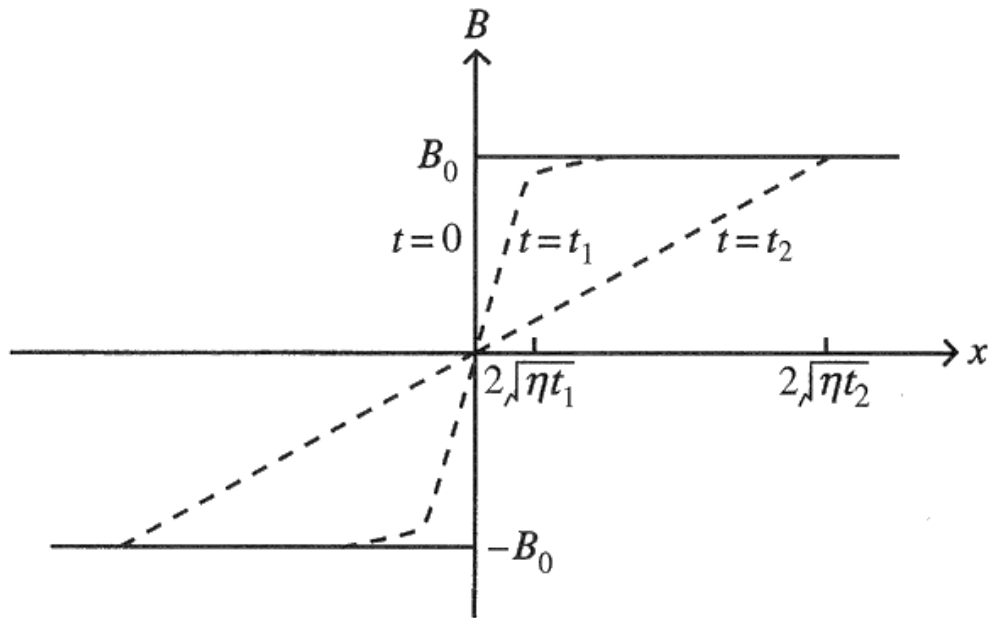


Fig. 3.1: The magnetic field (B) as a function of distance (x) in a 1-D current sheet that is diffusing from sheet of zero thickness initially, for times $t = 0, t_1, t_2$, where $0 < t_1 < t_2$.

Let us consider a current sheet described as

$$\begin{aligned} B(x, 0) &= B_0, \quad x > 0, \\ B(-x, 0) &= -B(x, 0). \end{aligned} \quad (3.1)$$

and the plasma velocity $\mathbf{v} = 0$ everywhere in the system. Then the induction equation is reduced to the diffusion one:

$$\frac{\partial B}{\partial t} = \eta \frac{\partial^2 B}{\partial x^2}, \quad (3.2)$$

whose solution is

$$B(x, t) = \frac{2B_0}{\sqrt{\pi}} \int_0^{x/\sqrt{4\eta t}} e^{-u^2} du. \quad (3.3)$$

Solution (3.3) has the form shown in Fig. 3.1 and may be verified a posteriori by substituting it back into Eq. (3.2).

Remark:

$$\frac{\partial}{\partial \alpha} \int_{\phi_1(\alpha)}^{\phi_2(\alpha)} f(x, \alpha) dx = \int_{\phi_1(\alpha)}^{\phi_2(\alpha)} \frac{\partial f(x, \alpha)}{\partial \alpha} dx + \phi_2' f(\phi_2(\alpha), \alpha) - \phi_1' f(\phi_1(\alpha), \alpha). \quad (3.4)$$

The magnetic field diffuses away in time at a speed η/l , where the width (l) of the sheet is of the order of $(\eta t)^{1/2}$ and so increases in time. The resulting magnetic field strength at a fixed position decreases with time, so the field is annihilated. The total magnetic flux ($\int_{-\infty}^{\infty} B dx$) remains constant (namely zero) and the total current

$$J = \int_{-\infty}^{\infty} j dx = \frac{1}{\mu} \int_{-\infty}^{\infty} \frac{\partial B}{\partial x} dx = \frac{2B_0}{\mu} \quad (3.5)$$

is conserved, since it simply spreads out in space. However, the magnetic energy decreases in time at a rate

$$\frac{\partial}{\partial t} \int_{-\infty}^{\infty} \frac{B^2}{2\mu} dx = \int_{-\infty}^{\infty} \frac{B}{\mu} \frac{\partial B}{\partial t} dx. \quad (3.6)$$

Substituting for $\partial B/\partial t$ from Eq. 3.2 and integrating by parts, we find that this becomes

$$\int_{-\infty}^{\infty} \frac{B\eta}{\mu} \frac{\partial^2 B}{\partial x^2} dx = \frac{1}{\mu^2 \sigma} \left(\left| B \frac{\partial B}{\partial x} \right|_{-\infty}^{\infty} - \int_{-\infty}^{\infty} \left(\frac{\partial B}{\partial x} \right)^2 dx \right). \quad (3.7)$$

Since $\partial B/\partial x$ remains equal to zero at infinity, the first term on the right vanishes, and, since the electric current is $j = \mu^{-1} \partial B/\partial x$, we finally have

$$\frac{\partial}{\partial t} \int_{-\infty}^{\infty} \frac{B^2}{2\mu} dx = - \int_{-\infty}^{\infty} \frac{j^2}{\sigma} dx. \quad (3.8)$$

In other words, magnetic energy is converted entirely into heat by ohmic dissipation (j^2/σ per unit volume).

Concept of frozen flux and field-line motion

The term "magnetic reconnection" is intimately lined to the concept of field-line motion. In a plasma with a very small resistivity the Ohm law becomes $\mathbf{E} + \mathbf{v} \times \mathbf{B} = 0$, and the induction equation reduces to

$$\frac{\partial \mathbf{B}}{\partial t} = \nabla \times (\mathbf{v} \times \mathbf{B}). \quad (3.9)$$

Then, if we consider a curve C (bounding a surface S) which is moving with the plasma, in a time dt an element $d\mathbf{s}$ of C sweeps out an element of area $\mathbf{v} \times d\mathbf{s} dt$. The rate of change of magnetic flux through C is

$$\frac{d}{dt} \int_S \mathbf{B} \cdot d\mathbf{S} = \int_S \frac{\partial \mathbf{B}}{\partial t} \cdot d\mathbf{S} + \int_C \mathbf{B} \cdot \mathbf{v} \times d\mathbf{s}. \quad (3.10)$$

As C moves, so the flux changes, both because the magnetic field changes with time and because the boundary moves in space. By setting $\mathbf{B} \cdot \mathbf{v} \times d\mathbf{s} = -\mathbf{v} \times \mathbf{B} \cdot d\mathbf{s}$ and applying Stokes theorem we obtain

$$\frac{d}{dt} \int_S \mathbf{B} \cdot d\mathbf{S} = \int_S \left(\frac{\partial \mathbf{B}}{\partial t} - \nabla \times (\mathbf{v} \times \mathbf{B}) \right) \cdot d\mathbf{S}, \quad (3.11)$$

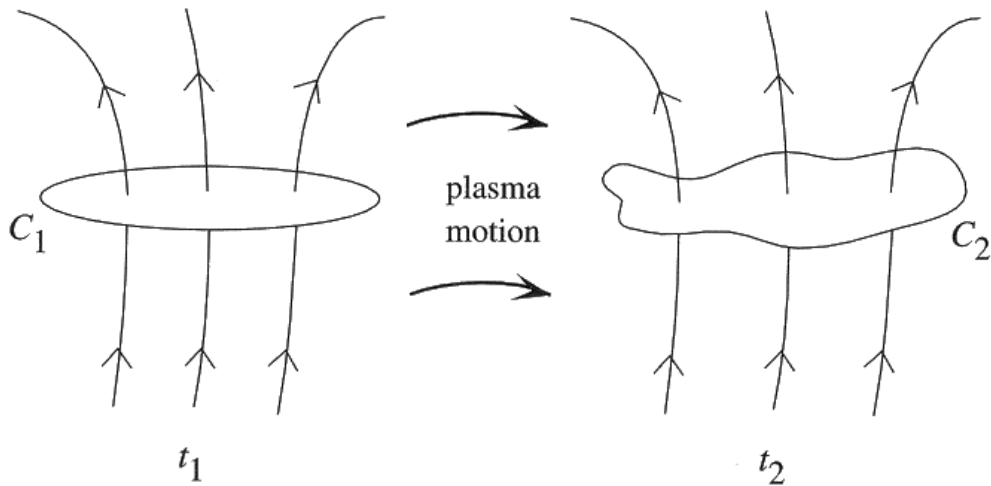


Fig. 3.2: Magnetic flux conservation: if a curve C_1 is distorted into C_2 by plasma motion, the flux through C_1 at t_1 equals the flux through C_2 at t_2 .

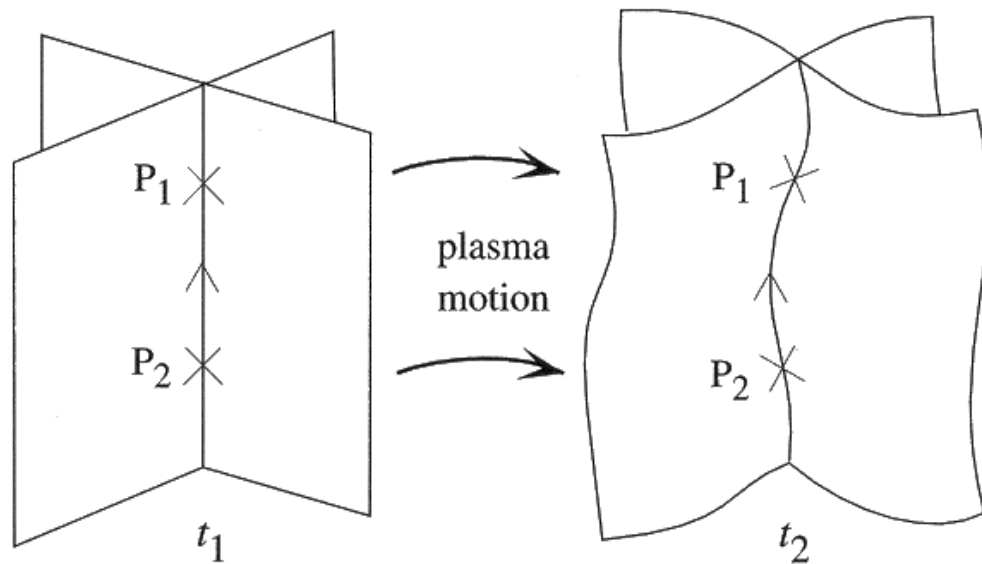


Fig. 3.3: Magnetic field-line conservation: if plasma elements P_1 and P_2 lie on a field line at time t_1 , then they will lie on the same line at a later time t_2 .

which vanishes in the ideal limit. Thus, the total magnetic flux through C remains constant as it moves with the plasma. In other words, we have proved magnetic flux conservation, namely the plasma elements that initially form a flux tube continue to do so at all later times (Fig. 3.2). There is also magnetic field line conservation, namely that, if two plasma elements lie on a field line initially, then they will always do so (Fig. 3.3).

Line conservation can be proved as follows. Applying the vector identity $(\nabla \times (\mathbf{a} \times \mathbf{b}) = (\mathbf{b} \cdot \nabla)\mathbf{a} - (\mathbf{a} \cdot \nabla)\mathbf{b} + \mathbf{a}(\nabla \cdot \mathbf{b}) - \mathbf{b}(\nabla \cdot \mathbf{a}))$ to the ideal induction equation gives

$$\frac{\partial \mathbf{B}}{\partial t} = (\mathbf{B} \cdot \nabla)\mathbf{v} - (\mathbf{v} \cdot \nabla)\mathbf{B} - \mathbf{B}(\nabla \cdot \mathbf{v}). \quad (3.12)$$

Using the mass continuity equation to eliminate $\nabla \cdot \mathbf{v}$, we then obtain

$$\begin{aligned} \frac{d\rho}{dt} &= \frac{\partial\rho}{\partial t} + \mathbf{v} \cdot \nabla\rho = -\rho\nabla \cdot \mathbf{v}, \\ \frac{\partial\mathbf{B}}{\partial t} + (\mathbf{v} \cdot \nabla)\mathbf{B} &= (\mathbf{B} \cdot \nabla)\mathbf{v} - \mathbf{B}(\nabla \cdot \mathbf{v}), \\ \frac{d\mathbf{B}}{dt} - \frac{\mathbf{B}}{\rho} \frac{d\rho}{dt} &= (\mathbf{B} \cdot \nabla)\mathbf{v}, \\ \frac{d}{dt} \left(\frac{\mathbf{B}}{\rho} \right) &= \left(\frac{\mathbf{B}}{\rho} \cdot \nabla \right) \mathbf{v}, \end{aligned} \quad (3.13)$$

where $d/dt = \partial/\partial t + \mathbf{v} \cdot \nabla$ is the total or convective derivative. To see how this result leads to the conclusion that the field lines are "frozen" to the plasma, consider an element segment $\delta\mathbf{l}$ along a line moving with the plasma. If \mathbf{v} is the plasma velocity at one end of the element and $\mathbf{v} + \delta\mathbf{v}$ is the velocity at the other end, then the differential velocity between the two ends is $\delta\mathbf{v} = (\delta\mathbf{l} \cdot \nabla)\mathbf{v}$. During the time interval dt , the segment $\delta\mathbf{l}$ changes at the rate

$$\frac{d\delta\mathbf{l}}{dt} = \delta\mathbf{v} = (\delta\mathbf{l} \cdot \nabla)\mathbf{v}. \quad (3.14)$$

Since this equation has exactly the same form as Eq. (3.13) for the vector \mathbf{B}/ρ , it necessarily follows that, if $\delta\mathbf{l}$ and \mathbf{B}/ρ are initially parallel, then they will remain parallel for all time.

Advection of magnetic field lines

If $R_m \gg 1$, plasma can move freely along magnetic field lines, but in motion perpendicular to them they are dragged with the plasma or vice versa.

As an example (Fig.3.4), consider the effect of a flow

$$v_x = -\frac{v_0 x}{a}, \quad v_y = \frac{v_0 y}{a} \quad (3.15)$$

on a field that is initially

$$\mathbf{B} = B_0 \cos \frac{x}{a} \mathbf{y}, \quad t = 0 \quad (3.16)$$

between $x = -\frac{1}{2}\pi a$ and $x = \frac{1}{2}\pi a$. The equations of the streamlines (namely, $xy = \text{constant}$) are obtained from $dy/dx = v_y/v_x = -y/x$ (Remark: $dy/y = -dx/x, \ln y = -\ln x + C, xy = \text{constant}$). These are rectangular hyperbolae (Fig. 3.4) with inflow along the X -axis and outflow along the y -axis when $v_0 > 0$.

The velocity field corresponds to a hydrodynamic stagnation-point flow. The effect of this flow on the magnetic field is to carry the field lines inwards from the sides and accumulate them near $x = 0$, increasing the field strength there. Since the component (v_x) of the velocity perpendicular to the field lines is constant along a particular field line ($x = \text{constant}$), the field lines are not distorted but remain straight as they come in.

Now, the y -component of the induction equation is $\partial B/\partial t = (\nabla \times (\mathbf{v} \times \mathbf{B}))_y = -\partial(v_x B)/\partial x$ or

$$\frac{\partial B}{\partial t} - \frac{v_0 x}{a} \frac{\partial B}{\partial x} = \frac{v_0 B}{a}, \quad (3.17)$$

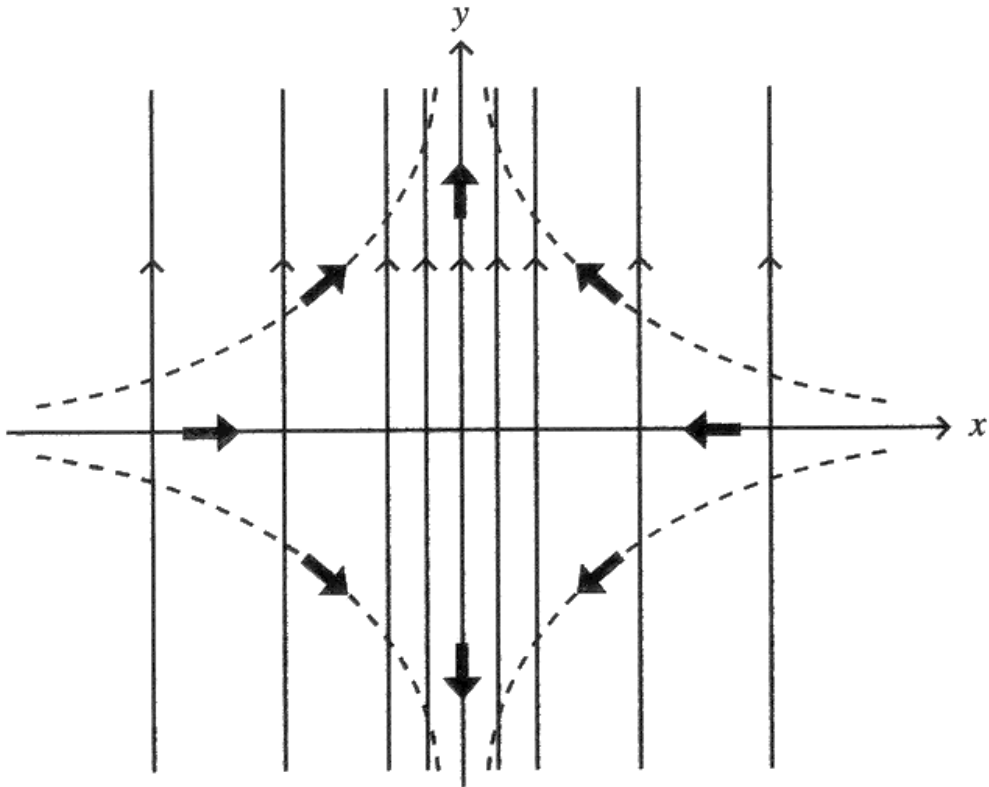


Fig. 3.4: A sketch of the magnetic lines (thin-headed arrows) and streamlines (thick-headed arrows) at $t = 0$ for $|x| < \pi a/2$.

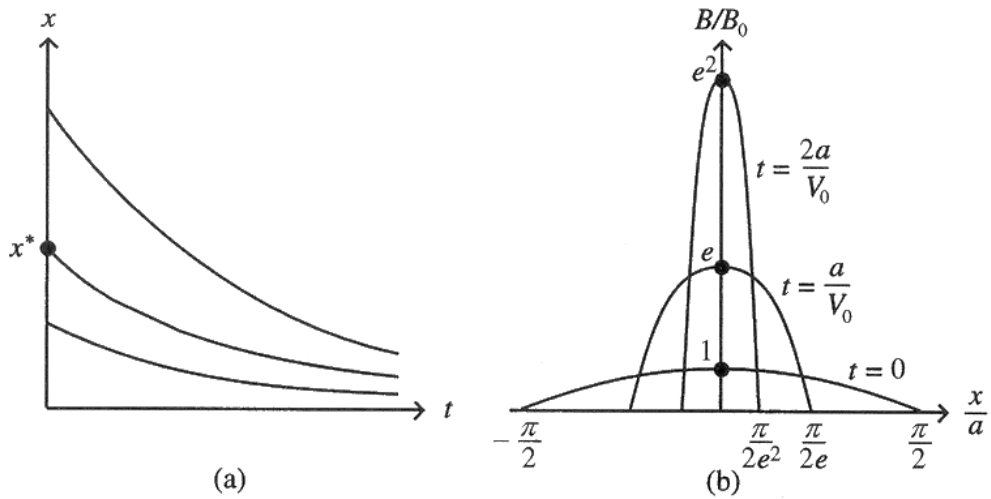


Fig. 3.5: (a) Characteristic curves $x = x^* \exp(-v_0 t/a)$; (b) the solution for B as a function of x for several times.

and this determines $B(x, t)$. In order to solve such a partial differential equation, we consider characteristic curves in the xt -plane, which are defined as

$$\frac{dx}{dt} = v_x = -\frac{v_0 x}{a}, \tag{3.18}$$

with solution

$$x = x^* e^{-v_0 t/a}, \quad (3.19)$$

where $x = x^*$ at $t = 0$. We wish to determine $B(x, t)$ at every point of the xt -plane, and the elegance of considering characteristic curves, $x = x(t)$ given by Eq. (3.19) (Fig. 3.5a), is that on such curves $B(x(t), t)$ has the derivative

$$\frac{dB}{dt} = \frac{\partial B}{\partial t} + \frac{dx}{dt} \frac{\partial B}{\partial x} = \frac{\partial B}{\partial t} - \frac{v_0 x}{a} \frac{\partial B}{\partial x}, \quad (3.20)$$

by Eq. (3.18), or, from Eq. (3.17), $dB/dt = v_0 B/a$. In other words, on the characteristic curves we have a simple ordinary differential equation to solve in place of Eq. (3.17): the solution is $B = \text{constant } e^{v_0 t/a}$ or, since $x = x^*$ and $B = B_0 \cos(x^*/a)$ at $t = 0$, we have

$$B(x, t) = B_0 \cos(x^*/a) e^{v_0 t/a}. \quad (3.21)$$

However, in this solution x^* is a constant which we have introduced for convenience and which was not present in the initial statement of the problem, so we should eliminate it by Eq. (3.19), with the final result

$$B(x, t) = B_0 \cos\left(\frac{x}{a} e^{v_0 t/a}\right) e^{v_0 t/a}. \quad (3.22)$$

This solution is plotted in Fig. 3.5b against x for several times. It can be seen that the field does indeed, as expected, concentrate near $x = 0$ as time proceeds. The field strength at the origin is $B(0, t) = B_0 e^{v_0 t/a}$, which grows exponentially in time (or decreases if the flow is reversed by taking $v_0 < 0$).

Stagnation-point flow model

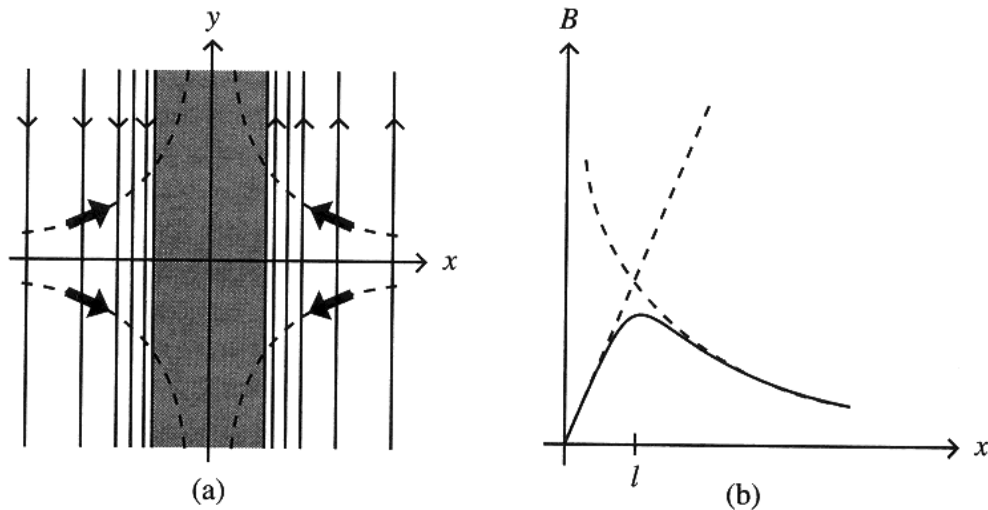


Fig. 3.6: (a) Stagnation-point flow creating a steady current sheet (shaded). (b) Magnetic field profile, with small- x and large- x approximations shown as dashed curves.

The standard equations for 2-D steady-state incompressible flow are

$$\mathbf{E} + \mathbf{v} \times \mathbf{B} = \eta \nabla \times \mathbf{B}, \quad (3.23)$$

$$\rho(\mathbf{v} \cdot \nabla)\mathbf{v} = -\nabla \left(p + \frac{B^2}{2\mu} \right) + (\mathbf{B} \cdot \nabla) \frac{\mathbf{B}}{\mu}, \quad (3.24)$$

where

$$\nabla \cdot \mathbf{B} = 0, \nabla \cdot \mathbf{v} = 0, \mathbf{j} \times \mathbf{B} = (\nabla \times \mathbf{B}) \times \mathbf{B} / \mu = (\mathbf{B} \cdot \nabla)\mathbf{B} / \mu - \nabla(B^2 / (2\mu)), \quad (3.25)$$

and the components v_x, v_y, B_x, B_y depend on x and y alone. Faraday's law ($\nabla \times \mathbf{E} = 0$) implies that $\partial E / \partial y = \partial E / \partial x = 0$, so that $\mathbf{E} = E\mathbf{z}$ is uniform.

Considering a steady-state flow

$$v_x = -\frac{v_0 x}{a}, v_y = \frac{v_0 y}{a}, \quad (3.26)$$

for which $\nabla \cdot \mathbf{v} = 0$. The steady-state continuity equation $(\mathbf{v} \cdot \nabla)\rho + \rho(\nabla \cdot \mathbf{v}) = 0$ then reduces to $(\mathbf{v} \cdot \nabla)\rho = 0$, which implies that the density ρ is uniform if it is constant at the inflowing sides. The flow vanishes at the origin and therefore represents an incompressible, stagnation-point flow.

Suppose now that the magnetic field lines are straight with $\mathbf{B} = B(x)\mathbf{y}$ and they reverse sign at $x = 0$. Then in Ohm law (Eq. 3.23), both $\mathbf{v} \times \mathbf{B}, \nabla \times \mathbf{B}$, and therefore \mathbf{E} are directed purely in the z -direction and in the present case it reduces to

$$E - \frac{v_0 x}{a} B = \eta \frac{dB}{dx}. \quad (3.27)$$

From this equation the magnetic field B can be estimated in two extreme cases as (see also Fig.3.6):

$$B \approx \frac{Ea}{v_0 x}, x \gg 1, \quad (3.28)$$

$$B \approx \frac{Ex}{\eta}, x \ll 1. \quad (3.29)$$

Steady reconnection: classical solutions

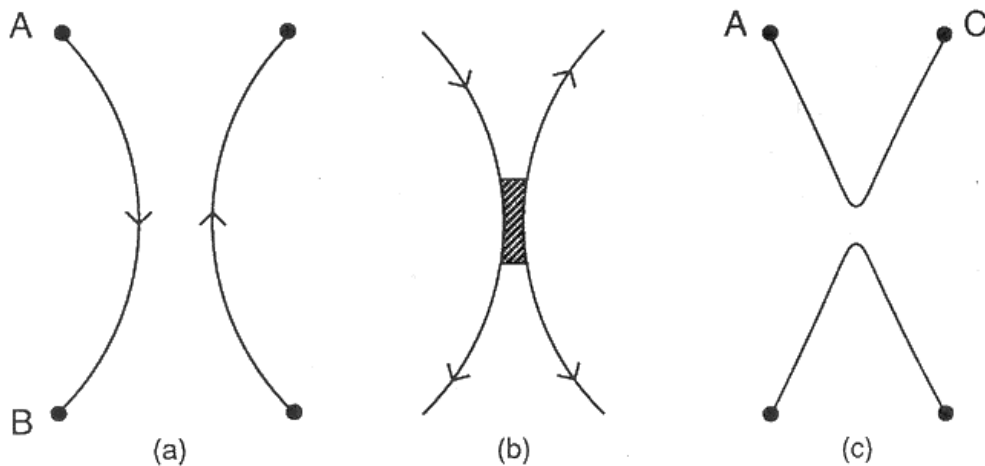


Fig. 3.7: Breaking and reconnection of magnetic field lines.

In most of the universe the magnetic Reynolds number is very much larger than unity and so the magnetic field is frozen to the plasma, but in very small singular regions it can slip (diffuse)

through the plasma (Fig. 3.7). There are several important effects of this local process:

- a) Changes of global topology and connectivity of field lines, which affect the paths of fast particles and heat, since these travel mainly along field lines.
- b) Conversion of magnetic energy to heat, kinetic energy and fast particle energy.
- c) Creation of large electric currents, large electric fields, shocks, all of which may help to accelerate fast particles.

a) Formation of a current sheet

X-type collapse

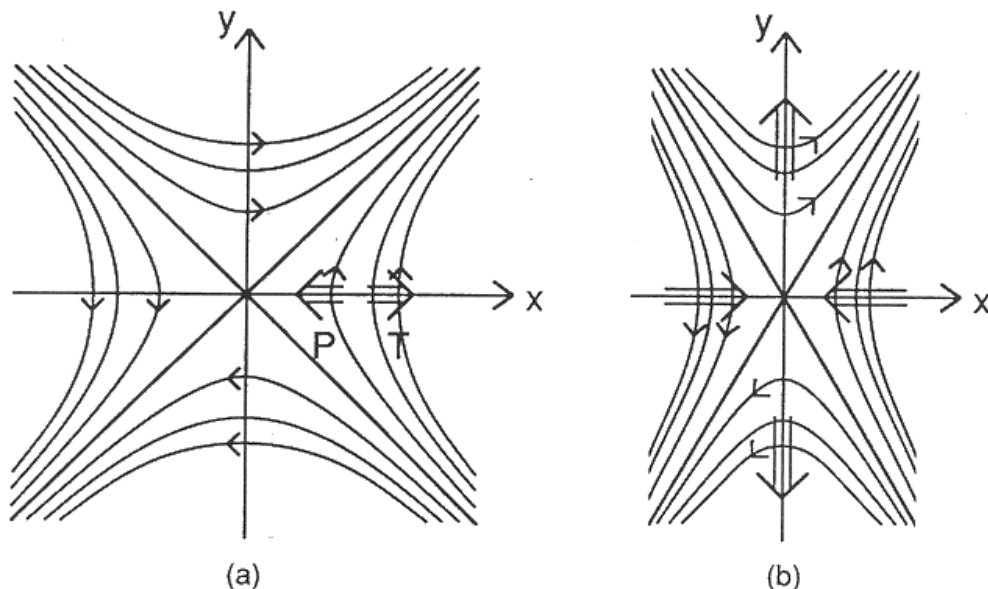


Fig. 3.8: Collapse of the field near an X-point.

There are several ways of forming current sheets. One is through the collapse of the field near an X-type neutral point such as

$$B_x = y, B_y = x, \quad (3.30)$$

which has field lines $y^2 - x^2 = \text{constant}$ ($dy/dx = B_y/B_x = x/y$). The field is in equilibrium since the electric current $\mu^{-1}(\partial B_y/\partial x - \partial B_x/\partial y)$ vanishes and so there is a balance everywhere between the magnetic pressure force (P) acting inwards and the magnetic tension force (T) acting outwards (Fig. 3.8a).

Suppose now the field is distorted to $B_x = y, B_y = \alpha^2 x$, where $\alpha^2 > 1$, with field lines $y^2 - \alpha^2 x^2 = \text{constant}$, as sketched in Fig. (3.8b), and electric current $j = (\alpha^2 - 1)/\mu$.

Physically, we expect an inwards force on the x -axis since the tension force is smaller and the magnetic pressure force larger, whereas along the y -axis we expect an outwards force since the tension force is increased by the larger curvature. Mathematically, the magnetic force has components

$$\mathbf{j} \times \mathbf{B} = -\frac{(\alpha^2 - 1)\alpha^2 x}{\mu} \mathbf{x} + \frac{(\alpha^2 - 1)y}{\mu} \mathbf{y}. \quad (3.31)$$

These act in such a sense as to increase the perturbation and so the initial equilibrium is unstable.

Current sheet formation: description by complex variables

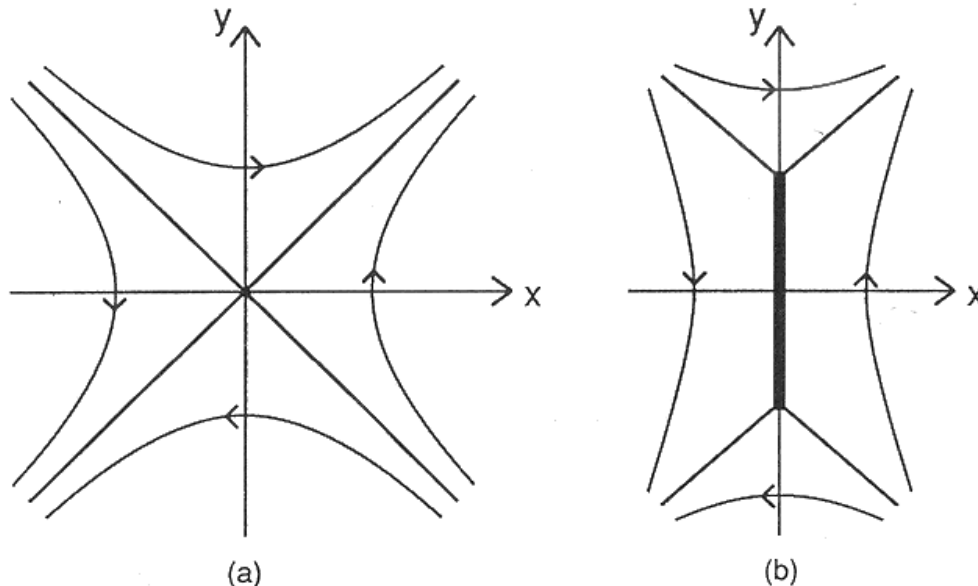


Fig. 3.9: Creation of a current sheet from an X-point configuration.

Suppose the sources of the magnetic field move slowly together and drive the formation of a series of equilibria containing a current sheet (Fig. 3.9a). Initially $B_x = y, B_y = x$. Then the question is how to describe the resulting equilibrium containing a current sheet as in Fig. 3.9b. Outside the sheet, where the current vanishes, the magnetic field satisfies $\nabla \times \mathbf{B} = 0$ and $\nabla \cdot \mathbf{B} = 0$ or, in two dimensions,

$$\frac{\partial B_y}{\partial x} - \frac{\partial B_x}{\partial y} = 0, \quad \frac{\partial B_x}{\partial x} + \frac{\partial B_y}{\partial y} = 0. \quad (3.32)$$

Now, it may be shown as follows that if

$$B_y + iB_x = f(z) \quad (3.33)$$

is any analytic function of the complex variable $z = x + iy$, then Eq. (3.32) is automatically satisfied. We are familiar with the fact that the derivative $f'(x)$ of a function of x exists if the gradient at x has the same value whether x is approached from the left or the right. In a similar way if $f(z)$ is analytic the gradient has the same value when z is approached from any direction, in particular keeping y constant (so that $z = x$) and keeping x constant (so that $z = iy$). In other words

$$\frac{\partial}{\partial x}(B_y + iB_x) = \frac{1}{i\partial y}(B_y + iB_x), \quad (3.34)$$

or, by equating real and imaginary parts, we obtain Eq. 3.32 as required. Thus, we can treat the current sheet as a cut in the complex plane and the object is to find a function $f(z)$ which has such a cut.

Now the initial state (3.33) has $B_y + iB_x = z$ and when a sheet stretches from $z = -iL$ to $z = iL$ we may use

$$B_y + iB_x = (z^2 + L^2)^{1/2}, \quad (3.35)$$

which behaves like z when $z \gg L$ and reduces to z when $L = 0$ (for $z = 0$, $B_y = L$, $B_x = 0$). Thus the evolution through a series of equilibria with a slowly growing sheet may simply be modelled by letting L slowly increase in value in (3.35). The field has limiting field lines (separatrices) through the ends of the sheet, field lines which are inclined to one another at the ends of the sheet by $2\pi/3$. This may be shown by noting that near the upper end of the sheet at $z = iL$, (3.35) becomes approximately $B_y + iB_x = \sqrt{(iL + Z)^2 + L^2} \approx \sqrt{2iL}Z^{1/2}$ where $Z = z - iL$. This may be written as

$$B_y + iB_x = \frac{da}{dZ}, \quad (3.36)$$

where

$$a = \sqrt{2iL} \frac{2}{3} Z^{3/2} = \sqrt{2L} \frac{2}{3} e^{i\pi/4} R^{3/2} e^{3i\Theta/2}, \quad (3.37)$$

and the complex number Z has been written in polar form as $Z = Re^{i\Theta}$, ($\sqrt{i} = (e^{i\pi/2})^{1/2}$). However, if A is the real part of a , then (3.36) implies that $B_y = \partial A / \partial X$, $B_x = -\partial A / \partial Y$, where X and Y are the real and imaginary parts of Z and the magnetic field lines are given by

$$\frac{dY}{dX} = \frac{B_y}{B_x} = -\frac{\partial A / \partial X}{\partial A / \partial Y}, \quad \frac{\partial A}{\partial X} dX + \frac{\partial A}{\partial Y} dY = 0. \quad (3.38)$$

In other words $dA = 0$ and so $A = \text{constant}$.

By taking the real part of (3.37) we can see that

$$A = \sqrt{2L} \frac{2}{3} R^{3/2} \cos\left(\frac{3\Theta}{2} + \frac{\pi}{4}\right). \quad (3.39)$$

Thus the particular field lines $A = 0$ are given by

$$\frac{3\Theta}{2} + \frac{\pi}{4} = -\frac{\pi}{2}, \frac{\pi}{2}, \frac{3\pi}{2}, \frac{5\pi}{2}, \quad (3.40)$$

and so $\Theta = -\pi/2, \pi/6, 5\pi/6$ or $3\pi/2$. In other words the current sheet (at $-\pi/2$ or $3\pi/2$) is inclined to the separatrices ($\pi/6$ and $5\pi/6$) by $2\pi/3$, as required.

b) Sweet-Parker model

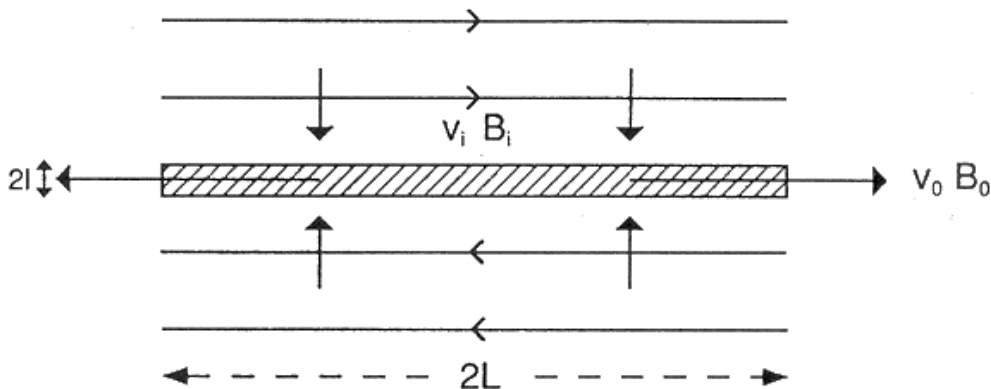


Fig. 3.10: Sweet-Parker reconnection.

This model consists of a simple diffusion region of length $2L$ and width $2l$ between oppositely directed fields. Let us suppose the input flow speed and magnetic field are v_i, B_i . (Fig.3.10).

The electric current is about $j \approx B_i/(\mu l)$ and so the Lorentz force along the sheet is $(\mathbf{j} \times \mathbf{B})_x \approx jB_0 = B_i B_0/(\mu l)$. This force accelerates the plasma from rest at the neutral point to v_0 over distance L and so, by equating the magnitude of $\rho(\mathbf{v} \cdot \nabla)v_x$ to the above Lorentz force, we have

$$\rho \frac{v_0^2}{L} \approx \frac{B_i B_0}{\mu l}. \quad (3.41)$$

From $\nabla \cdot \mathbf{B} = 0$ follows

$$\frac{B_0}{l} \approx \frac{B_i}{L}, \quad (3.42)$$

and so the right-hand side of Eq.3.41 may be written as $B_i^2/(\mu L)$ and we have

$$v_0^2 = \frac{B_i^2}{\mu \rho} = v_{Ai}^2, \quad (3.43)$$

where v_{Ai} is the Alfven speed at the inflow.

Now a question is: how fast can field lines and plasma enter the diffusion region. Note that for a steady state the plasma must carry the field lines in the same speed that they are trying to diffuse outward, so that

$$v_i = v_{Diffuse} = \frac{\eta}{l}. \quad (3.44)$$

Conservation of mass implies that the rate ($4\rho L v_i$) at which mass is entering the sheet must equal the rate ($4\rho l v_0$) at which it is leaving, so that

$$L v_i = l v_{Ai}. \quad (3.45)$$

The width l may be eliminated between these two equations to give $v_i^2 = \eta v_{Ai}/L$, or in dimensionless form

$$M_i = \frac{1}{R_m^{1/2}} \quad (3.46)$$

in terms of the Alfven Mach number

$$M = \frac{v}{v_A} \quad (3.47)$$

and the magnetic Reynolds number

$$R_m = \frac{L v_A}{\eta} \quad (3.48)$$

based on the Alfven speed.

Now, let us consider the energetics of this model. Because $l \ll L$ then $v_i \ll v_{Ai}$. The rate of inflow of electromagnetic energy is the Poynting flux $\mathbf{E} \times \mathbf{H}$ per unit area, or, since $E = v_i B_i$ in magnitude,

$$EHL = E \frac{B_i}{\mu} L = v_i \frac{B_i^2}{\mu} L. \quad (3.49)$$

Therefore by Eq. 3.47 the ratio of the inflow of kinetic to electromagnetic energy is

$$\frac{Inflow K.E.}{Inflow E.M.} = \frac{v_i 1/2 \rho v_i^2 L}{v_i L B_i^2 / \mu} = \frac{1/2 \rho v_i^2}{B_i^2 / \mu} = \frac{v_i^2}{2 v_{Ai}^2} \ll 1. \quad (3.50)$$

In other words, most of the inflowing energy is magnetic. Next consider the energy outflow. By conservation of flux

$$v_0 B_0 = v_i B_i, \quad (3.51)$$

(which is consistent with Eq. 3.42 and 3.45) and so $B_0 \ll B_i$. Outflow of electromagnetic energy is $EB_0 l/\mu$, which is much less than the inflow of electromagnetic energy since both $B_0 \ll B_i$ and $l \ll L$. So what has happened to the inflowing magnetic energy? The ratio of outflowing kinetic to inflowing magnetic energy is

$$\frac{\text{outflow } K.E.}{\text{inflow } E.M.} = \frac{1/2 \rho v_0^2 (v_0 l)}{v_i B_i^2 L / \mu} = \frac{1/2 v_0^2}{v_{Ai}^2} = \frac{1}{2}. \quad (3.52)$$

Thus half of the inflowing magnetic energy is converted to kinetic energy, while the remaining half is converted to thermal energy. In other words, the effect of the reconnection is to create hot fast streams of plasma. In this connection it is useful to remember, that by substituting for $\nabla \times \mathbf{H}$ from Ampere law and for $\nabla \times \mathbf{E}$ from Faraday law, we can write

$$-\nabla \cdot (\mathbf{E} \times \mathbf{H}) = \mathbf{E} \cdot \nabla \times \mathbf{H} - \mathbf{H} \cdot \nabla \times \mathbf{E} \quad (3.53)$$

$$-\nabla \cdot (\mathbf{E} \times \mathbf{H}) = \mathbf{E} \cdot \mathbf{j} + \frac{\partial}{\partial t} \left(\frac{B^2}{2\mu} \right), \quad (3.54)$$

which implies that an inflow of electromagnetic energy can produce electrical energy ($\mathbf{E} \cdot \mathbf{j}$) for the plasma and a rise in the magnetic energy. Furthermore, by taking the scalar product of \mathbf{j} with Ohm law $\mathbf{E} = \mathbf{j}/\sigma - \mathbf{v} \times \mathbf{B}$, we obtain

$$\mathbf{E} \cdot \mathbf{j} = \frac{j^2}{\sigma} + \mathbf{v} \cdot \mathbf{j} \times \mathbf{B}, \quad (3.55)$$

so that the electrical energy appears partly as ohmic heat and partly as the work done by the Lorentz force (accelerating plasma). In our case the inflow of electromagnetic energy goes into electrical energy, half of which appears as heat and half as kinetic energy.

There is also fast regime of the Sweet-Parker reconnection (see Fig. 3.11). The flow speed and magnetic field at large distances L_e from X-point are denoted by v_e and B_e . The properties of reconnection models depend on two dimensionless parameters: the reconnection rate ($M_e = v_e/v_{Ae}$) and global magnetic Reynolds number ($R_{me} = L_e v_{Ae}/\eta$).

Reconnection is "fast" when the reconnection rate (M_e) is much greater than the rate expressed in Eq. (3.46). Properties at the inflow to the diffusion to the diffusion region (denoted by "i") may be related to the external values at large distances (denoted by "e"). Thus flux conservation ($v_i B_i = v_e B_e$, through the same length, a part of flux is going out of diffusion region) may be written as

$$\frac{M_i}{M_e} = \frac{B_e^2}{B_i^2}. \quad (3.56)$$

Then the relations (3.44) and (3.45) may be rewritten into

$$\frac{L}{L_e} = \frac{1}{R_{me}} \frac{1}{M_i^{3/2}} \frac{1}{M_e^{1/2}}, \quad (3.57)$$

$$\frac{l}{L_e} = \frac{1}{R_{me}} \frac{1}{M_e^{1/2}} \frac{1}{M_i^{1/2}}. \quad (3.58)$$

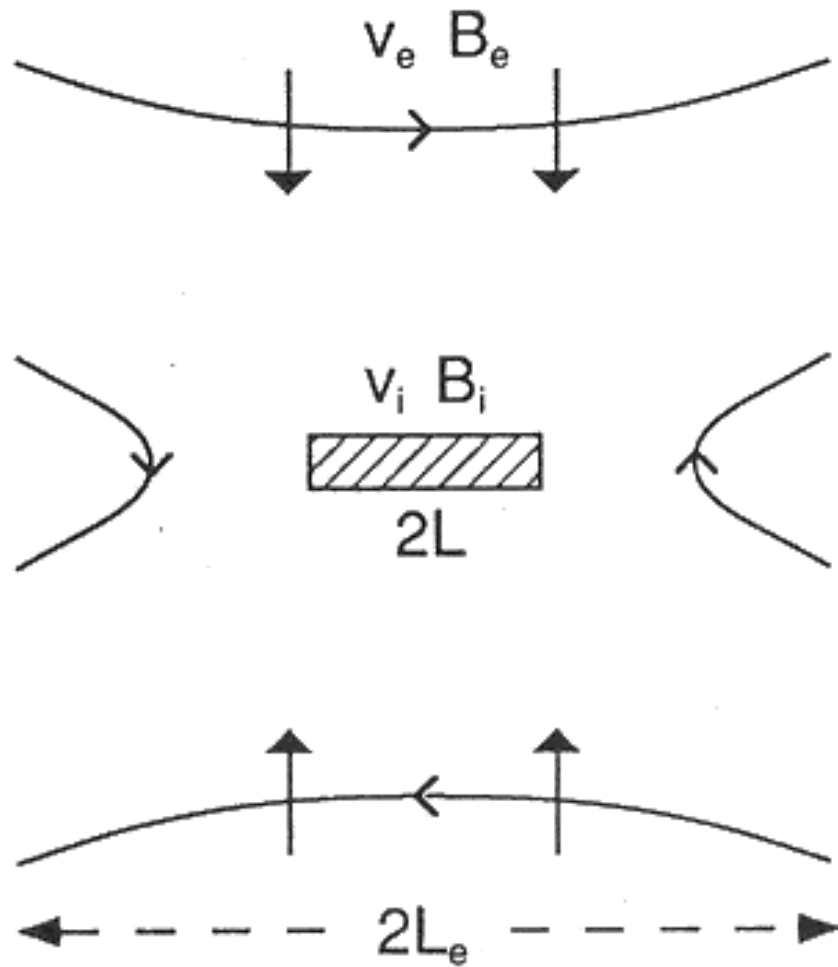


Fig. 3.11: The notation for fast regimes.

Thus, once B_i/B_e is determined from a model of the external region outside the diffusion region last three equations determine M_i/M_e and the dimensions of the diffusion region in terms of M_e and R_{me} .

c) Petschek model

In this model, most of the energy conversion takes place at standing slow-mode shocks (Fig. 3.12). These shocks accelerate and heat the plasma, with $2/5$ of the inflowing magnetic energy being changed to heat and $3/5$ to kinetic energy.

The inflow region consists of slightly curved field lines and the magnetic field is a uniform horizontal field ($B_e \mathbf{x}$), plus a solution of Laplace equation which vanishes at large distances and which has a normal component B_N at the shock waves and zero at the diffusion region. To lowest order, the inclination of the shocks may be neglected, and so the problem is to find a solution in the upper half-plane which vanishes at infinity and which equals $2B_N$ between L and L_e on the x -axis and, by symmetry $-2B_N$ between $-L_e$ and $-L$. Now, we may regard the normal component on the x -axis as being produced by a continuous series of poles. If each pole produces a field m/r at distance r , then the flux produced in the upper half plane by that pole will be πm : if the pole occupies a distance dx of the x -axis, the flux is also $2B_N dx$, so that $m = 2B_N/\pi$ and integrating along the x -axis gives the field at the **origin** produced by the poles

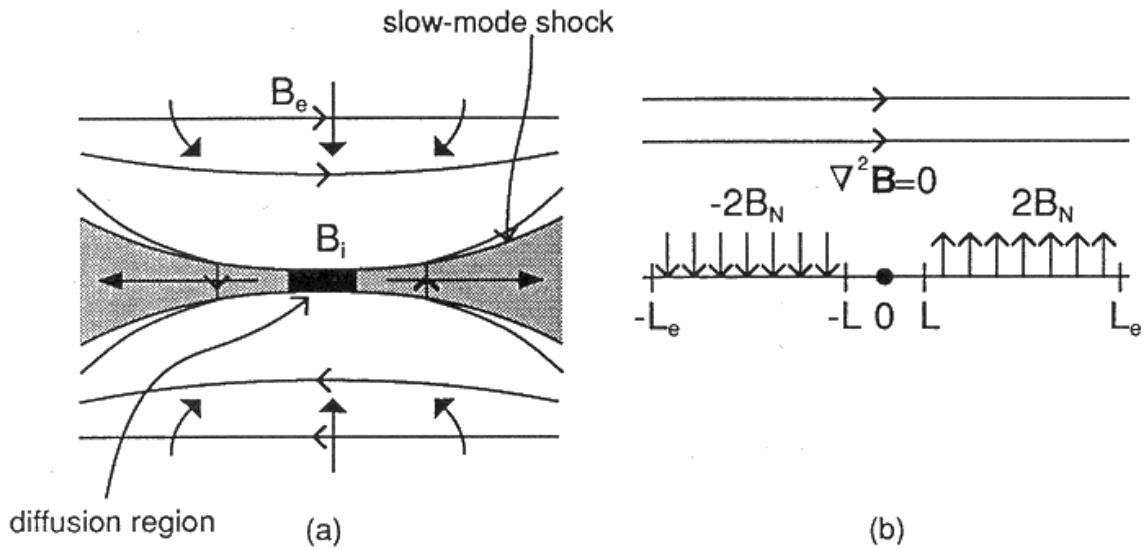


Fig. 3.12: (a) Petschek model, (b) notation for the inflow region.

as

$$\frac{1}{\pi} \int_{-L_e}^{-L} \frac{2B_N}{x} dx - \frac{1}{\pi} \int_L^{L_e} \frac{2B_N}{x} dx. \quad (3.59)$$

Adding this to the uniform field (B_e) at infinity gives

$$B_i = B_e - \frac{4B_N}{\pi} \log \frac{L_e}{L}. \quad (3.60)$$

But at the shock waves (slow shocks travel at the Alfvén speed based on the normal field, $B_N/\sqrt{\mu\rho}$), so that (3.60) becomes

$$B_i = B_e \left(1 - \frac{4M_e}{\pi} \log \frac{L_e}{L} \right), \quad (3.61)$$

which is the expression for B_i that we have been seeking.

Since $M_e \ll 1$ and $B_i \approx B_e$, the scalings (3.57) and (3.58) become

$$\frac{L}{L_e} \approx \frac{1}{R_{me} M_e^2}, \quad \frac{l}{L_e} \approx \frac{1}{R_{me} M_e}, \quad (3.62)$$

which show that the dimensions of the central region decrease as the magnetic Reynolds number (R_{me}) or reconnection rate (M_e) increase. Petschek suggests that the mechanism chokes itself off when B_i becomes too small, and so he estimates a maximum reconnection rate (M_e^*) by putting $B_i = 1/2 B_e$ in (3.61) to give

$$\frac{1}{2} = \frac{4M_e}{\pi} \log \frac{L_e}{L}, \quad \frac{L_e}{L} \approx R_{me}, \quad (3.63)$$

$$M_e^* \approx \frac{\pi}{8 \log R_{me}}. \quad (3.64)$$

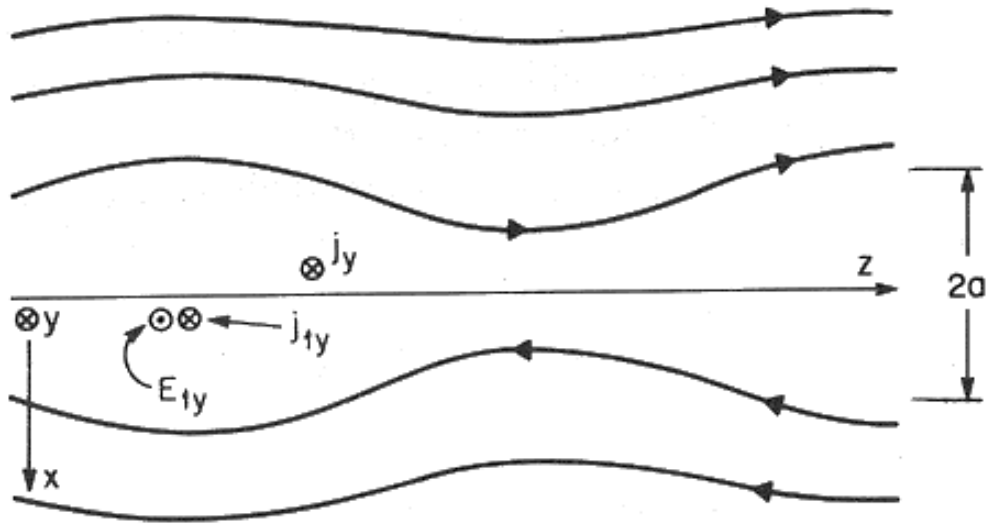


Fig. 3.13: Coordinate system used in the derivation of the tearing-mode instability condition for a sheet current.

Unsteady reconnection: tearing mode

Let us consider instability in the sufficiently long current sheet (Fig. 3.13); \mathbf{J}_1 and \mathbf{B}_1 are perturbations. This type of instability is that with finite resistivity, so Ohm law may be written as

$$\mathbf{E}_1 + \mathbf{v}_1 \times \mathbf{B}_0 - \eta_e \mathbf{J}_1 = 0. \quad (3.65)$$

We can see that the effect of finite resistivity becomes important at the neutral layers at $x \sim 0$, where the z -directed magnetic field $B_0 \sim 0$. On the other hand, at distances sufficiently far from the neutral layer, the $\mathbf{v} \times \mathbf{B}$ term can dominate, and the plasma can be regarded as lossless. Thus, the current sheet can be divided into two regions:

a) In the first region $|x| < \epsilon$ the diffusion equation is valid

$$\frac{\partial \mathbf{B}_1}{\partial t} = \frac{\eta_e}{\mu} \nabla^2 \mathbf{B}_1. \quad (3.66)$$

If the solution in the form $B_{1x} \sim \exp(ikz + \gamma t)$ is assumed then the equation may be rewritten into

$$\frac{d^2 B_{1x}}{dx^2} - \left(k^2 + \frac{\gamma \mu}{\eta_e} \right) B_{1x} = 0, \quad (3.67)$$

where

$$B_{1x} \sim A \cosh \left(k^2 + \frac{\gamma \mu}{\eta_e} \right)^{1/2} x. \quad (3.68)$$

is the solution of this equation.

b) Similarly in the lossless region $a > |x| > \epsilon$ this equation has a form

$$\frac{d^2 B_{1x}}{dx^2} + \left(\frac{1}{\lambda^2} - k^2 \right) B_{1x} = 0, \quad (3.69)$$

which solution can be expressed as

$$B_{1x} = C \sin \left(\frac{1}{\lambda^2} - k^2 \right)^{1/2} x. \quad (3.70)$$

If we now connect the solutions from both these regions at $x = \epsilon$, then we can derive the growth rate as

$$\gamma = \frac{\eta_e}{\mu \epsilon^2}. \quad (3.71)$$

Namely, for small x

$$\cosh x \approx 1 + x, \quad \sin x \approx x, \quad (3.72)$$

$$1 + \left(k^2 + \frac{\gamma \mu}{\eta_e} \right)^{1/2} \epsilon = \left(\frac{1}{\lambda^2} - k^2 \right)^{1/2} \epsilon \approx 0, \quad k \rightarrow 0. \quad (3.73)$$

Reference:

Hasegawa, A.: 1975, Plasma instabilities and non-linear effects, Springer-Verlag, Berlin.

Reconnection in three dimensions

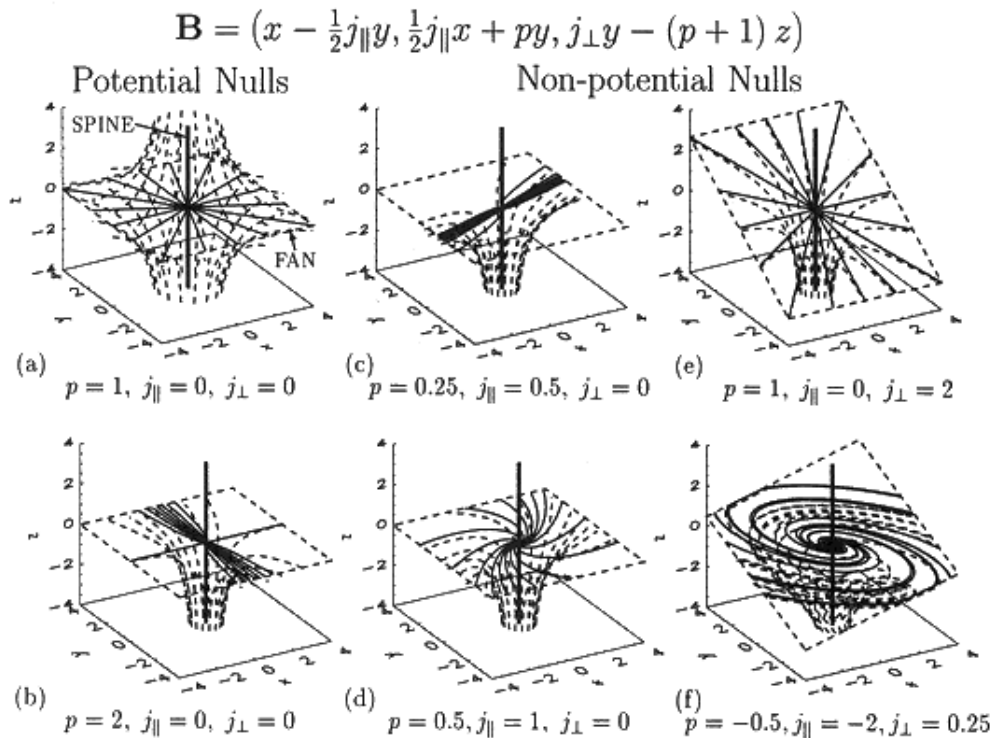


Fig. 3.14: Linear three-dimensional nulls. Potential nulls: (a) radial and (b) improper. Non-potential nulls: (c) improper and (d) spiral, both with only parallel current; (e) radial and (f) spiral, both with perpendicular current.

Reconnection in three dimension differs essentially from that of in two dimensions. For a 3-D neutral point, the structure consists of two main features (Fig. 3.14a): a *spine* and *fan* surface.

The spine is made up of two field lines that are directed into (or out of) the null. The fan consists of a surface of field lines that are pointing away from (or into) the null. Other flux surfaces in the vicinity of the null consist of field lines that run almost parallel to the spine before spreading out below the fan plane. In a positive null the field along the spine is directed into the null and the fan field lines spread out from the null; similarly, a negative null has field lines pointing towards the null in the fan and directed out along the spine.

The structure of any null is defined by four parameters $(p, q, j_{\parallel}, j_{\perp})$; the current is equal to

$$\mathbf{j} = (j_{\perp}, 0, j_{\parallel}), \quad (3.74)$$

so the parameters j_{\parallel} and j_{\perp} represent components of current parallel and perpendicular to the spine, respectively, while p and q are associated with the potential part of the field. We define j_{thresh} , called the threshold current, to be equal to

$$j_{thresh} = \sqrt{(p-1)^2 + q^2}. \quad (3.75)$$

To investigate the different types of 3-D null points we first consider potential null points, which have a general form

$$\mathbf{B} = (x, py, -(p+1)z). \quad (3.76)$$

They can either be radial ($p = 1$) or improper nulls ($p > 0$ and $p \neq 0$) (see Fig. 3.14a and Fig. 3.14b).

Non-potential nulls, however, have the form

$$\mathbf{B} = (x + (q - j_{\parallel})y/2, (q + j_{\parallel})x/2 + py, j_{\perp}y - (p+1)z). \quad (3.77)$$

These nulls may be divided into two categories: those that only have current parallel to the spine and those that have a component of current perpendicular to the spine. For example, two types of null with only parallel current are illustrated in (Fig. 3.14c and Fig. 3.14d); an improper null where $j_{\parallel} < j_{thresh}$ and a spiral null where $j_{\parallel} > j_{thresh}$, respectively. Two examples of nulls with the perpendicular current are radial null ($j_{\parallel} = 0$) and a spiral null ($j_{\parallel} > j_{thresh}$) (Fig. 3.14e and Fig. 3.14f).

Reference:

Parnell, C.E.: 1996, Proceedings of YOHKOH Conference, Bath, England, p. 19.

Kinetic reconnection

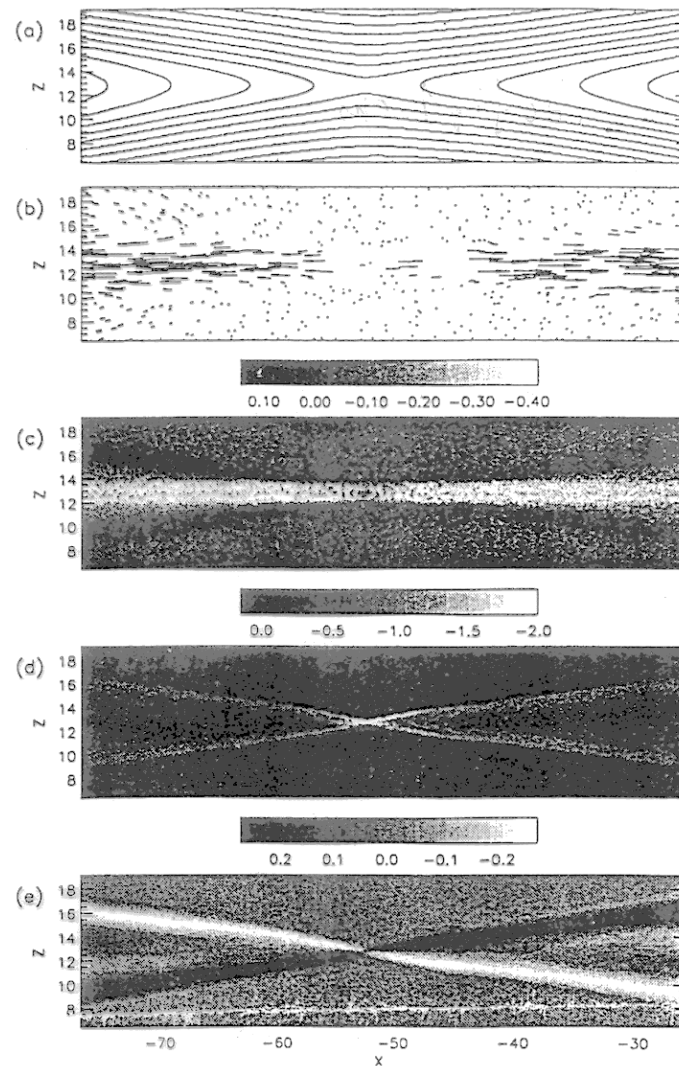


Fig. 3.15: Structure of the x-line: (a) in-plane magnetic field, (b) in-plane velocity, (c) out-of-plane ion current, (d) out-of-plane electron current, out-of-plane magnetic field.

There are attempts to simulate the magnetic reconnection not only in the MHD approximation, but in a more general kinetic approach. In Fig. 3.15 the results of the hybrid modelling with 2048×512 grid points and 20 million particles are shown. Here, differences between electron and ion currents can be seen, which it is not possible to simulate in the MHD models.

Reference:

Shay, M.A., Drake, J.F, Rogers, B.N., Denton, R.E.: 1999, *Geophys. Research Letters*, Vol. 26 (14), 2163.

Connectivity and quasi-separatrix layers

As seen in Fig. 3.16 magnetic field lines form domains in which they connect the photosphere.

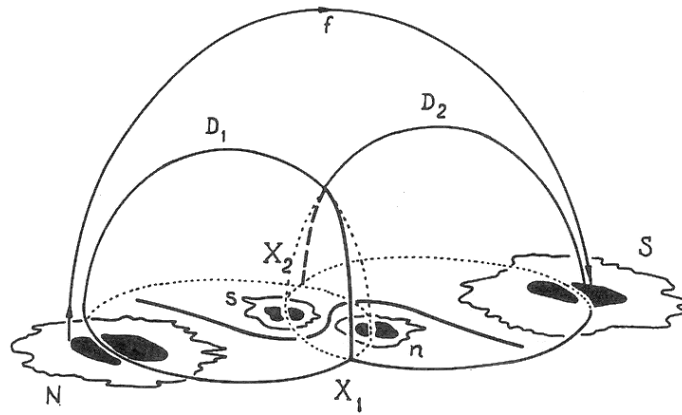


Fig. 3.16: The model of the magnetic field of four sunspots of pairwise opposite polarity. The boundary surfaces D_1 and D_2 cross in the corona at a topologically singular magnetic field line, the separator, which connects the points X_1 and X_2 in the photosphere. The contour f is an example of a field line connecting the distant sunspots N and S .

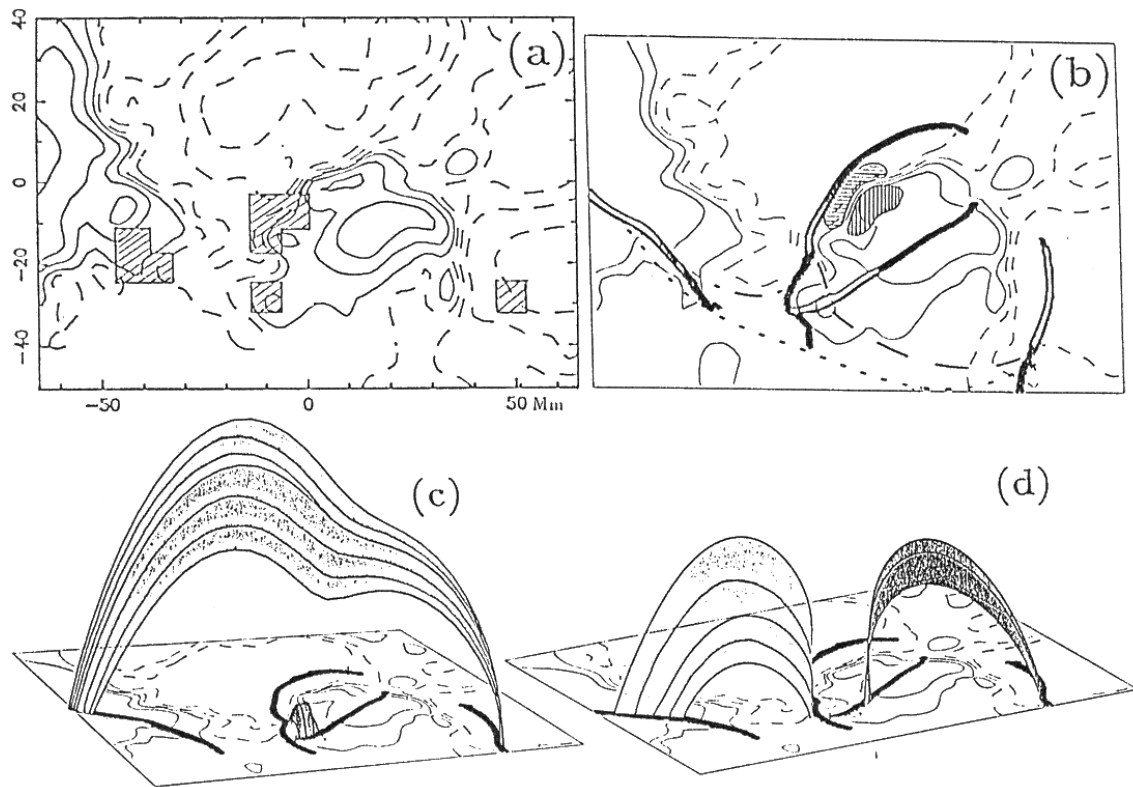


Fig. 3.17: Flaring AR 2779 on November 12, 1980: example of quadrupolar region formed by two extended bipoles. (a) Observational data: hatched regions - $H\alpha$ flare kernels and longitudinal magnetic field. (b) Intersection of the QSLs with the photosphere for a linear force-free extrapolation ($\alpha = -0.019 \text{ Mm}^{-1}$) with field lines and current-density regions. (c,d) Perspective views of (b), with field lines drawn as surfaces.

These domains are separated by separatrices, which can cross in the separators. The separator can be formed by null magnetic field line. If there is non-zero component of the magnetic field along these separatrices then it is useful to define so called quasi-separatrix layers (QSL). These

QSL are regions where a drastic change in field-line connectivity occurs, i.e. where field lines initially close separate widely over a short distance. Let us integrate over a distance s in both directions the field line passing at a point $P(x, y, z)$ of the corona. The end points of coordinates (x', y', z') and (x'', y'', z'') define a vector $D(x, y, z) = X_1, X_2, X_3 = x'' - x', y'' - y', z'' - z'$. A drastic change in field-line connectivity means that for a slight shift of the point $P(x, y, z)$, $D(x, y, z)$ varies greatly.

The function N , defined by

$$N(x, y) = \sqrt{\sum_{i=1,2} \left(\left(\frac{\partial X_i}{\partial x} \right)^2 + \left(\frac{\partial X_i}{\partial y} \right)^2 \right)}, \quad (3.78)$$

$N(x, y)$ is defined only at the photospheric boundary and is the norm of the displacement gradient tensor defined when mapping, by field lines, points from one section to another of the photosphere. The locations where $N(x, y)$ takes its highest values define the field lines involved in the QSLs. By following these lines we can locate the coronal portion of the QSLs - see Fig. 3.17.

Reference:

Demoulin, P., Bagala, L.G., Mandrini, C.H., Henoux, J.C., Rovira, M.G.: 1997, *Astron. Astrophys.* 325, 305-317.

Triggering of reconnection by a passage of the shock wave through the current sheet

See file `trigger.pdf`

Reference:

Odstrčil, D., Karlický, M.: 1997, Triggering of magnetic reconnection in the current sheet by shock waves, *Astron. Astrophys.* 326, 1252-1258.

Shear magnetic field reconnection near the the 3-D null point

Numerical Model

Computations are performed in the 3-D numerical box with $41 \times 41 \times 41$ grid points ($800 \times 800 \times 800$ km). The numerical code which solves the set of MHD equations is based on the FCT algorithm.

In the initial state the magnetic configuration corresponding to the 3-D null point is generated (Fig. 3.18).

$$\mathbf{B}(G) = \left(\frac{x - x_0}{x_{00}}, \frac{y - y_0}{y_{00}}, -\frac{2(z - z_0)}{z_{00}} \right), \quad (3.79)$$

where $x_0 = 4 \times 10^5$ m, $x_{00} = 4 \times 10^4$ m, $y_0 = 4 \times 10^5$ m and $z_{00} = 4 \times 10^4$ m. The layer near the plane $Z = 1$ is called the fan, and the central vertical line in the structure is called the spine.

The initial temperature of 10^6 K and the plasma density of 10^{-8} kg m $^{-3}$ is put constant through the system (coronal conditions). The plasma parameter β is thus everywhere $\beta \gg 1$.

The shear plasma flow which continuously deforms the initial magnetic field lines is used in the following form:

$$\mathbf{v} = v_0 \tanh \left(\frac{z - z_0}{z_v} \right), \quad (3.80)$$

where $v_0 = -10^5 \text{ m s}^{-1}$, $z_0 = 4 \times 10^5$ and $z_v = 10^5$ m. Free boundaries around the computational box are considered.

For a modelling of reconnections the anomalous resistivity was assumed in the $X - Y$ layer between 320 and 480 km, and its value was chosen to be $\eta_e = 2 \times 10^{-6}$ s.

Results

We made two types of computations: with and without the anomalous resistivity at the fan layer. Namely, at this layer where the electric current density is increasing during the shear plasma flow the anomalous resistivity can be naturally generated. The case without this resistivity is considered for comparison.

First, the current density in the central box point for both cases are compared (Fig. 3.19). While in the case without the resistivity the current density is linearly increasing as expected from theoretical estimations, in the case with the resistivity the current density increases more slowly up to the saturated value corresponding to the steady-state of reconnection.

The results of computations are shown in Figs 3.20 and 3.21. Figure 3.20 shows a deformation of magnetic field lines due to the shear plasma flow without taking into account the resistivity; on the other hand Figure 3.21 shows this deformation simultaneously with the flipping of lines due to the anomalous resistivity. Comparing the magnetic field lines in these figures we can see that the magnetic field lines reconnect in the fan layer. Thus, the magnetic field lines from one side of the fan connect magnetic lines on the opposite side and crossing the plane $Z = 1$. Simultaneously, their connections in the fan layer are changed over a broad range of angles: the maximum is near the spine (180°); this angle is decreasing with the distance increase from the spine.

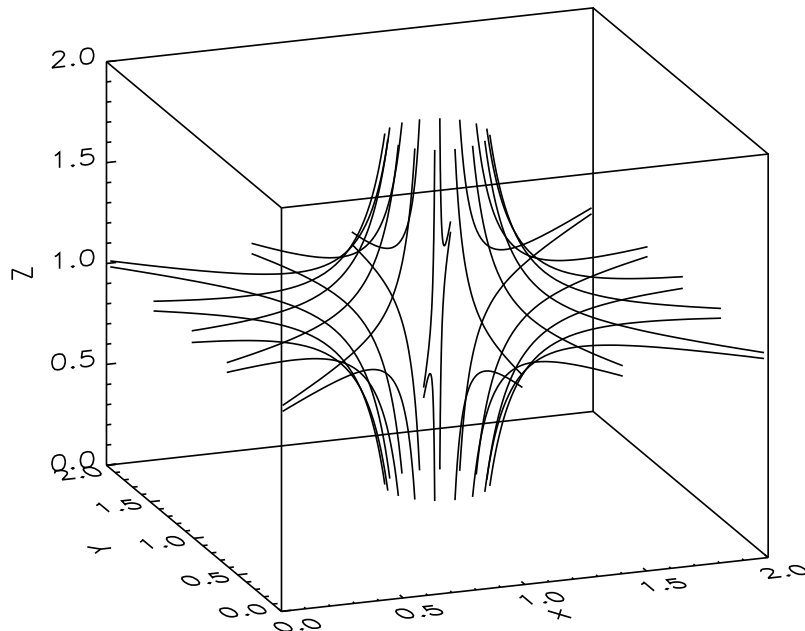


Fig. 3.18: The initial state of the magnetic field configuration.

Reference

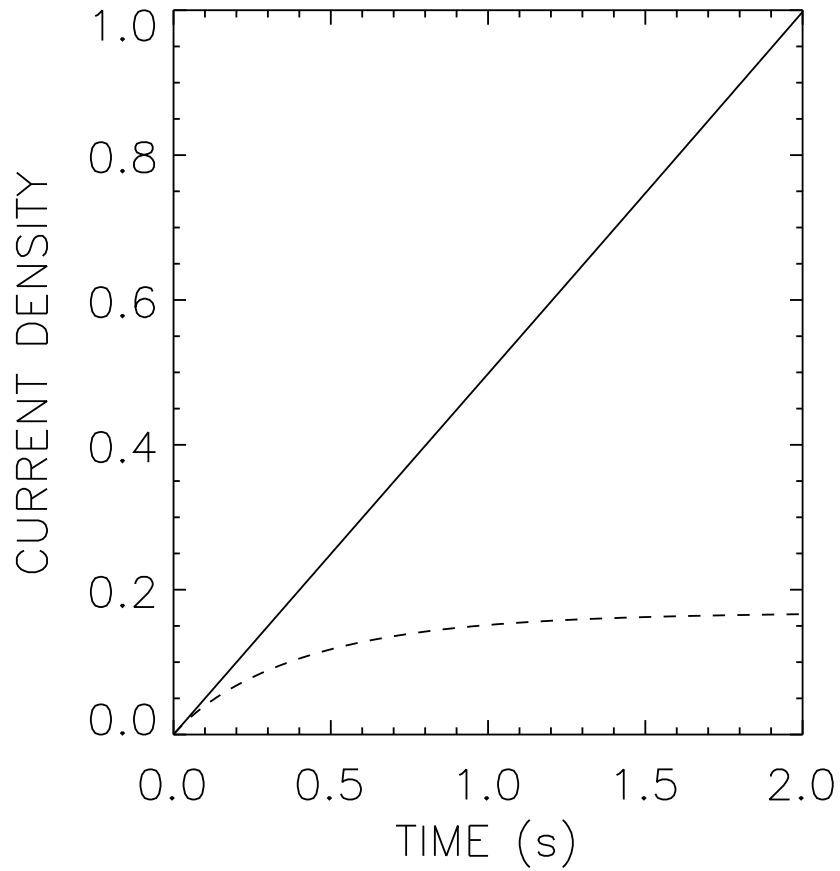


Fig. 3.19: Evolution of the normalized electric current density at the central box point for the case without (full line) and with (dashed line) the anomalous resistivity in the fan layer.

Karlický, M.: 1997, Shear magnetic field reconnection near the 3-D null point, *Hvar Obs. Bull.* 21, 1, 91-96.

Priest, E., Forbes, T.: 2000, *Magnetic reconnection: MHD theory and applications*, Cambridge University Press, Cambridge, UK.

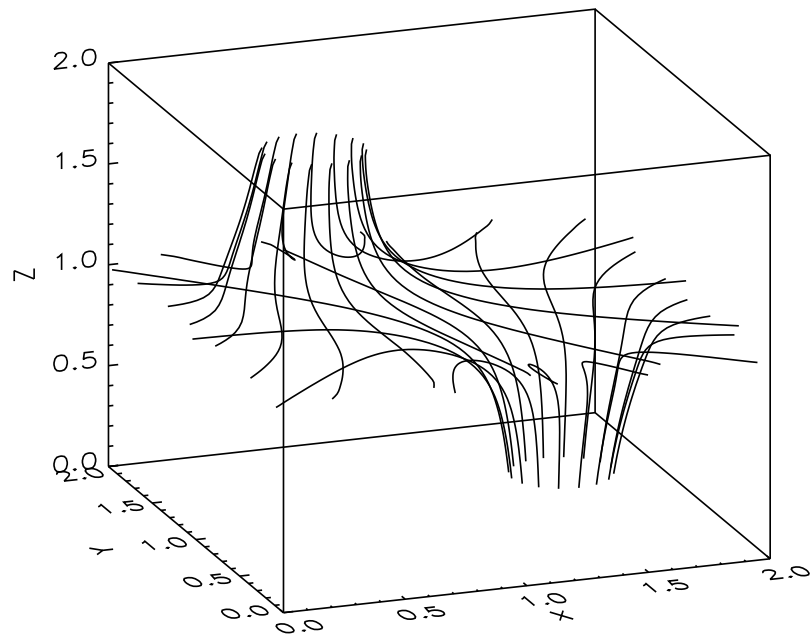


Fig. 3.20: Magnetic field lines at 2 s for the case without the anomalous resistivity. X,Y, and Z scale units are 400km.

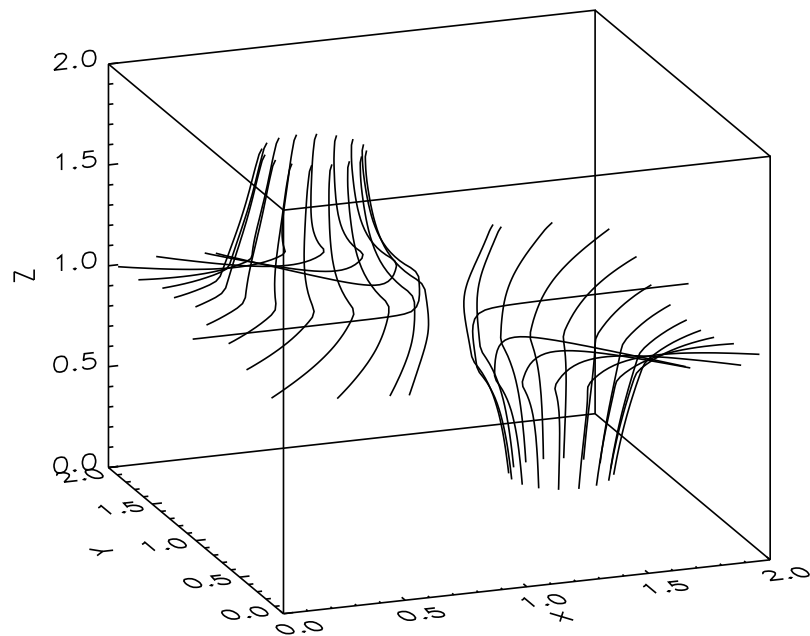


Fig. 3.21: Magnetic field lines at 2 s for the case with the anomalous resistivity. X,Y, and Z scale units are 400km.

Chapter 4

Helicity

An evolution of some energy integrals of physical systems is commonly used for a system description. In the solar corona for a description of e.g. flares or prominences we can use the volume integral of the magnetic field energy:

$$E_{mag} = \int_V \frac{B^2}{2\mu_0} dV. \quad (4.1)$$

A disadvantage of this approach is that the coronal magnetic field consists of a strong component of the potential magnetic field which is produced by sub-photospheric electric currents. This part of magnetic energy remains constant during active processes in the solar atmosphere. On the other hand, only a small part of the magnetic field energy, corresponding to electric currents in the solar atmosphere, can be transformed into other energy forms and can be dissipated. For these reasons an another volume integral, called helicity, was proposed for a physical description of these phenomena

$$H = \int_V \mathbf{A} \cdot \mathbf{B} dV, \quad (4.2)$$

where

$$\mathbf{B} = \nabla \times \mathbf{A},$$

where \mathbf{A} is the vector potential.

It can be shown that the helicity is directly connected with twists and linkings of magnetic field lines, which simultaneously expresses electric currents in the system. Thus, the helicity describes a part of the magnetic field energy which can be released during solar flares, and therefore the helicity is useful tool for active phenomena description.

Helicity conservation

Let us calculate a time change of the helicity:

$$\frac{\partial}{\partial t} \int \mathbf{A} \cdot \mathbf{B} dV = \int \mathbf{A} \cdot \frac{\partial \mathbf{B}}{\partial t} dV + \int \frac{\partial \mathbf{A}}{\partial t} \cdot \mathbf{B} dV.$$

Now, using the induction equation

$$\frac{\partial \mathbf{B}}{\partial t} = \nabla \times (\mathbf{v} \times \mathbf{B}),$$

$$\frac{\partial \nabla \times \mathbf{A}}{\partial t} = \nabla \times (\mathbf{v} \times \mathbf{B}),$$

$$\nabla \times \frac{\partial \mathbf{A}}{\partial t} = \nabla \times (\mathbf{v} \times \mathbf{B}),$$

$$\frac{\partial \mathbf{A}}{\partial t} = (\mathbf{v} \times \mathbf{B}) = -\mathbf{E},$$

(where the last equation expresses Ohm law) we can continue in the helicity conservation calculations

$$\int \mathbf{A} \cdot \frac{\partial}{\partial t} (\nabla \times \mathbf{A}) dV + \int \frac{\partial \mathbf{A}}{\partial t} \cdot \mathbf{B} dV = \int \mathbf{A} \cdot \nabla \times \frac{\partial \mathbf{A}}{\partial t} dV + \int \frac{\partial \mathbf{A}}{\partial t} \cdot \nabla \times \mathbf{A} dV. \quad (4.3)$$

The right side of this equation can be rewritten using the vector identity

$$\nabla \cdot (\mathbf{A} \times \frac{\partial \mathbf{A}}{\partial t}) = \frac{\partial \mathbf{A}}{\partial t} \cdot \nabla \times \mathbf{A} - \mathbf{A} \cdot \nabla \times \frac{\partial \mathbf{A}}{\partial t},$$

as

$$= - \int \nabla \cdot (\mathbf{A} \times \frac{\partial \mathbf{A}}{\partial t}) dV + \int 2 \frac{\partial \mathbf{A}}{\partial t} \cdot \nabla \times \mathbf{A} dV.$$

The last term is zero, because $\partial \mathbf{A} / \partial t = \mathbf{v} \times \mathbf{B}$ and $\nabla \times \mathbf{A} = \mathbf{B}$, and thus their scalar product is zero.

It means that for time change of helicity we can write

$$\frac{\partial}{\partial t} \int \mathbf{A} \cdot \mathbf{B} dV = - \int \nabla \cdot (\mathbf{A} \times \frac{\partial \mathbf{A}}{\partial t}) dV,$$

and using Gauss theorem

$$\frac{\partial}{\partial t} \int \mathbf{A} \cdot \mathbf{B} dV = - \int_S \mathbf{A} \times \frac{\partial \mathbf{A}}{\partial t} d\mathbf{S}. \quad (4.4)$$

Then, if $\partial \mathbf{A} / \partial t = -\mathbf{E} = 0$ at the system boundary then the helicity in the system is conserved.

Now, let us show that the helicity is invariant to a gauge transformation. Performing this transformation $\mathbf{A}' = \mathbf{A} + \nabla \chi$ (namely $\nabla \times \nabla \chi = 0$) we can write

$$H' - H = \int \nabla \chi \cdot \mathbf{B} dV,$$

and using

$$\nabla \cdot (\chi \mathbf{B}) = \nabla \chi \cdot \mathbf{B} + \chi \nabla \cdot \mathbf{B}, \quad \nabla \cdot \mathbf{B} = 0,$$

the helicity difference is

$$H' - H = \int \nabla (\chi \mathbf{B}) dV = \int_S \chi \mathbf{B} d\mathbf{S}, \quad (4.5)$$

which vanishes only if $B_n = 0$ at the system boundary, since χ is arbitrary. Thus, in infinite or closed system the helicity is conserved and it is gauge-invariant. But this general statement is

not very useful for practical purposes. Therefore other forms of the helicity integrals need to be constructed.

Let us define the so called relative helicity in a finite system as

$$\overline{H} = \int_V (\mathbf{A} + \mathbf{A}_0) \cdot (\mathbf{B} - \mathbf{B}_0) dV, \quad (4.6)$$

where \mathbf{A}_0 and \mathbf{B}_0 correspond to the potential magnetic field with the same boundary conditions as \mathbf{A} and \mathbf{B} .

Now, let us calculate the time derivative of this helicity: (The auxiliary relations are $\mathbf{E}_0 = 0$; $\nabla\chi_0 = 0$; $\partial\mathbf{A}_0/\partial t = 0$; $\partial\mathbf{B}_0/\partial t = 0$; $\partial\mathbf{A}/\partial t = -\mathbf{E} - \nabla\chi$; $\partial\mathbf{B}/\partial t = -\nabla \times \mathbf{E}$.)

$$\frac{\partial\overline{H}}{\partial t} = \int \left(\frac{\partial(\mathbf{A} + \mathbf{A}_0)}{\partial t} \cdot (\mathbf{B} - \mathbf{B}_0) + (\mathbf{A} + \mathbf{A}_0) \cdot \frac{\partial(\mathbf{B} - \mathbf{B}_0)}{\partial t} \right) dV,$$

$$\frac{\partial\overline{H}}{\partial t} = \int \left(\frac{\partial\mathbf{A}}{\partial t} \cdot (\mathbf{B} - \mathbf{B}_0) + (\mathbf{A} + \mathbf{A}_0) \cdot \frac{\partial\mathbf{B}}{\partial t} \right) dV,$$

$$\frac{\partial\overline{H}}{\partial t} = \int \left((-\mathbf{E} - \nabla\chi) \cdot (\mathbf{B} - \mathbf{B}_0) - (\mathbf{A} + \mathbf{A}_0) \cdot (\nabla \times \mathbf{E}) \right) dV,$$

$$\frac{\partial\overline{H}}{\partial t} = \int \left(-\mathbf{E} \cdot \mathbf{B} + \mathbf{E} \cdot \mathbf{B}_0 - \nabla\chi \cdot (\mathbf{B} - \mathbf{B}_0) - (\mathbf{A} + \mathbf{A}_0) \cdot (\nabla \times \mathbf{E}) \right) dV.$$

In the following the vector identity

$$\begin{aligned} \nabla \cdot (\chi(\mathbf{B} - \mathbf{B}_0) + \mathbf{E} \times (\mathbf{A} + \mathbf{A}_0)) = \\ \chi \nabla \cdot (\mathbf{B} - \mathbf{B}_0) + \nabla\chi \cdot (\mathbf{B} - \mathbf{B}_0) + (\mathbf{A} + \mathbf{A}_0) \cdot \nabla \times \mathbf{E} - \mathbf{E} \cdot \mathbf{B} - \mathbf{E} \cdot \mathbf{B}_0, \end{aligned} \quad (4.7)$$

where $\mathbf{E} \cdot \nabla \times \mathbf{A} = \mathbf{E} \cdot \mathbf{B}$, $\mathbf{E} \cdot \nabla \times \mathbf{A}_0 = \mathbf{E} \cdot \mathbf{B}_0$, $\nabla \cdot (\mathbf{B} - \mathbf{B}_0) = 0$, is used. After a manipulation and using Gauss theorem we can write

$$\frac{\partial\overline{H}}{\partial t} = -2 \int_V \mathbf{E} \cdot \mathbf{B} dV - \int_S (\chi(\mathbf{B} - \mathbf{B}_0) + \mathbf{E} \times (\mathbf{A} + \mathbf{A}_0)) d\mathbf{S}. \quad (4.8)$$

The first term on the right side of this relation expresses the Ohm dissipation as can be seen replacing the electric field as $\mathbf{E} = \mathbf{B} \times \mathbf{v} + \eta_e \mathbf{j}$, where \mathbf{j} is the electric current density. Thus the relative helicity is conserved in the spatially limited system when the Ohm dissipation is low (in coronal conditions it is usually fulfilled) and $\mathbf{B}_n = B_{0n}$; $\mathbf{E} = 0$.

If the Ohm dissipation is neglected and $\mathbf{A} = \mathbf{A}_0$ then the change of the relative helicity in the system is given by two term:

$$\begin{aligned} \frac{\partial\overline{H}}{\partial t} &= -2 \int_S \mathbf{A}_0 \times \mathbf{E} d\mathbf{S} = -2 \int_S \mathbf{A}_0 (\mathbf{B} \times \mathbf{v}) d\mathbf{S} = \\ &= -2 \int_S (\mathbf{A}_0 \cdot \mathbf{v}) \mathbf{B} d\mathbf{S} + 2 \int_S (\mathbf{A}_0 \cdot \mathbf{B}) \mathbf{v} d\mathbf{S}, \end{aligned} \quad (4.9)$$

the first term expresses a change of the relative helicity due to shearing motions at the system boundary and the second one represents a direct 'inflow' of the helicity.

In the solar physics studies there are attempts to evaluate the helicity change caused by photospheric shearing motions. For simplicity, let us assume that the photosphere is locally planar at the scale size of the active region. Then a change of the helicity can be written as

$$\frac{\partial \overline{H}}{\partial t} = 2 \int_S (\mathbf{A}_0 \cdot \mathbf{v}) B_n dS = \frac{1}{\pi} \int_S \int_{S'} \frac{\mathbf{R} \times \mathbf{v}(\mathbf{r})}{R^2} \Big|_n B_n(\mathbf{r}) B_n(\mathbf{r}') dS dS', \quad (4.10)$$

where $\mathbf{R} = \mathbf{r} - \mathbf{r}'$ is the difference between two spatial positions on the photospheric plane, and B_n is the magnetic field component perpendicular to the photosphere. This equation involves a double integration on the boundary. Since the integrations are done on the same surfaces, $S = S'$, we can exchange \mathbf{r} and \mathbf{r}' . This yields a new equation that summed up with previous equation gives:

$$2 \frac{\partial \overline{H}}{\partial t} = \frac{1}{\pi} \int_S \int_{S'} \frac{\mathbf{R} \times [\mathbf{v}(\mathbf{r}) - \mathbf{v}(\mathbf{r}')] }{R^2} \Big|_n B_n(\mathbf{r}) B_n(\mathbf{r}') dS dS'. \quad (4.11)$$

Let us define θ as the angle between \mathbf{R} and a fixed direction (e.g. the east-west direction) with trigonometric convection (counterclockwise), then:

$$\frac{d\theta}{dt} = \frac{\mathbf{R} \times d\mathbf{R}/dt}{R^2} \Big|_n \quad (4.12)$$

(with $d\mathbf{R}/dt = \mathbf{v}(\mathbf{r}) - \mathbf{v}(\mathbf{r}')$) the equation (4.11) is transformed to:

$$\frac{\partial \overline{H}}{\partial t} = \frac{1}{2\pi} \int_S \int_{S'} \frac{d\theta}{dt} B_n(\mathbf{r}) B_n(\mathbf{r}') dS dS'. \quad (4.13)$$

This equation shows that the helicity injection rate can be understood as the summation of the rotation rate of all the pairs of elementary fluxes weighted with their magnetic flux.

Chapter 5

Simple numerical schemes for a solution of MHD equations

Using a simple equation

$$\frac{\partial u}{\partial t} = -v \frac{\partial u}{\partial x} \quad (5.1)$$

as an example, let us show some numerical methods which may be used for a solution of general MHD equations. Namely, $\partial u/\partial t + v\partial u/\partial x \dots$ is a part of these equations. A numerical approximation of Eq. 5.1 may be

$$\frac{u_j^{n+1} - u_j^n}{\Delta t} = -v \frac{u_{j+1}^n - u_{j-1}^n}{2\Delta x}, \quad (5.2)$$

where Δt and Δx are the time step and grid step, respectively. Rearranging this equation we have

$$u_j^{n+1} = u_j^n - \frac{v\Delta t}{2\Delta x} (u_{j+1}^n - u_{j-1}^n). \quad (5.3)$$

Let u vary like $u_j^n \sim e^{i(kx_j - \omega n\Delta t)}$, where x_j is the j -th grid point coordinate $j\Delta x$. From Eq.5.3 we obtain

$$e^{i(kj\Delta x - \omega(n+1)\Delta t)} = e^{i(kj\Delta x - \omega n\Delta t)} - \frac{v\Delta t}{2\Delta x} \left(e^{i(k(j+1)\Delta x - \omega n\Delta t)} - e^{i(k(j-1)\Delta x - \omega n\Delta t)} \right), \quad (5.4)$$

and after dividing by $e^{i(kj\Delta x - \omega n\Delta t)}$

$$e^{-i\omega\Delta t} = 1 - \frac{v\Delta t}{2\Delta x} (e^{ik\Delta x} - e^{-ik\Delta x}). \quad (5.5)$$

The amplification factor $g \equiv u_j^{n+1}/u_j^n = e^{-i\omega\Delta t}$ is then according to the previous equation

$$g = 1 - i \frac{v\Delta t}{\Delta x} \sin(k\Delta x), \quad (5.6)$$

and its modulus

$$|g|^2 = 1 + \left(\frac{v\Delta t}{\Delta x} \right)^2 \sin^2(k\Delta x) > 1, \quad (5.7)$$

which shows that this scheme is always numerically unstable.

Lax scheme

In this approach we write Eq. 5.1 as

$$u_j^{n+1} = \frac{1}{2}(u_{j+1}^n + u_{j-1}^n) - \frac{v\Delta t}{2\Delta x}(u_{j+1}^n - u_{j-1}^n). \quad (5.8)$$

Then it can be rewritten into

$$e^{i(kj\Delta x - \omega(n+1)\Delta t)} = \frac{1}{2} \left(e^{i(k(j+1)\Delta x - \omega n\Delta t)} + e^{i(k(j-1)\Delta x - \omega n\Delta t)} \right) - \frac{v\Delta t}{2\Delta x} \left(e^{i(k(j+1)\Delta x - \omega n\Delta t)} - e^{i(k(j-1)\Delta x - \omega n\Delta t)} \right), \quad (5.9)$$

and after dividing by $e^{i(kj\Delta x - \omega n\Delta t)}$ the amplification factor is

$$g = \cos(k\Delta) - i \frac{v\Delta t}{\Delta x} \sin(k\Delta), \quad (5.10)$$

and its modulus is

$$|g|^2 = 1 - \sin^2(k\Delta) \left(1 - \left(\frac{v\Delta t}{\Delta x} \right)^2 \right). \quad (5.11)$$

The scheme is stable when $|g|^2 \leq 1$. This condition is fulfilled if

$$\Delta t \leq \Delta x/v. \quad (5.12)$$

Lax-Wendroff scheme

Let us consider a simple equation

$$\frac{\partial u}{\partial t} + \frac{\partial F}{\partial x} = 0, \quad (5.13)$$

where $F = uv$ (v is constant), as an example. The Lax-Wendroff scheme consists of two steps: The first one is according to Lax scheme over a half time step

$$u_j^{n+1/2} = 1/2(u_{j-1}^n + u_{j+1}^n) - \frac{\Delta t/2}{2\Delta x}(F_{j+1}^n - F_{j-1}^n), \quad (5.14)$$

and the second one over a full time step follows as

$$u_j^{n+1} = u_j^n - \frac{\Delta t}{2\Delta x}(F_{j+1}^{n+1/2} - F_{j-1}^{n+1/2}). \quad (5.15)$$

There are many further explicit as well as implicit schemes. The leap-frog scheme was described in details in the above mentioned particle code. Further important approach is so called "flux corrected transport method", which is successfully used in MHD tasks with shock waves.

Chapter 6

Plasma emission processes

In this chapter, only a general approach is presented. For more details and applications see:

Melrose, D.B.: 1980, Plasma Astrophysics, Gordon and Breach, New York.

6.1 Waves in plasmas

6.1.1 Wave equation

Due to many types of particle motions, in plasmas (especially in plasmas with the magnetic field) many types of waves can exist. This broad variety follows from a high complexity of the plasma response to electric or magnetic field perturbations. The electric (\mathbf{E}) and magnetic (\mathbf{B}) fields in plasmas are described by the system of Maxwell equations:

$$\begin{aligned}\nabla \times \mathbf{E} &= -\frac{\partial \mathbf{B}}{\partial t} & \nabla \cdot \mathbf{E} &= \frac{1}{\varepsilon_0} \rho \\ \nabla \times \mathbf{B} &= \mu_0 \mathbf{j} + \frac{1}{c^2} \frac{\partial \mathbf{E}}{\partial t} & \nabla \cdot \mathbf{B} &= 0\end{aligned}\tag{6.1}$$

where \mathbf{j} is the electric current density and ρ the charge density. These two quantities satisfy the charge continuity equation

$$\frac{\partial \rho}{\partial t} + \nabla \cdot \mathbf{j} = 0,\tag{6.2}$$

what implies from the set (6.1) as follows

$$\begin{aligned}\nabla \cdot \frac{\partial \mathbf{E}}{\partial t} &= \frac{1}{\varepsilon_0} \frac{\partial \rho}{\partial t}, \\ \nabla \cdot (c^2 \nabla \times \mathbf{B} - \mu_0 c^2 \mathbf{j}) &= \frac{1}{\varepsilon_0} \frac{\partial \rho}{\partial t}.\end{aligned}$$

Another useful equation is that for energy conservation, which can be derived as

$$\begin{aligned}\mathbf{B} \cdot \nabla \times \mathbf{E} + \mathbf{B} \cdot \frac{\partial \mathbf{B}}{\partial t} &= 0, \\ \mathbf{E} \cdot \nabla \times \mathbf{B} - \mu_0 \mathbf{E} \cdot \mathbf{j} - \frac{1}{c^2} \mathbf{E} \cdot \frac{\partial \mathbf{E}}{\partial t} &= 0.\end{aligned}$$

Using now the vector identity

$$\nabla \cdot (\mathbf{E} \times \mathbf{B}) = \mathbf{B} \cdot \nabla \times \mathbf{E} - \mathbf{E} \cdot \nabla \times \mathbf{B},$$

we can write

$$\frac{\partial}{\partial t} \left(\frac{|\mathbf{B}|^2}{2\mu_0} + \varepsilon_0 \frac{|\mathbf{E}|^2}{2} \right) + \nabla \cdot (\mathbf{E} \times \mathbf{H}) = -\mathbf{E} \cdot \mathbf{j}. \quad (6.3)$$

This equation expresses the conservation of electromagnetic energy; its change is due to Poynting vector flux $\mathbf{E} \times \mathbf{B}/\mu_0$ and Ohm dissipation $\mathbf{E} \cdot \mathbf{j}$.

For the purpose of formal theory of waves it is convenient to express Maxwell equations in natural basis of harmonic functions. Thus Fourier transforming the set (6.1) one obtains:

$$\mathbf{k} \times \mathbf{E} = \omega \mathbf{B} \quad (6.4)$$

$$\mathbf{k} \times \mathbf{B} = -i\mu_0 \mathbf{j} - \frac{\omega}{c^2} \cdot \mathbf{E} \quad (6.5)$$

$$\mathbf{k} \cdot \mathbf{E} = -\frac{i}{\varepsilon_0} \rho \quad (6.6)$$

$$\mathbf{k} \cdot \mathbf{B} = 0. \quad (6.7)$$

It is clear that the equation (6.7) is redundant since it follows directly from eq. (6.4), but with one exception – in the case of $\omega = 0$, i.e. in the case of static fields, the reduction of the system of equations does not apply. Thus, static fields have to be treated explicitly in further considerations. This is closely related to the well known problem of the fourth Maxwell equation ($\nabla \cdot \mathbf{B} = 0$), which should be considered as the initial condition rather than independent relation.

From the set of three remaining equations the general wave equation in the form

$$\mathbf{k} \times (\mathbf{k} \times \mathbf{E}(\mathbf{k}, \omega)) + \frac{\omega^2}{c^2} \mathbf{E}(\mathbf{k}, \omega) = -i\omega\mu_0 \mathbf{j}(\mathbf{k}, \omega) \quad (6.8)$$

can be derived, where equations (6.4) and

$$\omega \rho(\mathbf{k}, \omega) = \mathbf{k} \cdot \mathbf{j}(\mathbf{k}, \omega),$$

which is just the Fourier transform of continuity equation (6.2), should be considered as definitions of auxiliary quantities \mathbf{B} and ρ in terms of basic quantities \mathbf{E} and \mathbf{j} , respectively.

The current density \mathbf{j} at the right-hand side of the general wave equation can consist of two parts:

1. The current caused by induced motion of particles in plasmas under influence of electromagnetic field \mathbf{j}^{ind} .
2. The extraneous current \mathbf{j}^{ext} .

In the first approximation the induced part of the current is linearly related to electric field according to generalized Ohm's law (in usual tensor notation):

$$j_i^{ind}(\mathbf{k}, \omega) = \sigma_{ij}(\mathbf{k}, \omega) \cdot E_j(\mathbf{k}, \omega) \quad (6.9)$$

where $\sigma_{ij}(\mathbf{k}, \omega)$ is the generalized conductivity tensor and usual Einstein's summation law was applied. For the formal purposes it is much more convenient to use another tensor describing

the linear plasma response to electric field perturbation. The dielectric tensor $\varepsilon_{ij}(\mathbf{k}, \omega)$ is defined as:

$$\varepsilon_{ij}(\mathbf{k}, \omega) \equiv \delta_{ij} + \frac{i}{\omega\varepsilon_0} \cdot \sigma_{ij}(\mathbf{k}, \omega) \quad (6.10)$$

with δ_{ij} being the Kronecker delta (the unit tensor). Separating the current density into induced and extraneous parts and using Ohms law (6.9) and dielectric tensor definition (6.10) the wave equation (6.8) may be re-written into the form:

$$\begin{aligned} \left(\frac{c^2 \mathbf{k} \times (\mathbf{k} \times \mathbf{E})}{\omega^2} \right)_i + E_i + \frac{i}{\omega\varepsilon_0} j_i^{ind} &= -\frac{i}{\omega\varepsilon_0} j_i^{ext}, \\ \left(\frac{c^2 \mathbf{k} \times (\mathbf{k} \times \mathbf{E})}{\omega^2} \right)_i + (\delta_{ij} + \frac{i}{\omega\varepsilon_0} \sigma_{ij}) E_j &= -\frac{i}{\omega\varepsilon_0} j_i^{ext}, \\ \Lambda_{ij}(\mathbf{k}, \omega) \cdot E_j(\mathbf{k}, \omega) &= -\frac{i}{\omega\varepsilon_0} j_i^{ext}(\mathbf{k}, \omega) \end{aligned} \quad (6.11)$$

where the dispersion tensor $\Lambda_{ij}(\mathbf{k}, \omega)$ is defined as

$$\Lambda_{ij}(\mathbf{k}, \omega) \equiv \frac{k^2 c^2}{\omega^2} \left(\frac{k_i k_j}{k^2} - \delta_{ij} \right) + \varepsilon_{ij}(\mathbf{k}, \omega). \quad (6.12)$$

The equation (6.11) represents a set of three linear equations with components of the extraneous current density $\mathbf{j}^{ext}(\mathbf{k}, \omega)$ as explicit source terms.

Except of this explicit source term there is also an implicit one hidden in the dielectric tensor. The dielectric tensor can be separated into two parts – hermitian and anti-hermitian

$$\varepsilon_{ij} = \varepsilon_{ij}^h + \varepsilon_{ij}^a,$$

$$\varepsilon_{ij}^h = 1/2(\varepsilon_{ij} + \varepsilon_{ji}^*),$$

$$\varepsilon_{ij}^a = 1/2(\varepsilon_{ij} - \varepsilon_{ji}^*),$$

whose describe different kinds of plasma response to an electric field perturbation. While the hermitian part of $\varepsilon_{ij}(\mathbf{k}, \omega)$ describes time-reversible component of the response, the anti-hermitian part causes wave energy changes, either negative (damping of waves) or positive (amplification or by other words negative damping/negative absorption of waves).

6.1.2 The dispersion equation of linear waves

The question arises what is behaviour of the electric field perturbation in the case without dissipation and extraneous sources. One has to solve homogeneous form of the equation (6.11) in which also the implicit source term in the dielectric tensor (the anti-hermitian part) is omitted, i.e.

$$\Lambda_{ij}^h(\mathbf{k}, \omega) \cdot E_j(\mathbf{k}, \omega) = 0, \quad (6.13)$$

where $\Lambda_{ij}^h(\mathbf{k}, \omega)$ is the hermitian part of the dispersion tensor. Solution of such a system of equations exist only if the relation

$$\Lambda(\mathbf{k}, \omega) \equiv \det \Lambda_{ij}^h(\mathbf{k}, \omega) = 0 \quad (6.14)$$

is fulfilled. The condition (6.14) represents the general dispersion equation for linear non-damped waves in plasmas. To rewrite it to the usual form of the dispersion relation for a specific wave mode one has to express the frequency ω as a function of the wave vector \mathbf{k} . This is not unique operation in general, however, many branches of waves with different dispersion relations

$$\omega^m = \omega^m(\mathbf{k}) \quad (6.15)$$

can be obtained. Each branch $\omega^m(\mathbf{k})$ represents one wave mode m .

6.1.3 Polarisation vectors

Inserting relation (6.15) into the homogeneous equation (6.13) a solution for specific wave mode can be found. According to known rules of linear algebra the vector that solves (6.13) has to be the eigen-vector corresponding to the zero eigen-value of the tensor

$$\Lambda_{ij}^h(\mathbf{k}) = \Lambda_{ij}^h(\mathbf{k}, \omega^m(\mathbf{k})).$$

Namely, one eigen-value of the matrix representing a homogenous set of equations is zero. The corresponding eigen-vector is not determined uniquely since in the homogenous set of equations, with its determinant equals to zero, the number of linearly independent equations is less than the number of vector components. Therefore it is convenient to choose an unimodular complex vector $\mathbf{e}^m(\mathbf{k})$ as a representative of all solutions of the equation (6.13) for given wave mode. Such vector is called the polarisation vector and besides the dispersion relation (6.15) it is one of the basic characteristics of the specific wave mode. For example, from the polarization vector the magnetic and induced current vectors can be derived; using Eq. (6.4) and (6.9).

6.1.4 Energetics in the waves

The electric perturbation in plasma waves induces also the perturbation of magnetic field and, due to medium response, also variations of plasma velocity, stresses and pressure. All these perturbations raise the total amount of energy contained in plasmas and the difference over the equilibrium state can be ascribed to the waves. Thus, for the total wave energy of the mode m we can write

$$w_T^m(\mathbf{k}) = w_E^m(\mathbf{k}) + w_M^m(\mathbf{k}) + w_p^m(\mathbf{k}).$$

It is straightforward to compute the electric or magnetic field energy in waves knowing the electric field amplitude:

$$w_E^m(\mathbf{k}) = \frac{\varepsilon_0 |\mathbf{E}^m(\mathbf{k})|^2}{V}. \quad (6.16)$$

and using Eq. (6.4)

$$w_M^m(\mathbf{k}) = \left(\frac{kc}{\omega}\right)^2 (1 - |\frac{\mathbf{k}}{k} \cdot \mathbf{e}^m|^2) w_E^m.$$

On the other hand, mechanical energy connected with plasma motions and stresses is hard to be identified in general. Nevertheless, the total amount of energy contained in particular wave mode can be, fortunately, related to the electric field energy in this mode independently. The first is to include the anti-hermitian part of the dielectric tensor ε_{ij}^a as a small correction in the dispersion equation. To first order one can write

$$\det(\Lambda_{ij}^h + \varepsilon_{ij}^a) = \Lambda + \lambda_{ij} \varepsilon_{ji}^a. \quad (6.17)$$

Now damping of the waves is taken into account by allowing ω to have a small imaginary part $-i\gamma/2$, such that the wave energy damps as $e^{-\gamma t}$. Then, to lowest order in the terms associated with wave damping, Eq. (6.17) gives

$$-\frac{i\gamma}{2} \frac{\partial \Lambda}{\partial \omega} + \lambda_{ij} \varepsilon_{ji}^a = 0, \quad (6.18)$$

which is evaluated at $\Lambda = 0$. Similarly we can allow \mathbf{k} to have a small imaginary part $-i\mu/2$. Then Eq. (6.18) has a form:

$$-\frac{i\gamma}{2} \frac{\partial \Lambda}{\partial \omega} - \frac{i\mu}{2} \frac{\partial \Lambda}{\partial \mathbf{k}} = -\lambda_{ij} \varepsilon_{ji}^a. \quad (6.19)$$

On the other hand, for the energy w^m damped as $e^{-\gamma t}$ and the energy flux \mathbf{F}^m damped as $e^{-\mu r}$ we can write

$$\begin{aligned} \frac{\partial w^m}{\partial t} + \nabla \cdot \mathbf{F}^m &= Q^m, \\ \gamma w^m + \mu \mathbf{F}^m &= -Q^m, \end{aligned} \quad (6.20)$$

where Q^m is the source or damping wave term. Now, comparing Eqs. (6.19) and (6.20) one has

$$\frac{\mathbf{F}^m}{w^m} = \left(\frac{\partial \Lambda}{\partial \mathbf{k}} / \frac{\partial \Lambda}{\partial \omega} \right)_{\omega=\omega^m} = \frac{\partial w^m}{\partial \mathbf{k}} = \mathbf{v}_g^m.$$

The result implies that the velocity of energy propagation is the group velocity.

Moreover, the term

$$\gamma = -\frac{Q^m}{w^m} = -\frac{2i\lambda_{ij}\varepsilon_{ji}^a}{\left(\frac{\partial \Lambda}{\partial \omega}\right)_{\omega=\omega^m}} \quad (6.21)$$

is the absorption coefficient. Besides this relation there is a theoretical procedure in which the ratio between Q^m and w_E^m can be derived. Then by a comparison of these ratios the quantity $R_E^m = w_E^m/w^m$, expressing the ratio between the electric and total wave energies, can be determined.

6.1.5 Specific wave modes

As an illustration of determination of particular wave mode and its characteristics from the general dispersion equation (6.14) one may choose well known Langmuir, transverse and ion-sound waves in plasmas without ambient magnetic field. The first thing has to be done is calculation of the dielectric tensor. The kinetic approach gives for unmagnetized plasmas following result (Melrose, 1980, p. 40):

$$\varepsilon_{ij}(\mathbf{k}, \omega) = \delta_{ij} + \sum_{\alpha} \frac{q_{\alpha}^2}{\varepsilon_0 \omega^2} \int \frac{(\omega - \mathbf{k} \cdot \mathbf{v}) \delta_{sj} + k_s v_j}{\omega - \mathbf{k} \cdot \mathbf{v} + iO} \cdot v_i \cdot \frac{\partial f_{\alpha}(\mathbf{p})}{\partial p_s} d^3 \mathbf{p}, \quad (6.22)$$

the sum is performed over each particle species α and small imaginary part in the denominator indicates that correct integration path according to Landau prescription has to be used. For isotropic medium the dielectric tensor can be separated into longitudinal (ε^l) and transversal (ε^t) parts as:

$$\varepsilon_{ij}(\mathbf{k}, \omega) = \varepsilon^l(k, \omega) \cdot \frac{k_i k_j}{k^2} + \varepsilon^t(k, \omega) \left(\delta_{ij} - \frac{k_i k_j}{k^2} \right) \quad (6.23)$$

and explicit calculation for Maxwellian distribution function gives (Melrose, 1980, p. 50):

$$\begin{aligned}\varepsilon^l(k, \omega) &= 1 + \sum_{\alpha} \frac{1}{k^2 \lambda_{D\alpha}^2} \left[1 - \phi(y_{\alpha}) + i\sqrt{\pi} y_{\alpha} \exp(-y_{\alpha}^2) \right] \\ \varepsilon^t(k, \omega) &= 1 + \sum_{\alpha} \frac{\omega_{p\alpha}^2}{\omega^2} \left[-\phi(y_{\alpha}) + i\sqrt{\pi} y_{\alpha} \exp(-y_{\alpha}^2) \right].\end{aligned}\tag{6.24}$$

Here, $\omega_{p\alpha}$ and $\lambda_{D\alpha}$ are appropriate plasma frequencies and Debye lengths, respectively:

$$\omega_{p\alpha}^2 \equiv \frac{n_{\alpha} q_{\alpha}^2}{m_{\alpha} \varepsilon_0}, \quad \lambda_{D\alpha} \equiv \frac{V_{\alpha}}{\omega_{p\alpha}},\tag{6.25}$$

and the following dispersion function ($V_{\alpha} \equiv k_B T / m_{\alpha}$ designates thermal velocity of particles of species α) was used:

$$\begin{aligned}\phi(y) &\equiv 2y \exp(-y^2) \int_0^y \exp(t^2) dt, \quad y_{\alpha} \equiv \frac{\omega}{\sqrt{2k} V_{\alpha}}, \\ \phi(y) &= 2y^2 - 4/3y^4 + \dots \quad \text{for } |y^2| \ll 1, \\ \phi(y) &= 1 + 1/(2y^2) + 3/(4y^4) + \dots \quad \text{for } |y^2| \gg 1.\end{aligned}\tag{6.26}$$

Inserting the hermitian part of the dielectric tensor (i.e. retaining real parts of longitudinal and transversal components only) in the form of (6.23) into the equation (6.14) the dispersion equation

$$\left(\text{Re} \left\{ \varepsilon^l(k, \omega) \right\} \right) \cdot \left(n^2 - \text{Re} \left\{ \varepsilon^t(k, \omega) \right\} \right)^2 = 0\tag{6.27}$$

is obtained with the refractive index n defined as

$$n \equiv \frac{ck}{\omega}.$$

Now, expanding the function $\phi(y)$ into series for the high-frequency limit ($y \gg 1$) and retaining only first few terms of electronic contribution to this function (the contribution of ions is reduced by factor of m_e/m_i relatively to that of electrons) the transversal part of the equation (6.27) becomes

$$n^2 = 1 - \frac{\omega_{pe}^2}{\omega^2}$$

or using the refractive index definition, it can be written in more familiar form

$$\omega^2(k) = \omega_{pe}^2 + c^2 k^2.\tag{6.28}$$

The just derived equation (6.28) represents the dispersion equation for transversal (electromagnetic) mode. Additional relations for this mode are:

$$\mathbf{e} \cdot \frac{\mathbf{k}}{k} = 0, \quad R_E^t = \frac{1}{2},$$

expressing transverse character of this mode and the ratio between electric and total wave energy.

The longitudinal part of Eq. (6.27) gives two wave modes depending on the frequency limit used. For $\omega \gg kV_e$, i.e. $y_e \gg 1$ the expansion of the function ϕ yields dispersion equation

$$1 + \frac{1}{k^2 \lambda_{De}^2} \left(1 - 1 - \frac{1}{2} \frac{2k^2 V_e^2}{\omega^2} - \frac{3}{4} \frac{4k^4 V_e^4}{\omega^4} \right) = 0, \quad \omega_{pe}^2 = \frac{V_e^2}{\lambda_{De}^2}$$

$$\omega^2(k) = \omega_{pe}^2 + 3k^2 V_e^2, \quad \mathbf{e} = \frac{\mathbf{k}}{k}, \quad R_E^l = \frac{\omega^2}{2\omega_{pe}^2}, \quad (6.29)$$

which describes well known Langmuir waves.

On the other hand, expanding formulae for longitudinal part of the dielectric tensor in the limit

$$kV_i \ll \omega \ll kV_e$$

the ion-sound mode with the dispersion equation is

$$\begin{aligned} \text{Re } \varepsilon^l &\approx 1 - \frac{\omega_{pi}^2}{\omega^2} + \frac{1}{k^2 \lambda_{De}^2}, \\ \omega^2(k) &\approx \frac{k^2 c_s^2}{1 + k^2 \lambda_{De}^2}, \quad \mathbf{e} = \frac{\mathbf{k}}{k}, \quad R_E^s = \frac{\omega^2}{2\omega_{pi}^2}, \end{aligned} \quad (6.30)$$

is found. Here, the ion-sound wave speed c_s is defined by

$$c_s \equiv \omega_{pi} \cdot \lambda_{De}.$$

6.2 Spontaneous emission

If wave emission processes are taken into account then, in general case, the inhomogeneous wave equation

$$\Lambda_{ij}^h(\mathbf{k}, \omega) \cdot E_j(\mathbf{k}, \omega) = -\frac{i}{\omega \varepsilon_0} j_i^{ext}(\mathbf{k}, \omega) \quad (6.31)$$

with the source term, needs to be solved. Specifically, \mathbf{j}^{ext} is assumed to include the the term with the anti-hermitian part of the dielectric tensor

$$j_i^{ext}(\mathbf{k}, \omega) = -i\omega \varepsilon_0 \varepsilon_{ij}^a(\mathbf{k}, \omega) E_j(\mathbf{k}, \omega) + \dots, \quad (6.32)$$

which includes not only the normal absorption of waves, but in specific situations also negative absorption (amplification) of waves. But in the source term can be also further contributions.

Remark: Analyzing the equation of continuity for electromagnetic waves

$$\frac{\partial}{\partial t} \left(\frac{|\mathbf{B}|^2}{2\mu_0} + \frac{|\mathbf{E}|^2}{2\varepsilon_0} \right) + \nabla \cdot (\mathbf{E} \times \mathbf{H}) = -\mathbf{E} \cdot \mathbf{j}, \quad (6.33)$$

it is important to see a difference in methods used in calculation of power radiated in plasma and in vacuo. In the plasma this power is calculated as a volume integral of the work done by the extraneous current against the electric field which it generates (the right-hand side of Eq. (6.33)). In vacuo the power escaping is found by integrating the radial component of the Poynting vector $\mathbf{E} \times \mathbf{H}$ over the surface of an infinite sphere. In the plasma this method makes problem because in this case the Poynting vector does not give the total energy flux in the waves, in general.

6.2.1 Energy radiated by extraneous current

The extraneous current on the R.H. side of the expression (6.11) represents a source term in the wave equation. The wave energy U radiated (or absorbed) by this source is given by the work of the extraneous current against the consistent electric field of the wave, i.e.:

$$\begin{aligned} U &= - \int_{-\infty}^{+\infty} \int_V \mathbf{j}^{ext}(\mathbf{r}, t) \cdot \mathbf{E}(\mathbf{r}, t) \, d^3\mathbf{r} \, dt = \\ &= - \int_{-\infty}^{+\infty} \int \operatorname{Re} \left\{ \mathbf{j}^{ext}(\mathbf{k}, \omega) \cdot \mathbf{E}(\mathbf{k}, \omega) \right\} \frac{d^3\mathbf{k}}{(2\pi)^3} \frac{d\omega}{2\pi}, \end{aligned} \quad (6.34)$$

where the Parseval's power theorem was used. Solution of the wave equation (6.31) can be expressed as

$$E_i(\mathbf{k}, \omega) = - \frac{i}{\omega \varepsilon_0} \Lambda_{ik}^{-1}(\mathbf{k}, \omega) \cdot j_k^{ext}(\mathbf{k}, \omega), \quad (6.35)$$

where the matrix $\Lambda_{ik}^{-1}(\mathbf{k}, \omega)$ is the inversion operator to the dispersion tensor (6.12) and according to the tensor algebra rules it is written down using its co-factors (sub-determinants of transposed matrix) λ_{ik} as:

$$\Lambda_{ik}^{-1}(\mathbf{k}, \omega) = \frac{\lambda_{ik}(\mathbf{k}, \omega)}{\Lambda(\mathbf{k}, \omega)}.$$

Now, inserting the particular solution (6.35) into the formula (6.34), the wave energy generated by the extraneous current density \mathbf{j}^{ext} can be computed. Contributions to integral over ω are zero (because the integral is from the real part of apparently imaginary quantity) with exceptions of the poles of function in integrand. Such residues have to be treated carefully, and the integration has to be performed over the path in the complex plane according to Landau prescription, i.e. near the zeros we approximate Λ as

$$\Lambda(\mathbf{k}, \omega) \approx (\omega - \omega^m(\mathbf{k}) + i0) \left(\frac{\partial \Lambda}{\partial \omega} \right)_{\omega=\omega^m(\mathbf{k})}.$$

Each residue is connected with one zero of $\Lambda(\mathbf{k}, \omega)$, and thus each pole represents the energy radiated in one specific wave mode. Explicit calculation gives for energy radiated by extraneous current in wave mode m the expressions:

$$\begin{aligned} U &= -2 \int_0^{+\infty} \int \operatorname{Re} \left\{ j_i^{ext} \left(-\frac{i}{\omega \varepsilon_0} \right) j_k^{ext} \frac{\lambda_{ik}}{\Lambda} \right\} \frac{d^3\mathbf{k}}{(2\pi)^3} \frac{d\omega}{2\pi}, \\ U &= -2 \int_0^{\infty} \int \operatorname{Re} \left\{ j_i^{ext} \left(-\frac{i}{\omega \varepsilon_0} \right) j_k^{ext} \frac{\lambda_{ik}}{(\omega - \omega^m(\mathbf{k}) + i0) \left(\frac{\partial \Lambda}{\partial \omega} \right)_{\omega=\omega^m(\mathbf{k})}} \right\} \frac{d^3\mathbf{k}}{(2\pi)^3} \frac{d\omega}{2\pi}. \end{aligned}$$

Now using the Plemelj formula,

$$\frac{1}{\omega - \omega_0 \pm i0} = P \frac{1}{\omega - \omega_0} \mp i\pi \delta(\omega - \omega_0),$$

where P denotes the Cauchy principal value:

$$\begin{aligned} P \frac{1}{\omega} &= \lim_{\eta \rightarrow 0} \frac{1}{\omega} \quad \text{for } |\omega| > |\eta|, \\ P \frac{1}{\omega} &= \lim_{\eta \rightarrow 0} 0 \quad \text{for } |\omega| < |\eta|, \end{aligned}$$

we can write

$$U = -2 \int_0^\infty \int \operatorname{Re} \left\{ j_i^{ext} \left(-\frac{i}{\omega \varepsilon_0} \right) j_k^{ext} \frac{\lambda_{ik}}{\frac{\partial \Lambda}{\partial \omega}} (-i\pi \delta(\omega - \omega^m)) \right\} \frac{d^3 \mathbf{k}}{(2\pi)^3} \frac{d\omega}{2\pi},$$

$$U = -2 \int_0^\infty \int \operatorname{Re} \left\{ j_i^{ext} \left(-\frac{i}{\omega \varepsilon_0} \right) j_k^{ext} \frac{\lambda_{ss} e_i^m e_k^m}{\frac{\partial \Lambda}{\partial \omega}} (-i\pi \delta(\omega - \omega^m)) \right\} \frac{d^3 \mathbf{k}}{(2\pi)^3} \frac{d\omega}{2\pi},$$

$$U^m = \int \frac{R_E^m(\mathbf{k})}{\varepsilon_0} \left| \overline{\mathbf{e}^m(\mathbf{k})} \cdot \mathbf{j}^{ext}(\mathbf{k}, \omega^m(\mathbf{k})) \right|^2 \frac{d^3 \mathbf{k}}{(2\pi)^3},$$

where the bar over the polarisation vector $\mathbf{e}^m(\mathbf{k})$ means complex conjugation as usual. Apparently, the quantity

$$u^m(\mathbf{k}) = \frac{R_E^m(\mathbf{k})}{\varepsilon_0} \left| \overline{\mathbf{e}^m(\mathbf{k})} \cdot \mathbf{j}^{ext}(\mathbf{k}, \omega^m(\mathbf{k})) \right|^2 \quad (6.36)$$

that represents the wave energy generated by current density $\mathbf{j}^{ext}(\mathbf{k}, \omega^m(\mathbf{k}))$ in the mode m per unit cube of \mathbf{k} -space, or its time derivative – the radiated power

$$p^m(\mathbf{k}) = \lim_{\tau \rightarrow \infty} \frac{u^m(\mathbf{k})}{\tau} \quad (6.37)$$

will be more relevant ones for computation of radiation in particular emission processes.

6.3 Plasma emission mechanism

Standard radiative mechanisms – the bremsstrahlung and gyrosynchrotron radiation are considered also for solar corona radio emission, particularly for quiet sun radiation and slowly-varying solar radio component. Nevertheless, solar radio bursts that often consist of intense narrow-band fine structures hardly could be explained in terms of these processes since they have by their nature broad-band emission spectrum. Moreover, there is quantitative disagreement in values of radio flux predicted considering these mechanisms.

On the other hand, very hot and sparse coronal plasmas may, due to lack of collisions, easily be in the state of thermodynamic non-equilibrium with non-Maxwellian distribution function, particularly during solar transient events (e.g. flares or CMEs). Under such circumstances the anti-hermitian part $\varepsilon_{ij}^a(\mathbf{k}, \omega)$ of the dielectric tensor (6.22) can result in negative values of the absorption coefficient (6.21) in some range of wave-vectors for the specific wave mode m . One then says, that distribution function is unstable with respect to generation of wave mode m within some range of \mathbf{k} -space. The negative absorption is also often called *stimulated* or *induced* emission.

Such self-generation of waves in unstable plasmas, similar to light amplification in lasers as will be seen further, represents the basis of so called *plasma emission mechanism*. Since there are many types of distribution functions unstable to large amount of wave modes the term “plasma emission” should be regarded as generic name for all radiative processes based primarily on the negative absorption of particular wave modes.

For the electromagnetic mode which only can escape from the coronal plasmas and reach Earth radiotelescopes the absorption coefficient (6.21) is always positive with one exception of so called electron-cyclotron maser radiation. Thus, some mechanism of conversion between unstable plasma modes and the electromagnetic one is required. Such mechanism is possible due to

non-linear coupling among variations of plasma parameters (e.g. electric and magnetic field, electron density etc.) in different wave modes.

To sum up, plasma emission mechanism is generic name for class of radiative processes working usually in the following two stages:

1. the wave mode m unstable in some range of \mathbf{k} -space is generated due to deviation of distribution function from equilibrium Maxwellian distribution.
2. this mode m is converted via non-linear coupling into the electromagnetic one that escapes solar corona and can be detected on Earth.

Since the region of unstable waves in \mathbf{k} -space is usually limited to small extent and also the wave mode conversion is strongly resonant process as will be seen later, resulting radio emission is narrowband and possibly with fine structures as usually observed during solar radio bursts.

Due to mentioned similarity with radiation amplification in lasers it is convenient to adopt principle of detailed balance between emission and absorption processes used in radiative transfer elementary physics and quantitatively expressed using the Einstein coefficients. The theory built on these axioms will be in usual quantum notation briefly reviewed in the following.

6.4 Weak turbulence theory

Stimulated emission and other induced processes such as wave-particle or wave-wave scattering can be under some assumptions described consistently within the weak turbulence theory. It is based on semi-classical formalism – the particles in states with momentum \mathbf{p} are described by distribution function $f(\mathbf{p})$ while the waves in mode m with wave-vector \mathbf{k} is described by the occupation number $N^m(\mathbf{k})$ (number of quanta of wave mode m in state with momentum $\hbar\mathbf{k}$) defined as:

$$N^m(\mathbf{k}) = \frac{w^m(\mathbf{k})}{\hbar\omega^m(\mathbf{k})} \quad (6.38)$$

Such description brings not only the advantage of uniform treatment of various induced processes from the wave generation point of view, but also it enables consistent estimation of back-reaction of particles to wave radiation or absorption since the principle of energetic balance is imposed on microscopic level here. On the other hand, approach (6.38) to wave distribution disables correct description of coherent processes since the phase information about mode depicted by occupation number is lost. Thus, the assumption that phases of waves are unimportant – so called *random phase approximation* – plays key role in the weak turbulence theory. Coherent processes will be discussed in the next section 6.5, however such general theory as in case of incoherent emission has not been available yet.

One may start with subset of this general description applied to stimulated emission of waves due to unstable particle distribution function and its back-reaction to wave generation – so called *quasi-linear theory*.

6.4.1 Quasi-linear theory

Transferring wave generation and/or absorption processes onto microscopic level one has to use, according to quantum physics, probabilistic description of each elementary emission/absorption action. This is usually done introducing the Einstein coefficients.

Einstein coefficients Consider two states described by particle momenta \mathbf{p} and \mathbf{p}^- . Let the total number of particles in state \mathbf{p} is N_p and N_{p^-} for the state \mathbf{p}^- , respectively. According to quantum theory the transition of one particle between states \mathbf{p} and \mathbf{p}^- is accompanied by emission or absorption of quantum of waves with frequency given by condition

$$\hbar\omega = |E(\mathbf{p}) - E(\mathbf{p}^-)|. \quad (6.39)$$

Here, $E(\mathbf{p}^-)$ and $E(\mathbf{p})$ are particle energies in the states \mathbf{p}^- and \mathbf{p} , respectively. In case of free particles the energy of the state \mathbf{p} reads in non-relativistic limit

$$E(\mathbf{p}) = \frac{\mathbf{p}^2}{2m} \quad (6.40)$$

with m being the particle mass, components of state vector \mathbf{p} are simply Cartesian components of particle momentum.

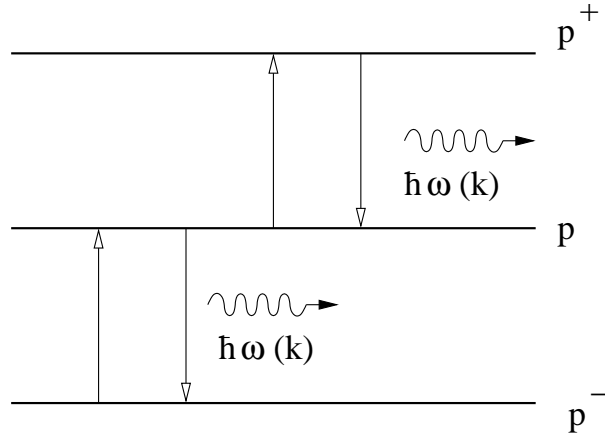


Fig. 6.1: Absorption and emission processes due to $\mathbf{p}^+ \leftrightarrow \mathbf{p}$ and $\mathbf{p} \leftrightarrow \mathbf{p}^-$ state transitions.

Now suppose that $E(\mathbf{p}^-) < E(\mathbf{p})$ (see Fig. 6.1) and consider probabilities (transition rates) $w_{p^-p}^{m,abs}(\mathbf{k})$, $w_{pp^-}^{m,sp}(\mathbf{k})$ and $w_{pp^-}^{m,ind}(\mathbf{k})$ of transitions between the states \mathbf{p} and \mathbf{p}^- due to absorption, spontaneous and induced emission of quantum of mode m with wave-vector \mathbf{k} (referred as (m, \mathbf{k}) quantum further) per unit time, respectively. The rates $w_{p^-p}^{m,abs}(\mathbf{k})$, $w_{pp^-}^{m,sp}(\mathbf{k})$ and $w_{pp^-}^{m,ind}(\mathbf{k})$ represents Einstein coefficients for transitions $\mathbf{p} \rightleftharpoons \mathbf{p}^-$. The total rate of transitions $\mathbf{p}^- \rightarrow \mathbf{p}$ due to absorption is

$$-\frac{dN^m(\mathbf{k})}{dt} = w_{p^-p}^{m,abs}(\mathbf{k})N_{p^-} - N^m(\mathbf{k}) \quad (6.41)$$

while total rate of transitions $\mathbf{p} \rightarrow \mathbf{p}^-$ as consequence of spontaneous or induced emission reads

$$\frac{dN^m(\mathbf{k})}{dt} = w_{pp^-}^{m,sp}(\mathbf{k})N_p + w_{pp^-}^{m,ind}(\mathbf{k})N_p N^m(\mathbf{k}). \quad (6.42)$$

The relations between the Einstein coefficients can be obtained in the state of thermodynamic equilibrium but it should be noted, that resulting relations are valid regardless of macroscopic state of plasma-waves system as they are fundamental characteristics of the $\mathbf{p} \rightleftharpoons \mathbf{p}^-$ transitions. In the state of thermodynamic equilibrium adopted principle of detailed balance applies implying that rate of change of occupation number $N^m(\mathbf{k})$ of (m, \mathbf{k}) quanta due to absorption and emission

processes during $\mathbf{p} \rightleftharpoons \mathbf{p}^-$ transitions together is zero. Thus combining equations (6.41) and (6.42) one obtain

$$\frac{dN^m(\mathbf{k})}{dt} = w_{pp^-}^{m,sp}(\mathbf{k})N_p + w_{pp^-}^{m,ind}(\mathbf{k})N_p N^m(\mathbf{k}) - w_{p^-p}^{m,abs}(\mathbf{k})N_{p^-} N^m(\mathbf{k}) = 0. \quad (6.43)$$

In the state of thermodynamic equilibrium the distribution of wave quanta is given by Planck law

$$N^m(\mathbf{k}) = \frac{1}{\exp\left(\frac{\hbar\omega^m(\mathbf{k})}{k_B T}\right) - 1}.$$

Inserting the Planck law into the eq. (6.43), considering

$$\frac{N_p}{N_{p^-}} = \exp\left(-\frac{E(\mathbf{p}) - E(\mathbf{p}^-)}{k_B T}\right) = \exp\left(-\frac{\hbar\omega}{k_B T}\right),$$

and taking into account that (6.43) has to apply for arbitrarily high temperature T the relation among three Einsteins coefficients is found:

$$w_{p^-p}^{m,abs}(\mathbf{k}) = w_{pp^-}^{m,sp}(\mathbf{k}) = w_{pp^-}^{m,ind}(\mathbf{k}) \equiv w_{pp^-}^m(\mathbf{k}). \quad (6.44)$$

Quasi-linear equations Using the relations (6.44) the rate the (m, \mathbf{k}) quanta are emitted at in the general (non-equilibrium) state due to all transitions that can be taken into account is (see eq. 6.43):

$$\frac{dN^m(\mathbf{k})}{dt} = \sum_{p,p^-} w_{pp^-}^m(\mathbf{k}) [N_p + N^m(\mathbf{k})(N_p - N_{p^-})]. \quad (6.45)$$

However, the actual number of possible transitions is much less than it seems from eq. (6.45) since the quantum condition

$$\mathbf{p} - \mathbf{p}^- = \hbar\mathbf{k}$$

selects only allowed ones. In particular, the transition rate $w_{pp^-}^m(\mathbf{k})$ can be expressed as:

$$w_{pp^-}^m(\mathbf{k}) = w^m(\mathbf{p}, \mathbf{k}) \cdot \delta(\mathbf{p} - \mathbf{p}^- - \hbar\mathbf{k}). \quad (6.46)$$

Now, one would like to change from discrete notation used hitherto to the continuous one. Thus, the number of particles N_p in the state \mathbf{p} should be replaced by distribution function $f(\mathbf{p})$ and double sum in the equation (6.45) by integration over \mathbf{p} and \mathbf{p}^- . Using the expression (6.46) for the transition rate $w(\mathbf{p}, \mathbf{p}^-, \mathbf{k})$, which is now re-interpreted as probability of quantum emission per unit cube of \mathbf{k} -space, the integration over p^- is performed trivially due to δ -function. The expression $f(\mathbf{p} - \hbar\mathbf{k})$ appeared in the result can be for $\hbar\mathbf{k} \ll \mathbf{p}$ expanded in Taylor series

$$f(\mathbf{p} \pm \hbar\mathbf{k}) = f(\mathbf{p}) \pm \hbar k_i \frac{\partial f(\mathbf{p})}{\partial p_i} + \frac{1}{2} \hbar^2 k_i k_j \frac{\partial^2 f(\mathbf{p})}{\partial p_i \partial p_j} + \dots$$

When only the terms that are meaningful in classical limit $\hbar \rightarrow 0$ (see the paragraph **Transition rates calculation**) are retained, the first quasi-linear equation describing wave generation (or absorption) in plasmas described by distribution function $f(\mathbf{p})$ is finally found:

$$\frac{dN^m(\mathbf{k})}{dt} = \int w^m(\mathbf{p}, \mathbf{k}) \left(f(\mathbf{p}) + N^m(\mathbf{k}) \hbar\mathbf{k} \cdot \frac{\partial f(\mathbf{p})}{\partial \mathbf{p}} \right) d^3\mathbf{p} \quad (6.47)$$

As was already mentioned, the advantage of this semi-classical approach consist besides other in possibility of homogeneous description of back-reaction of particle distribution to wave emission/absorption processes. On the microscopic level, each emission or absorption of quantum of

waves is connected with transition of particle between two states. Consequently, the time change of number N_p of particles in state \mathbf{p} is given by the difference between net rate the quanta (m, \mathbf{k}) are emitted at due to transition $(\mathbf{p}^+ = \mathbf{p} + \hbar\mathbf{k}) \rightarrow \mathbf{p}$ and net rate the quanta (m, \mathbf{k}) are emitted at due to transition $\mathbf{p} \rightarrow (\mathbf{p}^- = \mathbf{p} - \hbar\mathbf{k})$, i.e. (see Fig. 6.1):

$$\frac{dN_p}{dt} = \sum_{\mathbf{k}} w_{p^+p}^m(\mathbf{k}) [N_{p^+} + N^m(\mathbf{k})(N_{p^+} - N_p)] - \sum_{\mathbf{k}} w_{pp^-}^m(\mathbf{k}) [N_p + N^m(\mathbf{k})(N_p - N_{p^-})]. \quad (6.48)$$

Transferring from the discrete notation to the continuous one again and expressing the difference of the two sums in the previous relation as a derivative times the interval \mathbf{k} , the second quasi-linear equation describing back-reaction of particles distribution to the wave emission/absorption processes reads

$$\frac{df(\mathbf{p})}{dt} = \int \hbar\mathbf{k} \cdot \frac{\partial}{\partial \mathbf{p}} \left[w^m(\mathbf{p}, \mathbf{k}) \left(f(\mathbf{p}) + N^m(\mathbf{k}) \hbar\mathbf{k} \cdot \frac{\partial f(\mathbf{p})}{\partial \mathbf{p}} \right) \right] \frac{d^3\mathbf{k}}{(2\pi)^3}. \quad (6.49)$$

Transition rates calculation To make equations (6.47) and (6.49) meaningful for practical computation one has to calculate the emission rate $w^m(\mathbf{p}, \mathbf{k})$. It can be done when one re-interprets the power radiated $p^m(\mathbf{k})$ considered in the section 6.2.1 as continuous process to be – according to quantum physics ideas – the series of quanta emissions with emission probability per unit time $w(\mathbf{p}, \mathbf{k})$, i.e.:

$$p^m(\mathbf{k}) = \hbar\omega^m(\mathbf{k}) w^m(\mathbf{p}, \mathbf{k})$$

Thus, using relations (6.36) and (6.37) the emission rate can be expressed as:

$$w^m(\mathbf{p}, \mathbf{k}) = \lim_{\tau \rightarrow \infty} \frac{1}{\tau} \left(\frac{1}{\hbar\omega^m(\mathbf{k})} \frac{R_E^m(\mathbf{k})}{\varepsilon_0} \left| \overline{\mathbf{e}^m(\mathbf{k})} \cdot \mathbf{j}^{ext}(\mathbf{k}, \omega^m(\mathbf{k})) \right|^2 \right) \quad (6.50)$$

In the force-free collision-less plasmas particle moves on rectilinear trajectory. Consequently, the extraneous current density in the equation (6.50) is to be identified with that given by equation with rectilinear trajectory

$$\mathbf{r}(t) = \mathbf{r}_0 + \mathbf{v}t$$

inserted. Now using

$$\mathbf{j}(\mathbf{k}, \omega) = q \int_{-\infty}^{\infty} dt \int d^3\mathbf{r} \exp[-i(\mathbf{k} \cdot \mathbf{r}) - \omega t] \mathbf{v}(t) \delta^3(\mathbf{r} - \mathbf{r}(t)) = q \int_{-\infty}^{\infty} dt \mathbf{v}(t) \exp[-i(\mathbf{k} \cdot \mathbf{r}(t)) - \omega t],$$

$$\mathbf{j}(\mathbf{k}, \omega) = q\mathbf{v} \exp(-i\mathbf{k} \cdot \mathbf{r}_0) \int_{-\infty}^{\infty} dt \exp[i(\omega - \mathbf{k} \cdot \mathbf{v})t] = 2\pi q\mathbf{v} \exp(-i\mathbf{k} \cdot \mathbf{r}_0) \delta(\omega - \mathbf{k} \cdot \mathbf{v}),$$

$$[\delta(\omega)]^2 = \lim_{\tau \rightarrow \infty} \frac{\tau}{2\pi} \delta(\omega),$$

calculation gives

$$w^m(\mathbf{p}, \mathbf{k}) = \frac{2\pi q^2 R_E^m(\mathbf{k})}{\hbar\omega^m(\mathbf{k}) \varepsilon_0} \left| \overline{\mathbf{e}^m(\mathbf{k})} \cdot \mathbf{v} \right|^2 \delta(\omega^m(\mathbf{k}) - \mathbf{k} \cdot \mathbf{v}) \quad (6.51)$$

Absorption coefficient As was already mentioned, the first quasi-linear equation (6.47) expresses the emission or absorption of wave quanta due to medium described by distribution function. The rate of occupation number change can be separated to two parts – one independent of the occupation number itself

$$\left[\frac{dN^m(\mathbf{k})}{dt} \right]^{sp} = \int w^m(\mathbf{p}, \mathbf{k}) f(\mathbf{p}) d^3\mathbf{p}$$

and one linearly proportional to it

$$\left[\frac{dN^m(\mathbf{k})}{dt} \right]^{ind} = -\gamma^m(\mathbf{k})N^m(\mathbf{k})$$

where $\gamma^m(\mathbf{k})$ reads

$$\gamma^m(\mathbf{k}) = - \int w^m(\mathbf{p}, \mathbf{k}) \hbar \mathbf{k} \cdot \frac{\partial f(\mathbf{p})}{\partial \mathbf{p}} d^3 \mathbf{p}. \quad (6.52)$$

As the superscripts over each part indicate the former part describes spontaneous or thermal wave emission whereas the latter belongs to induced processes. The quantity $\gamma^m(\mathbf{k})$ is absorption coefficient by definition and its sign depend on what process prevails – whether absorption or stimulated emission of waves. In case of negative values also the term *growth rate* is often used.

It is clear from expression (6.52) that in case of positive slope of distribution function $f(\mathbf{p})$ in the direction of wave-vector \mathbf{k} the absorption coefficient $\gamma^m(\mathbf{k})$ can reach negative values implying so self-amplification or instability of waves. The positive slope corresponds to inequality

$$N_{p+\hbar k} > N_p$$

in the formula (6.45), which is only discrete form of the first quasi-linear equation (6.47), and thus inverse population of energetic levels is required (in unmagnetised plasmas) for self-amplification to work. This feature of the theory of induced processes in plasmas makes it very close to, now already classical, physics of lasers as was already mentioned in the introduction to this section. Probably the most known examples of amplification of waves due to such inverse population of energetic levels in the field of plasma physics are the “Bump-in-Tail” or “Two-stream” instabilities of Langmuir waves. The positive slope of the particle distribution function is reached by energetic particle stream propagating through the thermal background plasmas in this case.

Then, the resonant condition contained implicitly due to δ -function in the relation (6.51) can be fulfilled only if

$$v \geq v_\varphi \quad (6.53)$$

where $v_\varphi = \omega(\mathbf{k})/k$ is the wave phase velocity. Since refractive index for electromagnetic waves $n^T(\mathbf{k}) < 1$ for all \mathbf{k} -vectors, negative absorption of this mode is forbidden in the case of unmagnetized plasmas as a consequence of apparent inequality

$$v < c$$

Hence, the mode conversion between waves that can satisfy the condition (6.53), and their amplification is therefore possible, and the electromagnetic ones is required for plasma emission process to work.

6.5 Coherent processes

The weak-turbulence theory just reviewed in the previous section is capable to describe many types of particle-wave or wave-wave interactions, provided that wave field is sufficiently described by occupation numbers – i.e. that wave phases are unimportant. As was shown, such a condition is fulfilled in case of broad-band wave distributions as after the coherence time τ_c the phases of waves are completely mixed. Nevertheless, sometimes the region of unstable waves in the \mathbf{k} -space is so narrow, that before the phase mixing state is reached the waves have grown up substantially.

For such cases the weak-turbulence theory is inapplicable and its departure from the reality can be separated into two kinds of problems:

- the theory predicts qualitatively some process (e.g. instability) to be running, but further quantitative analysis gives wrong results – usually predicted growth rates of unstable waves are lower than in reality.
- the weak-turbulence version of coherent process does not exist at all.

Hence, processes where also wave phases are important have to be treated another way. Unfortunately, the general theory of coherent processes – as a counterpart of the weak-turbulence theory – has not been established yet. One particular case is discussed in the following.

6.5.1 Strong wave turbulence

Strong wave turbulence is term for non-linear wave-wave interactions that can not be sufficiently described within the weak-turbulence theory just due to great importance of wave phases for processes involved. The first description of coherent wave-wave interactions is that by Zakharov who treated the non-linear interaction between Langmuir and ion-sound waves. His approach was roughly as follows:

Firstly, let us consider linear Langmuir and ion-sound waves in homogeneous plasmas. The time evolution of plasma parameters variations in these waves can be derived most simply within the plasma two-fluid theory or alternatively they can be guessed Fourier transforming the dispersion relations (6.29) and (6.30) for relevant waves into the coordinate space. Hence, the electric field variation in Langmuir waves is governed by equation

$$\frac{\partial^2 \mathbf{E}}{\partial t^2} - 3V_e^2 \Delta \mathbf{E} + \omega_{pe}^2 \mathbf{E} = 0 \quad (6.54)$$

and similarly the electron density variation n in the ion-sound waves fulfils (for wavelengths $\lambda \ll \lambda_{De}$) relation

$$\frac{\partial^2 n}{\partial t^2} - c_s^2 \Delta n = 0. \quad (6.55)$$

Now suppose that both wave modes propagate through plasma simultaneously. Due to ion-sound wave the electron density is now distributed non-uniformly and as a consequence of the plasma frequency definition (6.25) the last term $\omega_{pe}^2 \mathbf{E}$ in the eq. (6.54) depends explicitly on time and space. Hence, the equation (6.54) can be rewritten in the form

$$\frac{\partial^2 \mathbf{E}}{\partial t^2} - 3V_e^2 \Delta \mathbf{E} + \omega_{pe}^2 \mathbf{E} = -\omega_{pe}^2 \frac{n(\mathbf{r}, t)}{n_0} \mathbf{E} \quad (6.56)$$

where the plasma frequency ω_{pe} is now re-interpreted as that connected with the background average density n_0 . Equation (6.56) describes Langmuir wave electric field evolution under the influence of ion-sound density perturbation. The effect of density distribution can be estimated qualitatively even without solving it by analogy with the Schrödinger wave equation describing an electron inside the crystal lattice (c.f. equation 6.59). Identifying the total density $n_0 + n$ with crystal single-electron potential one finds, that the Langmuir electric field tends to concentrate itself in the density holes, similarly as electron probability density in the crystal is high in places of low potential (in the vicinity of ions locations).

On the other hand, non-homogeneous (averaged over wavelength) electric field influences density distribution due to non-linear ponderomotive force F_{NL} whose volume density is (e.g. ??):

$$\mathbf{f}_{NL} = -\frac{\omega_{pe}^2}{\omega^2} \mathbf{grad} \frac{\varepsilon_0 \langle E^2 \rangle}{2}. \quad (6.57)$$

where $\langle \rangle$ denotes the fast-time (on scales of several plasma period) averaging. As a consequence, a source term has to appear on the R.H. side of equation (6.55), i.e.

$$\frac{\partial^2 n}{\partial t^2} - c_s^2 \Delta n = \frac{1}{m_i} \operatorname{div} \mathbf{f}_{NL}. \quad (6.58)$$

Since changes of electric field amplitude and ion-sound density variations are slow in comparison with plasma frequency it is convenient to separate the instantaneous Langmuir electric field time evolution into the fast (on plasma frequency) variations and the slowly varying complex amplitude

$$\mathbf{E}(\mathbf{r}, t) = \frac{1}{2} \left[\mathcal{E}(\mathbf{r}, t) \cdot \exp(-i\omega_{pe}t) + \bar{\mathcal{E}}(\mathbf{r}, t) \cdot \exp(+i\omega_{pe}t) \right]$$

Using this separation and relation (6.57) for ponderomotive force, further omitting the second derivative of slowly changing complex amplitude $\mathcal{E}(\mathbf{r}, t)$ the equations (6.56) and (6.58) can be rewritten in the form:

$$i \frac{\partial \mathcal{E}}{\partial t} + \frac{3V_e^2}{2\omega_{pe}} \Delta \mathcal{E} = \omega_{pe} \frac{n}{2n_0} \mathcal{E} \quad (6.59)$$

$$\frac{\partial^2 n}{\partial t^2} - c_s^2 \Delta n = \frac{\varepsilon_0}{4m_i} \Delta |\mathcal{E}|^2. \quad (6.60)$$

The relations (6.59, 6.60) are known as set of Zakharov equations and describe coherent non-linear interactions of Langmuir and ion-sound waves.

Chapter 7

Beams and two-stream instability

a) Beams in the solar atmosphere

See file `beams.ps`

Doplňit obrázky do SPA3.tex

Reference

Karlický, M: 1997, Effects of particle beams in the solar atmosphere, *Space Sci. Rev.* 81, 143-172.

b) Two-stream instability

Here the CGS unit system is used.

Dispersion equation

Let at times $t < 0$ a plasma exists in a stationary state, i.e. the plasma density, plasma velocity, magnetic and electric fields are:

$$n = n_0; \mathbf{v} = \mathbf{v}_0; \mathbf{B} = \mathbf{B}_0; \mathbf{E} = \mathbf{E}_0. \quad (7.1)$$

Then at times $t > 0$ small perturbations appear:

$$n = n_0 + n'; \mathbf{v} = \mathbf{v}_0 + \mathbf{v}'; \mathbf{B} = \mathbf{B}_0 + \mathbf{B}'; \mathbf{E} = \mathbf{E}_0 + \mathbf{E}'. \quad (7.2)$$

Let us assume that these perturbations have periodic form in time as:

$$X'(t, \mathbf{r}) = X'(\mathbf{r}) \exp(-i\omega t), \quad (7.3)$$

where \mathbf{r} is the position and ω is the frequency.

Then the mass conservation, momentum and Maxwell equations can be linearized. Thus, a set of equations for variables of zero-, first- and higher-orders of magnitude can be derived. The set of equations with first-order variables follows:

$$\begin{aligned} -i\omega n' + \nabla \cdot (n' \mathbf{v}_0 + n_0 \mathbf{v}') &= 0, \\ -i\omega \mathbf{v}' + (\mathbf{v}_0 \nabla) \mathbf{v}' + (\mathbf{v}' \nabla) \mathbf{v}_0 &= \frac{e}{m} (\mathbf{E}' + \frac{1}{c} (\mathbf{v}' \times \mathbf{B}_0) + \frac{1}{c} (\mathbf{v}_0 \times \mathbf{B}')), \\ \nabla \times \mathbf{B}' &= \frac{4\pi}{c} e (n' \mathbf{v}_0 + n_0 \mathbf{v}') - \frac{i\omega}{c} \mathbf{E}', \end{aligned}$$

$$\begin{aligned}\nabla \times \mathbf{E}' &= \frac{i\omega}{c} \mathbf{B}', \\ \nabla \cdot \mathbf{E}' &= 4\pi en', \\ \nabla \cdot \mathbf{B}' &= 0,\end{aligned}\tag{7.4}$$

where the Fourier transform in time ($\partial/\partial t \rightarrow -i\omega$) was done.

Oscillations of homogenous plasma

Let us assume a 1-D case with $\mathbf{B}_0 = 0$, $\mathbf{v}_0 = 0$, $\nabla n_0 = 0$ and the spatial perturbation in the form: $X'(\mathbf{r}) \sim \exp(i\mathbf{k}\mathbf{r})$. Then from the above mentioned equations follow:

$$\begin{aligned}-i\omega n' + n_0 ikv' &= 0, \\ -i\omega v' &= \frac{e}{m} E', \\ ikE' &= 4\pi en',\end{aligned}$$

Now, from these equations the dispersion equation for so called plasma oscillations can be written as:

$$\omega^2 = \frac{4\pi e^2 n_0}{m}.\tag{7.5}$$

Electromagnetic waves in homogenous plasma

Furthermore we can write

$$\begin{aligned}\nabla \times \mathbf{B}' &= \frac{4\pi}{c} en_0 v' + \frac{1}{c} \frac{\partial \mathbf{E}'}{\partial t}, \quad / \frac{\partial}{\partial t} \\ \nabla \times \frac{\partial \mathbf{B}'}{\partial t} &= \frac{4\pi}{c} en_0 \frac{\partial v'}{\partial t} + \frac{1}{c} \frac{\partial^2 \mathbf{E}'}{\partial t^2}, \\ -c\nabla \times \nabla \times \mathbf{E}' &= \frac{4\pi}{c} en_0 \frac{e}{m} \mathbf{E}' + \frac{1}{c} \frac{\partial^2 \mathbf{E}'}{\partial t^2}, \\ -ck^2 \mathbf{E}' &= \frac{\omega_p^2}{c} \mathbf{E}' - \frac{\omega^2}{c} \mathbf{E}', \\ \omega^2 &= \omega_p^2 + k^2 c^2,\end{aligned}\tag{7.6}$$

which is the dispersion equation for the electromagnetic waves in the plasma without static magnetic field.

Dispersion equation for plasma with moving components

Let us consider a potential perturbation of the electric field

$$\mathbf{E} = -\nabla\psi; \quad \mathbf{E} = -i\mathbf{k}\psi,$$

and let us look what a perturbation of the electric charge density ρ_e causes the electric field perturbation, i.e. let us look for the function χ in the relation $\rho_e = \chi\psi$.

In this case the linearized MHD equation has a following form:

$$-i\omega n' + \nabla \cdot (n' \mathbf{v}_0 + n_0 \mathbf{v}') = 0,$$

$$-i\omega \mathbf{v}' + (\mathbf{v}_0 \nabla) \mathbf{v}' + (\mathbf{v}' \nabla) \mathbf{v}_0 = \frac{e}{m} \mathbf{E}',$$

Using $\nabla \mathbf{v}_0 = 0$ and $\mathbf{E}' = -\nabla \psi'$ the equation can be rewritten into

$$-i\omega n' + in' \mathbf{k} \mathbf{v}_0 + in_0 \mathbf{k} \mathbf{v}' = 0,$$

$$-i\omega \mathbf{v}' + \mathbf{v}_0 i \mathbf{k} \mathbf{v}' = -i \frac{e}{m} \mathbf{k} \psi',$$

Now, we can express the density and plasma velocity perturbations as

$$n' = \frac{n_0 \mathbf{k} \mathbf{v}'}{\omega - \mathbf{k} \mathbf{v}_0}; \quad \mathbf{v}' = \frac{e \mathbf{k} \psi'}{m(\omega - \mathbf{k} \mathbf{v}_0)},$$

Combining these equations the perturbation of charge density is

$$\rho_e = n' e = \chi \psi' = \frac{e^2 n_0 k^2}{m(\omega - \mathbf{k} \mathbf{v}_0)^2} \psi', \quad (7.7)$$

i.e. the function χ for some specific plasma component α can be expressed as

$$\chi^\alpha = \frac{e^\alpha n_0^\alpha k^2}{m^\alpha (\omega - \mathbf{k} \mathbf{v}_0^\alpha)^2}. \quad (7.8)$$

Let us put these results into the Poisson equation. Then

$$\begin{aligned} k^2 \psi &= 4\pi \sum_{\alpha} \rho_e^\alpha, \\ k^2 \psi &= 4\pi \sum_{\alpha} \chi^\alpha \psi, \\ \left(1 - \frac{4\pi}{k^2} \sum_{\alpha} \chi^\alpha\right) \psi &= 0 \end{aligned} \quad (7.9)$$

In the last relation the term in brackets is the dispersion equation which can be formally written as

$$\epsilon_0 = 1 - \frac{4\pi}{k^2} \sum_{\alpha} \chi^\alpha, \quad (7.10)$$

where contributions of moving components of plasma into the dispersion equation are

$$\epsilon_0^\alpha = -\frac{4\pi}{k^2} \chi^\alpha = -\frac{(\omega_p^\alpha)^2}{(\omega - \mathbf{k} \mathbf{v}_0^\alpha)^2}. \quad (7.11)$$

Beam instabilities

a) Instability of two counter-streaming beams

Let us consider two counter-streaming beams of the same density, i.e.

$$n_{01} = n_{02} = n_0; \quad v_{01} = -v_{02} = v. \quad (7.12)$$

in this case the dispersion equation is

$$1 - \frac{\omega_p^2}{(\omega - k_{\parallel}v)^2} - \frac{\omega_p^2}{(\omega + k_{\parallel}v)^2} = 0. \quad (7.13)$$

This equation leads to the bi-quadratic equation with the following solutions:

$$\omega = \pm \sqrt{(k_{\parallel}v)^2 + \omega_p^2} \pm \omega_p(\omega_p^2 + 4k_{\parallel}^2v^2)^{1/2}. \quad (7.14)$$

If

$$(k_{\parallel}v)^2 + \omega_p^2 < \omega_p(\omega_p^2 + 4k_{\parallel}^2v^2)^{1/2},$$

i.e. if

$$(k_{\parallel}v)^4 + 2(k_{\parallel}v)^2\omega_p^2 + \omega_p^4 < \omega_p^2(\omega_p^2 + 4k_{\parallel}^2v^2),$$

and i.e. if $k_{\parallel} < \sqrt{2}\omega_p/v$ then there is one solution with $Im \omega > 0$, which for the perturbation in the form $X(t) \sim \exp^{-i\omega t}$ means an instability. Furthermore, if $k_{\parallel} \ll \omega_p/v$ then the term under the root can be written as

$$(k_{\parallel}v)^2 + \omega_p^2 - \omega_p^2\left(1 + \frac{2k_{\parallel}^2v^2}{\omega_p^2}\right) = (k_{\parallel}v)^2 - 2(k_{\parallel}v)^2,$$

which gives the growth rate of the instability as

$$Im \omega = |k_{\parallel}v|. \quad (7.15)$$

On the other hand, the maximum growth rate can be derived as follows:

$$\frac{d}{dk_{\parallel}}((k_{\parallel}v)^2 + \omega_p^2 - \omega_p(\omega_p^2 + 4k_{\parallel}^2v^2)^{1/2}) = 0,$$

$$2v^2k_{\parallel} - \frac{\omega_p}{2} \frac{8k_{\parallel}v^2}{(\omega_p^2 + 4k_{\parallel}^2v^2)^{1/2}} = 0,$$

$$\omega_p^2 + 4k_{\parallel}^2v^2 = 4\omega_p^2,$$

$$k_{\parallel max} = \frac{\sqrt{3}\omega_p}{2v}. \quad (7.16)$$

Now, putting this $k_{\parallel max}$ into the relation for ω (Eq.7.14), the maximum growth rate is

$$\gamma_{max} = \omega_p/2. \quad (7.17)$$

b) Beam-plasma instability

Let us assume a beam which density is much lower than that of background plasma ($n_1 \ll n_0$). Then the dispersion equation is

$$1 - \frac{\omega_{pe}^2}{\omega^2} - \frac{\alpha\omega_{pe}^2}{(\omega - k_{\parallel}v)^2} = 0. \quad (7.18)$$

where $\omega_{pe}^2 = 4\pi e^2 n_0 / m_e$, $\alpha = n_1 / n_0 \ll 1$, v is the beam velocity.

Solutions:

a) The non-resonant case, i.e. the case with $\omega_{pe} \neq k_{\parallel}v$.

The solution can be derived as follows:

$$(\omega - k_{\parallel}v)^2 - (\omega - k_{\parallel}v)^2 \frac{\omega_{pe}^2}{\omega^2} - \alpha\omega_{pe}^2 = 0,$$

$$(\omega - k_{\parallel}v)^2 \left(1 - \frac{\omega_{pe}^2}{\omega^2}\right) = \alpha\omega_{pe}^2,$$

$$(\omega - k_{\parallel}v)^2 = \alpha\omega_{pe}^2 \frac{1}{1 - \frac{\omega_{pe}^2}{\omega^2}},$$

$$\omega - k_{\parallel}v = \pm \sqrt{\alpha\omega_{pe}^2} \frac{1}{\sqrt{1 - \frac{\omega_{pe}^2}{\omega^2}}},$$

$$\omega = k_{\parallel}v \pm \sqrt{\alpha} \frac{\omega_{pe}}{\sqrt{1 - \frac{\omega_{pe}^2}{(k_{\parallel}v)^2}}}, \quad (7.19)$$

where, in the last equation, the approximate relation $\omega \simeq k_{\parallel}v$ was used.

As can be seen, if $k_{\parallel}v < \omega_{pe}$ the solution is complex and the growth rate is

$$\gamma = \sqrt{\alpha} \frac{\omega_{pe}}{\sqrt{(\omega_{pe}/k_{\parallel}v)^2 - 1}}, \quad (7.20)$$

b) The resonant case, i.e. the case with $\omega \simeq k_{\parallel}v \simeq \omega_{pe}$.

Let us assume that the frequency correction is

$$|\omega^{(1)}| \gg |\omega_{pe} - k_{\parallel}v|,$$

Then the dispersion equation can be written as

$$1 - \frac{\omega_{pe}^2}{\omega^2} - \frac{\alpha\omega_{pe}^2}{(\omega_{pe} + \omega^{(1)} - k_{\parallel}v)^2} = 0, / \cdot \omega^2$$

$$\omega^2 - \omega_{pe}^2 - \frac{\alpha\omega_{pe}^4}{(\omega^{(1)})^2} = 0.$$

Using now

$$\omega^2 \approx (\omega_{pe} + \omega^{(1)})^2 = \omega_{pe}^2 + 2\omega^{(1)}\omega_{pe},$$

we can continue in the simplification of the dispersion equation as follows

$$2\omega^{(1)}\omega_{pe} - \frac{\alpha\omega_{pe}^4}{(\omega^{(1)})^2} = 0,$$

$$((\omega^{(1)})^3 - \frac{\alpha\omega_{pe}^2}{2}) = 0,$$

which solution is

$$x_{1,2,3} = \frac{\alpha^{1/3}\omega_{pe}}{2^{1/3}}(\cos\phi + i\sin\phi)^{1/3}, \quad \phi = 0, 2\pi, 4\pi$$

Thus the correction of real frequency and growth rate of the instability ($\phi/3 = 4\pi/3$) are

$$Re\omega^{(1)} = -\omega_{pe}\frac{\alpha^{1/3}}{2^{4/3}}, \quad (7.21)$$

$$\gamma = \omega_{pe}\frac{\sqrt{3}\alpha^{1/3}}{2^{4/3}}. \quad (7.22)$$

c) Buneman instability

In this case the electron plasma component is in a relative motion to the proton component. In this case the dispersion equation is

$$1 - \frac{\omega_{pe}^2}{(\omega - k_{\parallel}v)^2} - \frac{\omega_{pp}^2}{\omega^2} = 0, \quad (7.23)$$

where $\omega_{pp}^2/\omega_{pe}^2 \ll 1$. Using the same procedure as in the previous case for $\alpha = m_e/m_p$ (the electron-proton mass ratio) the resonant growth rate can be obtained as

$$\gamma = \omega_{pe}\frac{\sqrt{3}(m_e/m_i)^{1/3}}{2^{4/3}}. \quad (7.24)$$

d) Kinetic beam instability

If a beam has some dispersion in velocities v_{T1} which is greater than $\alpha^{1/3}v$, where $\alpha = n_1/n_0$ is the ratio of beam and plasma densities and v is the beam velocity, then the results for the above mentioned beam-plasma instability are not valid and the kinetic approach to this instability is necessary. In this case the instability has a maximum for $k \approx \omega_{pe}/v$ with the growth rate

$$\gamma \simeq \frac{\omega_{pe}}{2}\alpha\left(\frac{v}{v_{T1}}\right)^2. \quad (7.25)$$

Comparing the relations (1.22) and (1.25) we can see that the growth rate of the kinetic instability is lower than that of the MHD one, and the both growth rates are equal if $v_{T1} = \alpha^{1/3}v$.

Chapter 8

Numerical particle code

At the end of fifties and at the beginning of sixties of the 20-century John Dawson and Oscar Buneman started to simulate a plasma by a big amount of numerical particles which were electromagnetically interacting. While at the beginning many scientists expressed scepticism to this approach, now it is well developed research field.

To fulfill basic characteristics of the plasma it is necessary to have a system which is large enough (its length $L \gg \lambda_D$) and the number of numerical particles in the Debye sphere is much greater than 1. It needs enormous amount of particles, especially in 3-dimensional case. Much better situation is in 1-D case and that is why all studies in this field started with the 1-D system where the number of particles in the Debye sphere is $N_D = n\lambda_D$ only; n is the plasma particle density. But generally, a relatively small number of particles in the system generates high level of noise.

In principle, it is possible to build a numerical piece of plasma considering particles which interact with all other particles, but this numerical approach is very time and memory consuming. Therefore a modified method called as particle-in-cell is used.

As an example, in the following, let us present a simple 1-D electrostatic code. A scheme of this numerical code is shown in Fig. 8.1. Particles are distributed in the system of the length L which is much greater than λ_D ; usually $L \approx 100\lambda_D$. In each Debye length is as minimum 100 electrons and 100 protons forming thus a quasi-neutral plasma. As known from numerical experiments these numbers are sufficient to fulfilled the condition about a big number of particles in the Debye sphere. Thus in our system simulating plasma we have about 10000+10000 numerical particles. Although, the electron-proton ratio is 1836, in numerical simulations this ratio is usually smaller in order to accelerate some plasma processes. On the other hand, this fact needs to be taken into account when we interpret results of numerical simulations.

First in the code, the initial state of the system needs to be generated; every particle needs to have initial position and velocity. Positions of particles can be regular or by some way modified, e.g. by the presence of initial electrostatic wave in some tasks. In the case of cold plasma all velocities are zero, otherwise Maxwell distribution of particles corresponding to some temperature is generated. Then we need to compute electrostatic forces among particles. As mentioned above a direct method through the Coulomb law is not used in such a model. Here, electrostatic forces are computed as a difference of the electrostatic potential computed from Poisson equation. For this purpose the charge density is calculated on the grids (hundreds grids per system) using some weighting procedure. Knowing the electric charge distribution in the system the Fourier transform is applied and the Poisson equation is solved in k-space. Then the inverse Fourier transform is made, and from the electrostatic potential the electric field is computed. Because the fast Fourier transform is used then it is useful to use powers of 2^n (128, 256, 512 ..) for the number of system grids. Furthermore, usually the periodic boundary conditions are used. Using now further weighting procedure the force on every particle

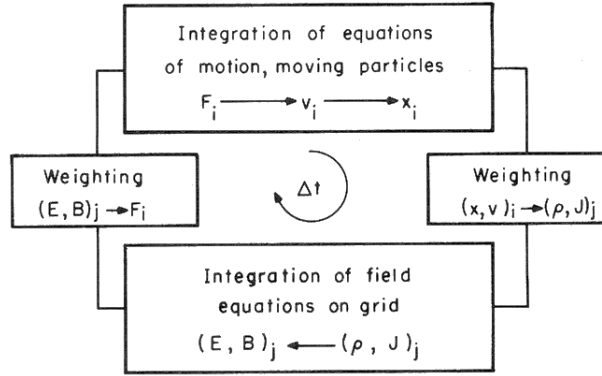


Fig. 8.1: One time step in a particle simulation program. The particles are numbered $i = 1, 2, \dots, NP$; the grid indices are j .

is calculated from the electric field computed on grids. Then solving Newton equation we obtain new positions and new velocities of all particles, and the full time step Δt is finished and further step can start. During computations it is important to record some important variables for diagnostic purposes.

Now let us describe the 1-D electrostatic code in more details.

Integration of the equations of motion

One commonly used integration is the leap-frog method. The use of high-order methods (e.g. Runge-Kutta) is possible, but they multiply the operations taken for each particle.

The two first-order differential equations to be integrated separately for each particle are

$$m \frac{d\mathbf{v}}{dt} = \mathbf{F}, \quad (8.1)$$

$$\frac{d\mathbf{x}}{dt} = \mathbf{v}, \quad (8.2)$$

where \mathbf{F} is the force. These equations are replaced by the finite-difference equations

$$m \frac{\mathbf{v}_{new} - \mathbf{v}_{old}}{\Delta t} = \mathbf{F}_{old}, \quad (8.3)$$

$$\frac{\mathbf{x}_{new} - \mathbf{x}_{old}}{\Delta t} = \mathbf{v}_{new}. \quad (8.4)$$

In the leap-frog method values of \mathbf{x} and \mathbf{v} are not known at the same time, they are shifted each other by $\Delta t/2$ (Fig. 8.2). The user must show care in at least two ways: first, initial conditions for particle velocities and positions given at $t = 0$ must be changed; we push $\mathbf{v}(0)$ back to $\mathbf{v}(-\Delta t/2)$ using the force \mathbf{F} calculated at $t = 0$; second, the energies calculated from \mathbf{v} (kinetic) and \mathbf{x} (potential, or field) must be adjusted to appear at the same time.

The leap-frog method has error, with the error vanishing as $\Delta t \rightarrow 0$. Applying this method to integration of a simple harmonic oscillator of frequency ω_0 , we will find that there is no amplitude error for $\omega_0 \Delta t \leq 2$ and that the phase advance for one step is given by

$$\omega_0 \Delta t + \frac{1}{24} (\omega_0 \Delta t)^3 + \dots \quad (8.5)$$

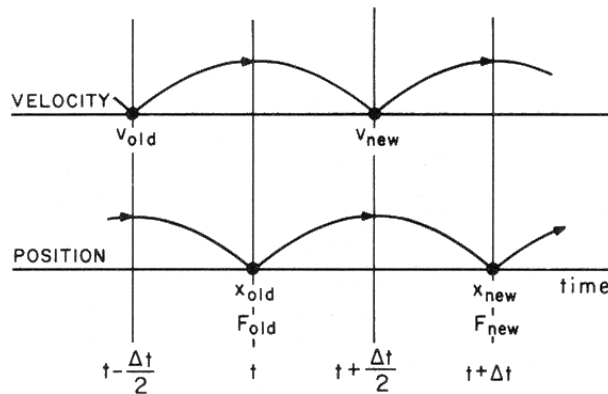


Fig. 8.2: Sketch of leap-frog integration method showing time-centering of force \mathbf{F} while advancing \mathbf{v} , and of \mathbf{v} while advancing \mathbf{x} .

Remark: This relation follows from two half-time steps and Taylor series for one half step as

$$\sin\left(\omega_0 \frac{\Delta t}{2}\right) \approx \omega_0 \frac{\Delta t}{2} - \frac{1}{6} \left(\omega_0 \frac{\Delta t}{2}\right)^3 + \dots \quad (8.6)$$

The error terms dictate a choice of $\omega_0 \Delta t \leq 0.3$ in order to observe oscillations or waves for some tens of cycles with acceptable accuracy.

Although the numerical system is 1-dimensional, in the limited sense (with the static magnetic field \mathbf{B} perpendicular to the x -coordinate of the system) we can consider two components of velocities (v_x, v_y). In this case the force \mathbf{F} has two parts,

$$\mathbf{F} = \mathbf{F}_{electric} + \mathbf{F}_{magnetic} = q\mathbf{E} + q(\mathbf{v} \times \mathbf{B}). \quad (8.7)$$

Here the electric field \mathbf{E} and magnetic field \mathbf{B} are to be calculated at the particle position. Hence, using a spatial grid, we must interpolate \mathbf{E} and \mathbf{B} from the grid to the particle. As we will see later, the electric force on a particle will depend not only on the distance to other particles (physical) but also on the position within the cell (nonphysical).

For our 1-D case, let us consider the particle displacement to be along x , and that we have velocities v_x and v_y , with a uniform static magnetic field B_0 , along z (Fig. 8.3). The $q(\mathbf{v} \times \mathbf{B})$ force is simply a rotation of \mathbf{v} ; that is, \mathbf{v} does not change in magnitude. However, the $q\mathbf{E} = qE_x \mathbf{x}$ force does alter the magnitude of \mathbf{v} (v_x); $E_y = 0$. Hence, a physically reasonable scheme which is centered in time is as follows (with t' and t'' as dummy variables, $t - \Delta t/2 < t' < t'' < t + \Delta t/2$):

Half acceleration

$$v_x(t') = v_x \left(t - \frac{\Delta t}{2} \right) + \left(\frac{q}{m} \right) E_x(t) \left(\frac{\Delta t}{2} \right) \quad (8.8)$$

$$v_y(t') = v_y \left(t - \frac{\Delta t}{2} \right)$$

Rotation

$$\begin{pmatrix} v_x(t'') \\ v_y(t'') \end{pmatrix} = \begin{pmatrix} \cos \omega_c \Delta t & \sin \omega_c \Delta t \\ -\sin \omega_c \Delta t & \cos \omega_c \Delta t \end{pmatrix} \begin{pmatrix} v_x(t') \\ v_y(t') \end{pmatrix} \quad (8.9)$$

Half acceleration

$$v_x \left(t + \frac{\Delta t}{2} \right) = v_x(t'') + \left(\frac{q}{m} \right) E_x(t) \left(\frac{\Delta t}{2} \right) \quad (8.10)$$

$$v_y \left(t + \frac{\Delta t}{2} \right) = v_y(t'')$$

The angle of rotation is

$$\Delta \theta = -\omega_c \Delta t \quad (8.11)$$

where ω_c is the cyclotron frequency.

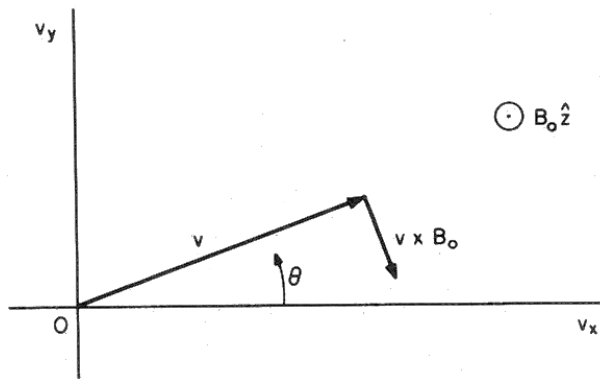


Fig. 8.3: The v_x and v_y plane, showing the $q(\mathbf{v} \times \mathbf{B})$ force normal to \mathbf{v} , which results in a rotation of \mathbf{v} , with no change in speed magnitude with $d\theta/dt < 0$ for $(q/m) > 0$, $B_0 > 0$.

Integration of the field equations

Starting from the charge density as assigned to the grid-points, we now obtain the electric field. In our 1-D case we need to solve the following differential equations

$$\mathbf{E} = -\nabla \phi, \quad E_x = -\frac{\partial \phi}{\partial x}, \quad (8.12)$$

$$\nabla \cdot \mathbf{E} = \frac{\rho}{\epsilon_0}, \quad \frac{\partial E_x}{\partial x} = \frac{\rho}{\epsilon_0}, \quad (8.13)$$

which are combined to obtain Poisson's equation

$$\nabla^2 \phi = -\frac{\rho}{\epsilon_0}, \quad \frac{\partial^2 \phi}{\partial x^2} = -\frac{\rho}{\epsilon_0}. \quad (8.14)$$

One approach is solve the finite difference versions of these equations as

$$E_j = \frac{\phi_{j-1} - \phi_{j+1}}{2\Delta x} \quad (8.15)$$

$$\frac{\phi_{j-1} - 2\phi_j + \phi_{j+1}}{(\Delta x)^2} = -\frac{\rho}{\epsilon}. \quad (8.16)$$

A very powerful approach for periodic systems is to use a discrete Fourier series for all grid quantities. This approach also provides spatial spectral information on ρ , ϕ , and E which is useful in relating results to plasma theory, and which also allows control (smoothing) over the spectrum of field quantities.

In such types of computations the fast Fourier transform is effectively used. This transformation allows us to obtain $\phi(k)$ from $\rho(k)$ from simple equation (transformed Poisson equation)

$$\phi(k) = \frac{\rho(k)}{\epsilon_0 k^2}. \quad (8.17)$$

The next step is to take the inverse Fourier transform of $\phi(k)$ in order to obtain $\phi(x)$ and then $E(x)$ using equation (8.15).

The solution using a finite Fourier series starts from the charge densities at the grid points, with values $\rho(X_j)$, $j = 0, 1, 2, \dots, \text{NG} - 1$ for a total of NG values. Letting the grid functions $G(X_j)$ (standing for field or potential or charge density) be periodic, $G(X_j) = G(X_j + L)$, then the finite discrete Fourier transform is (sum on $X_j = j\Delta x$)

$$G(k) = \Delta x \sum_{j=0}^{\text{NG}-1} G(X_j) e^{-ikX_j}. \quad (8.18)$$

The inverse transform is (the sum is on $k = n(2\pi/L)$)

$$G(X_j) = \frac{1}{L} \sum_{n=-\text{NG}/2}^{\text{NG}/2-1} G(k) e^{ikX_j}, \quad (8.19)$$

which produces NG distinct values of $G(X_j)$.

Weighting procedures

In the numerical code, it is necessary to calculate the charge density on the discrete grid points from the continuous particle positions and then to calculate the force at the particle positions from the fields known on grid points. There are several methods of such weighting.

Zero-order weighting

In this procedure (Fig. 8.4), we simply count the number of particles within distance $\pm\Delta x/2$ (one cell width) about the j^{th} grid point and assign that number [call it $N(j)$] to that point, that is, the grid density is simply $n_j = N(j)/\Delta x$. The common name for this weighting is nearest-grid-point. The electric field to be used in the force is that at X_j , for all particles in the j^{th} cell.

As a particle moves into the j^{th} cell (through cell boundaries at $x = X_j \pm \Delta x/2$), the grid density due to that particle jumps up; as the particle moves out ($x > X_j + \Delta x/2$ or $x < X_j - \Delta x/2$), the grid density jumps down. We can see two effects. One is that the particle appears to have a rectangular shape with a width of Δx . This leads us to think that we have a collection of

finite-size particles; hence, the physics observed will be that of such particles rather than that of point particles. Because close encounters between plasma particles are rare (i.e., for many particles in a Debye length, the plasma parameter $N_D \gg 1$), this new physics hardly alters the basic plasma effects to be studied. The second effect is that the jumps up and down as a particle passes through a cell boundary will produce a density and an electric field which are relatively noisy both in space and time; this noise may be intolerable in many plasma problems therefore a better weighting is necessary to look for.

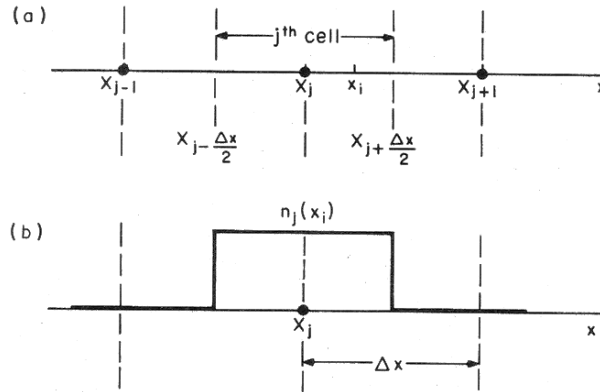


Fig. 8.4: Zero-order particle and field weighting, also called nearest-grid-point. Particles in the j^{th} cell, that is, with positions $x_i \in X_j \pm \Delta x/2$, are assigned to X_j to obtain grid density $n(X_j)$. All of these particles are acted on by the field at X_j , $E(X_j)$. b) The density $n_j(X_j)$ at point X_j due to a particle at x_i , as the particle moves through the cell centered on X_j . This density may be interpreted as the effective particle shape.

First-order weighting

This procedure smooths the density and field fluctuations, which reduces the noise (relative to zero-order weighting), but requires additional expense in accessing two grid points for each particle, twice per step. The charged particles seem to be finite-size rigid clouds which may pass freely through each other. The model is called cloud-in-cell (Fig. 8.5). For total cloud charge of q_c , the part assigned to j is

$$q_j = q_c \left(\frac{\Delta x - (x_i - X_j)}{\Delta x} \right) = q_c \frac{X_{j+1} - x_i}{\Delta x}, \quad (8.20)$$

and the part assigned to $j + 1$ is

$$q_{j+1} = q_c \left(\frac{x_i - X_j}{\Delta x} \right). \quad (8.21)$$

The net effect is to produce a triangle particle shape which has width $2\Delta x$. There are also higher-order weighting, but at the cost of more computations.

Initial state

Now, few words about initiating the program. In all cases we need to choose:

- The number of particles and grid cells.
- The weighting.
- The desired initial distribution functions of electrons, protons and further components (e.g. a beam)(random or ordered).

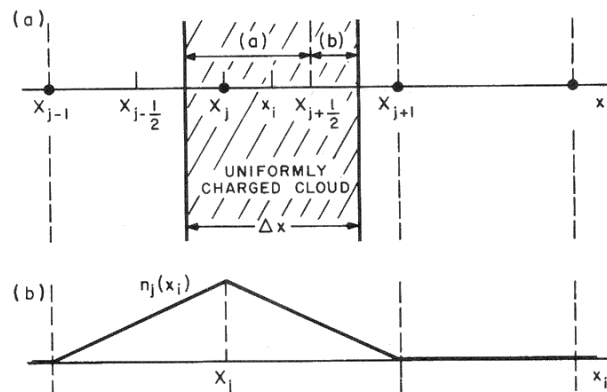


Fig. 8.5: First-order particle weighting. The finite-size charged particle, or cloud, is one cell wide, with center at x_i . This weighting puts that part of the cloud which is in the j^{th} cell at X_j , fraction (a), and that part which is in the $(j+1)^{\text{th}}$ cell at X_{j+1} , fraction (b). This weighting is the same as applying nearest-grid-point interpolation to each elemental part. (b) The grid density $n_j(x_i)$ at point x_i as the particle moves past X_j , again displaying the effective particle shape.

The next step is to place the particles in phase space (\mathbf{x}, \mathbf{v}) so that the problem desired is properly set up to run.

A cold, uniform periodic plasma of mobile electrons and immobile protons ($M_p/m_e \rightarrow \infty$) is simplest. The electrons can be put in uniformly. But sometimes we need in the initial state a plasma wave. It can be done by perturbing the uniform positions x_{i0} by

$$x_i(t=0) = x_{i0} + x_{i1} \cos(k_s x_{i0}), \quad (8.22)$$

where $k_{min} \leq k_s \leq k_{max}$ is some wave vector for which we want the plasma behavior of the system.

Diagnostics

For an interpretation of numerical results the diagnostic output of the code is very important. Information of our interest can be as follows:

a) For particles:

- Phase space, v_x versus x .
- Velocity space, v_y versus v_x .
- density in velocity, $f(v)$ versus v , or $f(v^2)$ versus v^2 , or $\ln(f(v^2))$ versus v^2 .

b) For grid quantities:

- Charge density $\rho(x)$ versus x or particle density $n(x)$ versus x .
- Potential $\phi(x)$ versus x .
- Field $E(x)$ versus x .
- distribution of electrostatic energy $1/2\rho_k\phi_k^*$ versus k .

Furthermore, the result at the end of a run will consist of plots of histories of various quantities versus time, such as:

- Electrostatic energy $\sum_k 1/2\rho_k\phi_k^*$.
- Particle kinetic energy by species $\sum_i 1/2m_iv_i^2$.
- Particle drift energy $\sum_i 1/2m_i\langle v_i \rangle^2$.
- Particle thermal energy $\sum_i 1/2m_i(\langle v_i^2 \rangle - \langle v_i \rangle^2)$.
- Total energy, electrostatic plus particle.
- Mode plots, $1/2\rho_k\phi_k^*$, for each k with plots versus ω - dispersion curves.

Chapter 9

Solar radio bursts

9.1 Classification of solar radio bursts

Solar radio bursts are observed in a very broad range of frequencies (see Fig. 9.1). Based on their spectral and time characteristics they are classified into five main classes:

a) Type III radio bursts

An example of these bursts is shown in Fig. 9.2. These bursts are characterized by very fast frequency drifts ($\sim 20 \text{ MHz s}^{-1}$ in the metric range) on the dynamic radio spectrum. The observed drifts correspond to exciter speeds between $0.2c$ and $0.6c$, where c is the speed of light. These bursts are observed at the beginning of solar flares, in so called impulsive phase and they are considered as a signature of electron beams propagating from the flare site upwards into the interplanetary space.

b) Type II radio bursts

An example of this burst is shown in Fig. 9.3. These bursts are characterized by relatively slow frequency drifts ($\sim 1 \text{ MHz s}^{-1}$ in the metric range) on the dynamic radio spectrum. The observed drifts correspond to exciter speeds between 500 km s^{-1} and 2000 km s^{-1} . These bursts are observed after the impulsive phase and they are considered to be a signature of the MHD flare shock propagating from the flare site upwards into the interplanetary space.

c) Type IV radio bursts

These broadband radio bursts (or continuum bursts) are typical bursts observed during solar flares, especially in long-lasting ones. While the high-frequency type IV bursts are generated by the gyro-synchrotron mechanism of superthermal electrons trapped in magnetic flare loops, on lower frequencies (those with relatively narrow band emission) are probably generated by the plasma emission processes.

There are many fine structures of these bursts, see the following examples.

d) Type I radio bursts - noise storm

These bursts express activity in solar active regions. They are observed in the metric range only and they consist of a continuum radiation and a cloud of short-lasting ($< 1 \text{ s}$) and narrowband ($\sim 5 \text{ MHz}$) bursts.

a) Type V radio bursts

The type V burst is similar to the type III burst, but its duration is longer (~ 1 min). It is believed that some electrons of fast electron beam are trapped for some time in coronal magnetic trap and thus the radio emission is prolonged.

Radio bursts during stellar flares

In Fig. 9.4 an example of the dynamic radio spectrum of the AD Leo star flare in the decimetric range is shown for comparison.

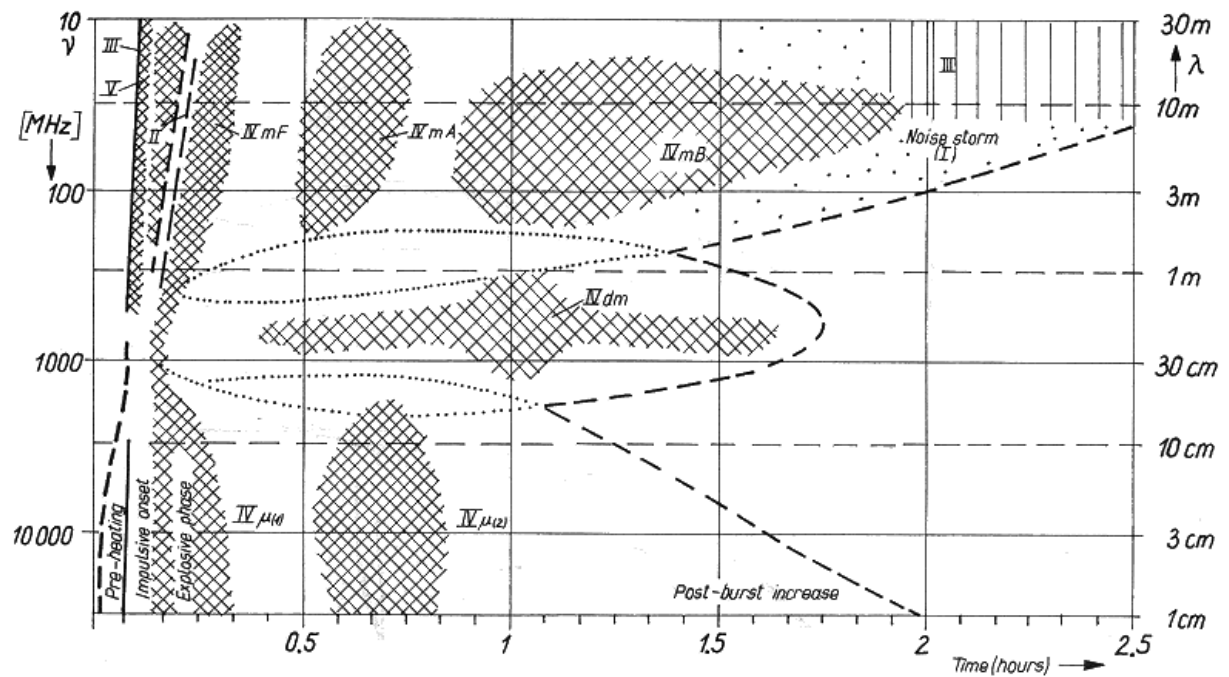


Fig. 9.1: Schematic representation of different solar radio bursts.

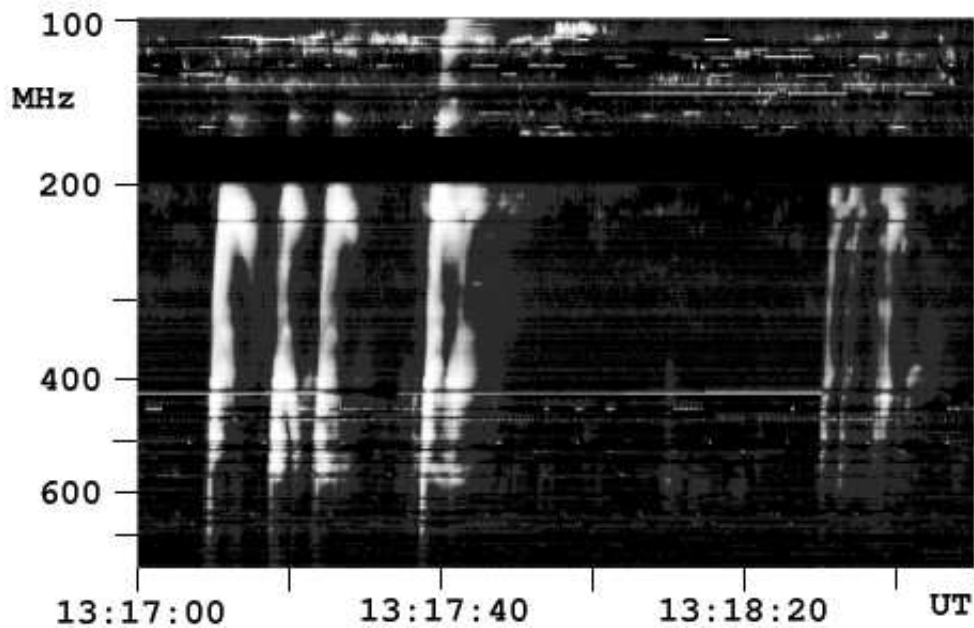


Fig. 9.2: Type III solar radio burst observed at Tremsdorf Observatory, Germany on May 17, 1999 (courtesy Dr. A. Klassen).

Examples of solar radio bursts

In this chapter new results and new types of solar radio bursts are presented.

a) High-frequency zebras

See file `zebras.ps`

Reference:

Sawant, H.S., Karlický, M., Fernandes, F.C.R., Cecatto, J.R.: 2002, Observation of harmonically related solar radio zebra patterns in the 1-4 GHz frequency range, *Astron. Astrophys.* 396, 1015-1018.

b) Narrowband dm-spikes

See file `spikes.ps`

Reference:

Bárta, M., Karlický, M.: 2001, Turbulent plasma model of the narrowband dm-spikes, *Astron. Astrophys.* 379, 1045-1051.

c) Lace bursts

See file `laces.ps`

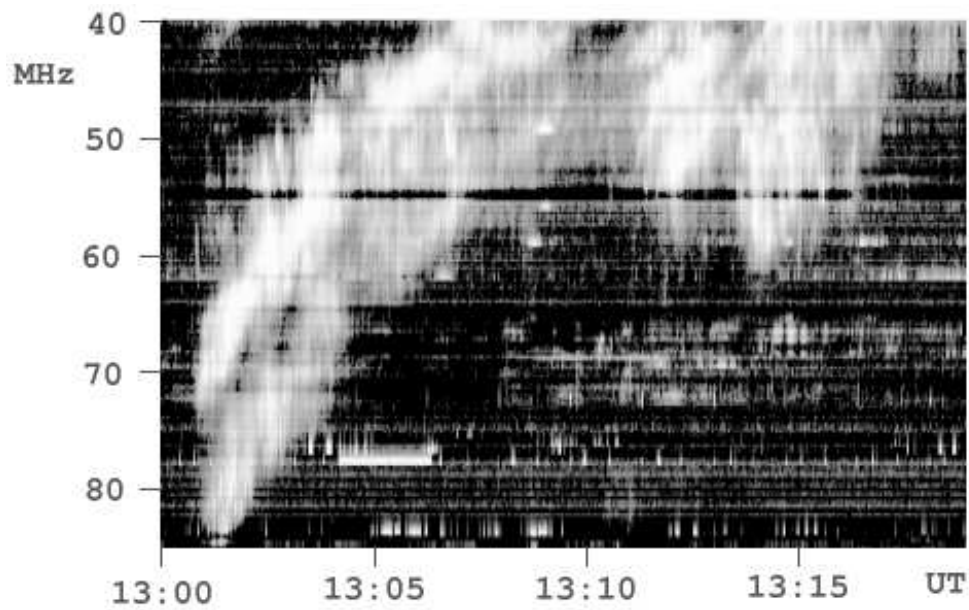


Fig. 9.3: Dynamic spectrum of type II solar radio burst observed at Trensdorf Observatory on October 22, 1999 (courtesy Dr. A. Klassen).

Reference:

Karlický, M., Bárta, M., Jiříčka, K., Mészárosová, H., Sawant, H.S., Fernandes, F.C.R., Cecatto, J.R.: 2001, Radio bursts with rapid frequency variations - Lace bursts, *Astron. Astrophys.* 375, 638-642.

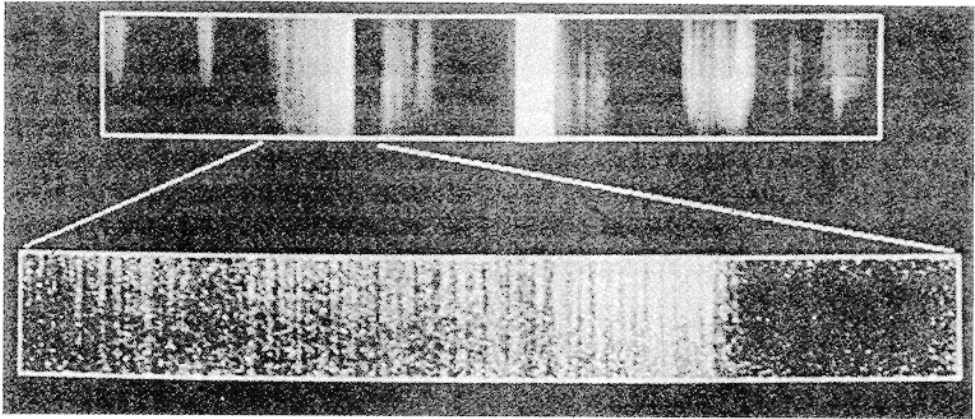


Fig. 9.4: Decimetric radio spectrum of the AD Leo star obtained by Arecibo radioheliograph.

Chapter 10

Solar flares and coronal mass ejections

Examples of solar flare studies

a) Magnetic field reconnection

See file **reconnection.ps**

Reference:

Karlický, M.: 2002, Plasma resonance surfaces in the magnetic field reconnection and radio fine structures, *Solar Physics*, in press.

b) Plasmoid ejection

See file **plasmoid.ps**

Reference:

Karlický, M., Fárník, F., Mészárosová, H.: 2002, High-frequency slowly drifting structures in solar flares, *Astron. Astrophys.* 395, 677-683.

c) Impact polarization of optical chromospheric lines

See file **impact.ps**

Reference:

Karlický, M., Henoux, J.C.: 2002, Impact H-alpha line polarization and return current, *Astron. Astrophys.* 383, 713-718.

c) Flare hard X-rays from neutral beams

See file **nhardx-ray.pdf**

Reference:

Karlický, M., Brown, J.C., Conway, A.J., Penny, G.: 2000, Flare hard X-rays from neutral beams, *Astron. Astrophys.* 353, 729-740.

c) Return current in solar flares

See file **return.pdf**

Reference:

Karlický, M., Hénoux, J.C.: 1992, Return current losses in pulse beam heating of the solar atmosphere, *Astron. Astrophys.* 264, 679-685.

Priest, E., Forbes, T.: 2000, *Magnetic reconnection: MHD theory and applications*, Cambridge University Press, Cambridge, UK.

Gallery of the models of solar flares and coronal mass ejection

Characteristic values of the total energy \mathcal{E} [erg] and power \mathcal{P} [erg/s] released in various forms in large and small flares.

Form of energy release	Largest flares		Subflares	
	\mathcal{E}	\mathcal{P}	\mathcal{E}	\mathcal{P}
1. Hydrodynamic plasma flows:				
a) Interplanetary ejections and shock waves	$(1-3) \times 10^{32}$	—	—	—
b) Surges above photosphere	$\approx 10^{32}$	$\approx 10^{29}$	$\lesssim 10^{29}$	$\lesssim 10^{27}$
2. Radiation:				
a) Soft X-ray and UV	$(3-5) \times 10^{31}$	$(3-5) \times 10^{28}$	$\lesssim 10^{29}$	$\lesssim 10^{27}$
b) optical continuum	3×10^{31}	3×10^{28}	none?	none?
c) H_α line	3×10^{30}	3×10^{27}	$\approx 10^{26}$	$\approx 10^{24}$
d) hard X-ray	$(3-5) \times 10^{26}$	$(3-5) \times 10^{23}$	$\lesssim 10^{24*}$	$\lesssim 10^{22}$
e) gamma-ray	$(1-3) \times 10^{25}$	$(1-3) \times 10^{22}$	none?	none?
f) radio waves	$\approx 10^{24}$	$\approx 10^{21}$	$\lesssim 10^{21}$	$\lesssim 10^{19}$
3. Accelerated particles:				
a) electrons ($E_e \geq 20$ keV)	$(1-3) \times 10^{31}$	$(1-3) \times 10^{28}$	10^{27*}	10^{25}
b) protons ($E_p \geq 20$ MeV)	$(1-3) \times 10^{31}$	$(1-3) \times 10^{28}$	none?	none?

* In vast majority of flares not detected.

Fig. 10.1: Energies in large and small solar flares.

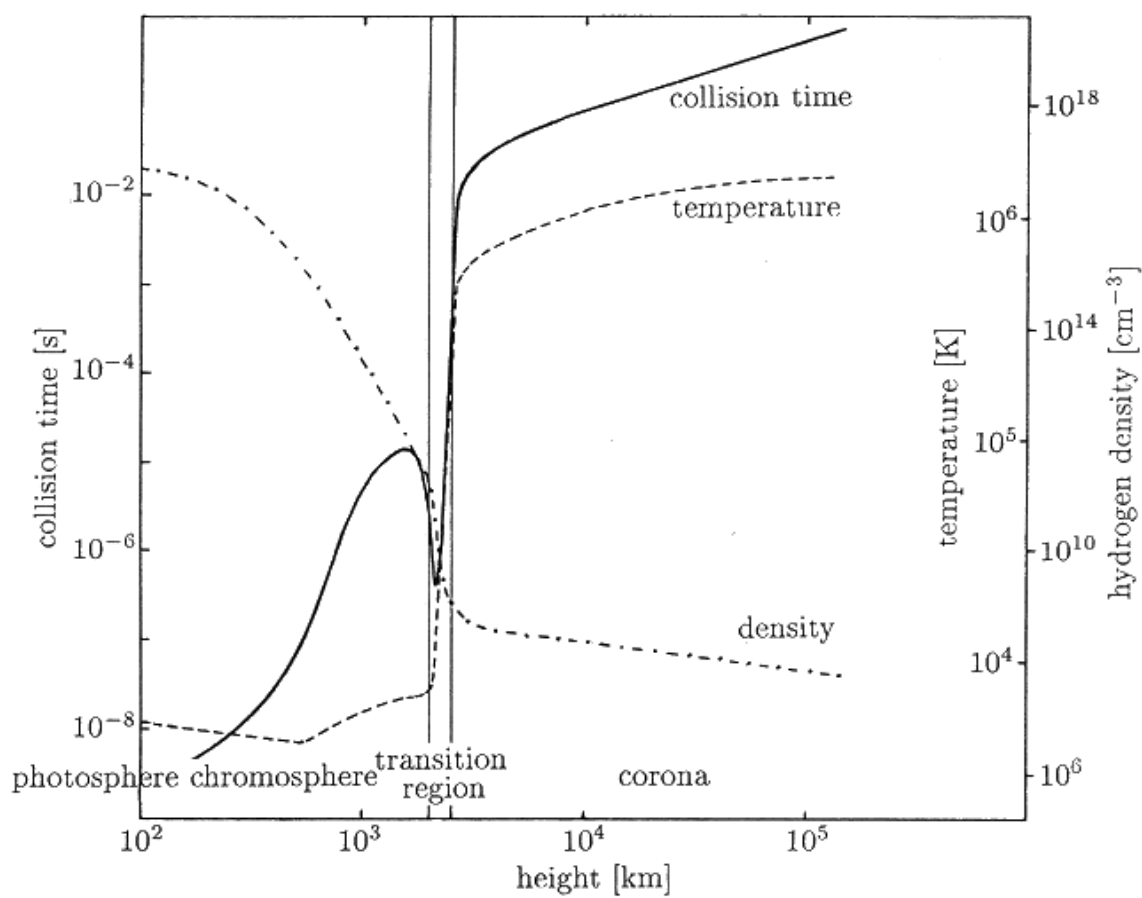


Fig. 10.2: Schematic drawing of the collision time vs. height of an electron moving at the mean thermal velocity in the quiet solar atmosphere. The relevant plasma parameters are from standard models and are also shown (dashed). The hydrogen density includes both neutral atoms and ions.

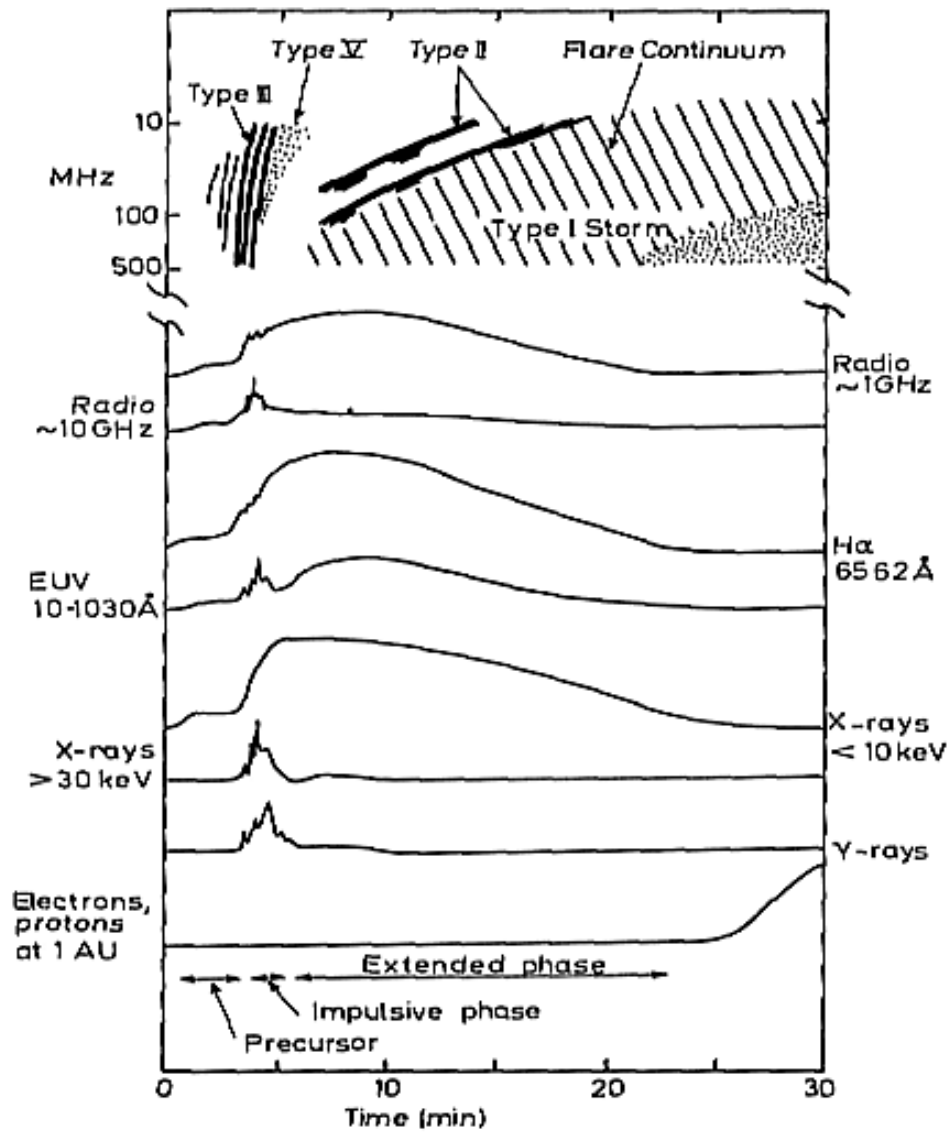


Fig. 10.3: Characteristic profile of a solar flare in various wavelengths.

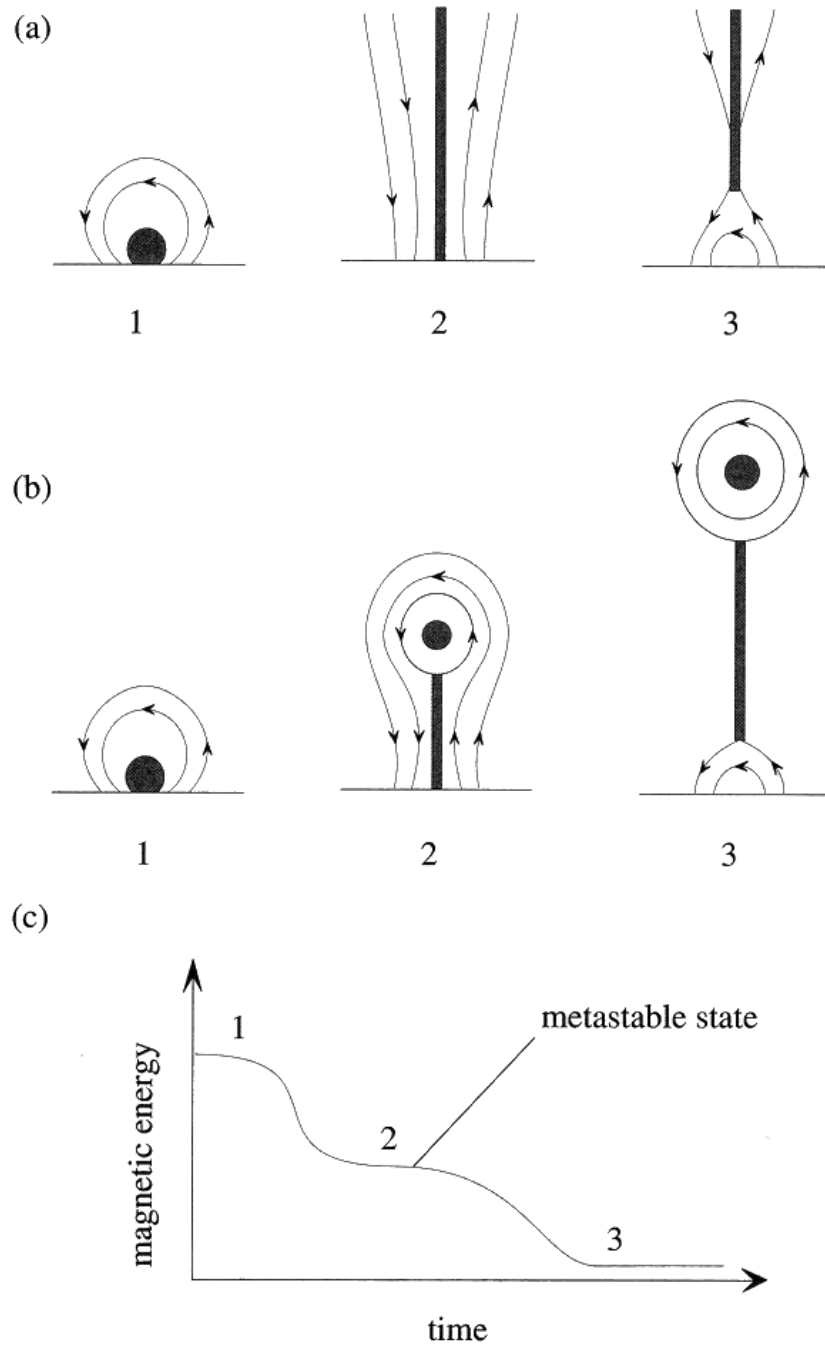


Fig. 10.4: Two scenarios which have been proposed for opening the magnetic field during large solar flares and coronal mass ejections. (a) In the first scenario an ideal MHD process changes the closed-field configuration (1) into an open configuration (2) during the impulsive phase, and reconnection re-closes the field (3) during the gradual phase. (b) In the second scenario an ideal MHD process creates a relatively short current sheet without opening the field, but magnetic flux can still escape into space if rapid reconnection occurs in this sheet. If there is no input of the magnetic energy during the eruption, then the magnetic energy continuously decreases during both the impulsive and gradual phases of the flare, as shown in (c).

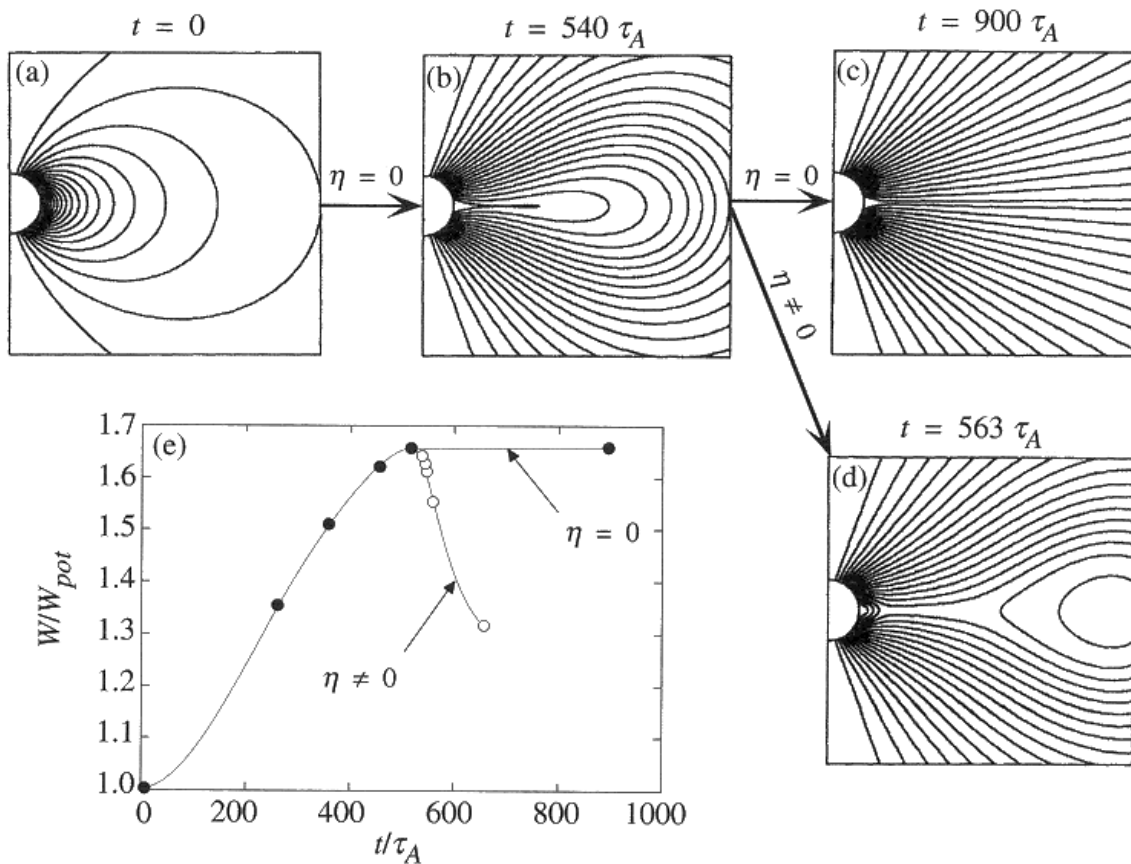


Fig. 10.5: Quasi-static evolution of an axially symmetric arcade in response to shearing of its footpoints. (a) The initial field is a Sun-centered dipole which (b) evolves into a force-free field when its footpoints in the upper and lower hemispheres are rotated in opposite directions. (c) After a rotation of 126° , the field becomes fully opened as long as the diffusivity (η) remains zero. (d) A plot of the corresponding time evolution of the total energy divided by the potential energy.

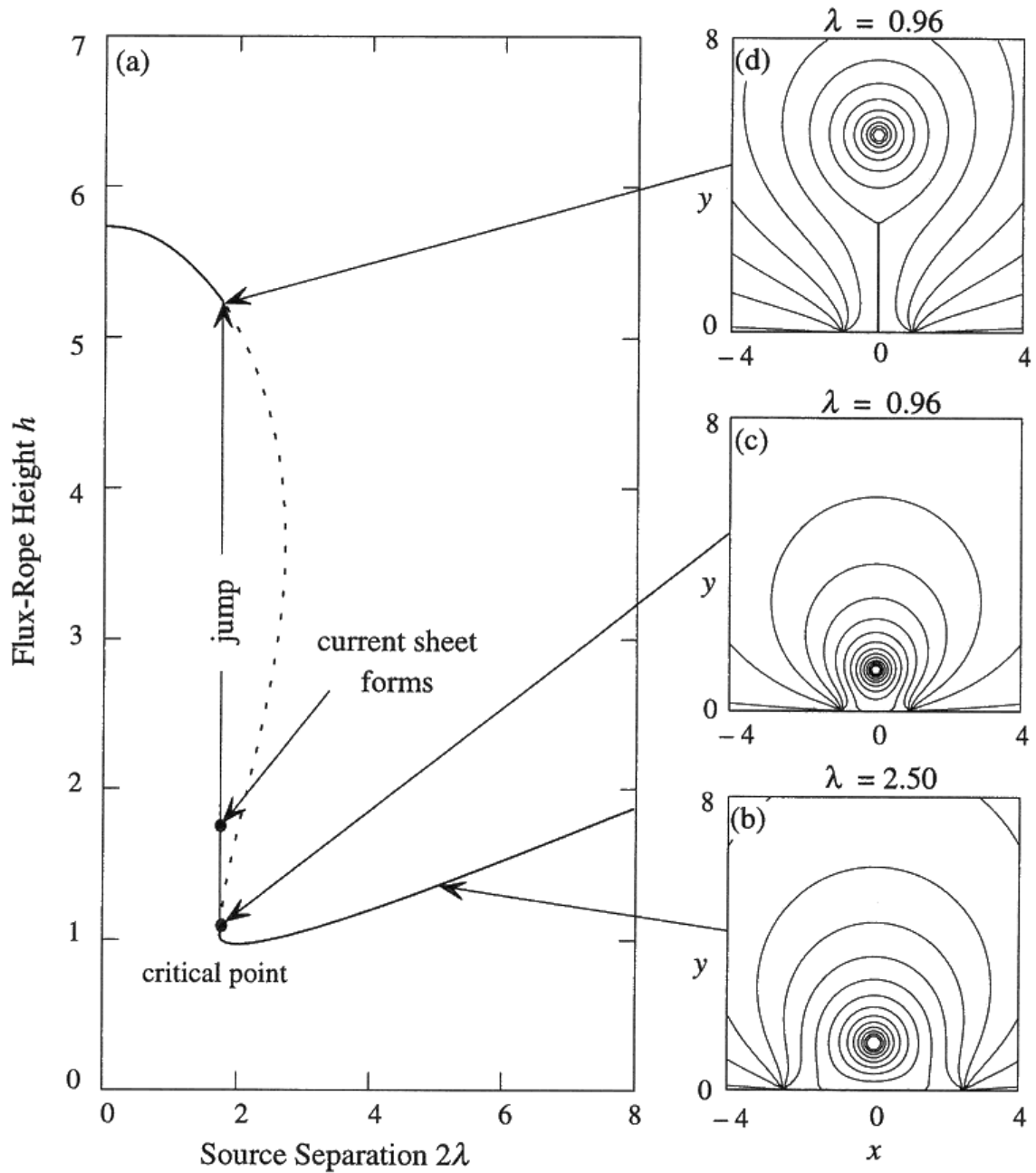


Fig. 10.6: A flux-rope model. (a) Ideal MHD evolution of a two-dimensional arcade containing an unshielded flux rope of height h as the source separation (2λ) decrease. (b), (c) The flux rope and arcade move upwards when the two photospheric field sources are pushed too close to one another. (d) In the absence of reconnection the eruption leads to a new equilibrium containing a current sheet.

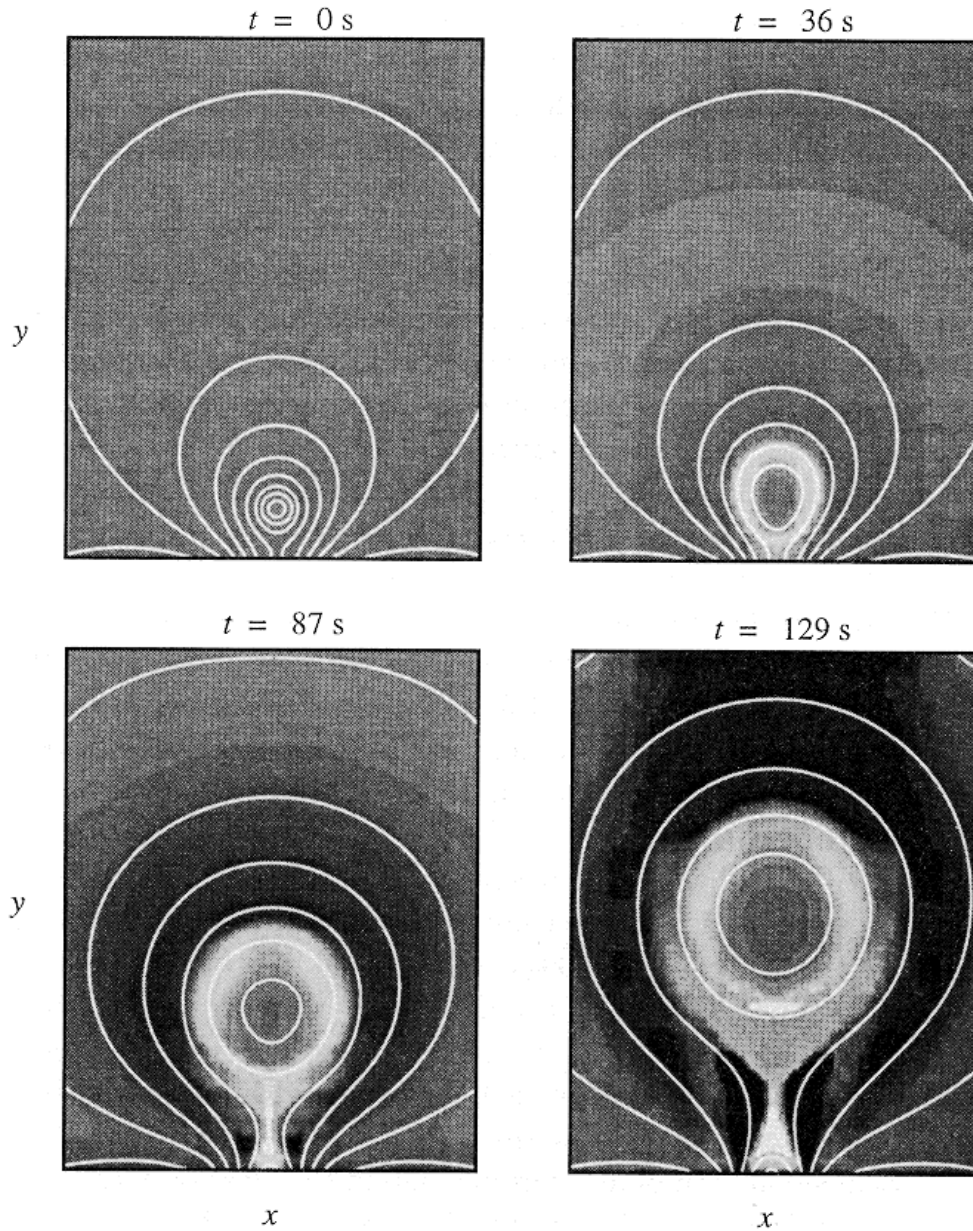


Fig. 10.7: Resistive MHD simulation based on the two-dimensional flux-rope model. White curves are magnetic field lines, while the grey scale corresponds to temperature variations. White regions have the highest temperature ($> 10^8\text{ K}$ in the absence of cooling processes), while black regions have the lowest. The magnetic Reynolds number is about 200, many orders of magnitude smaller than expected for the Sun.

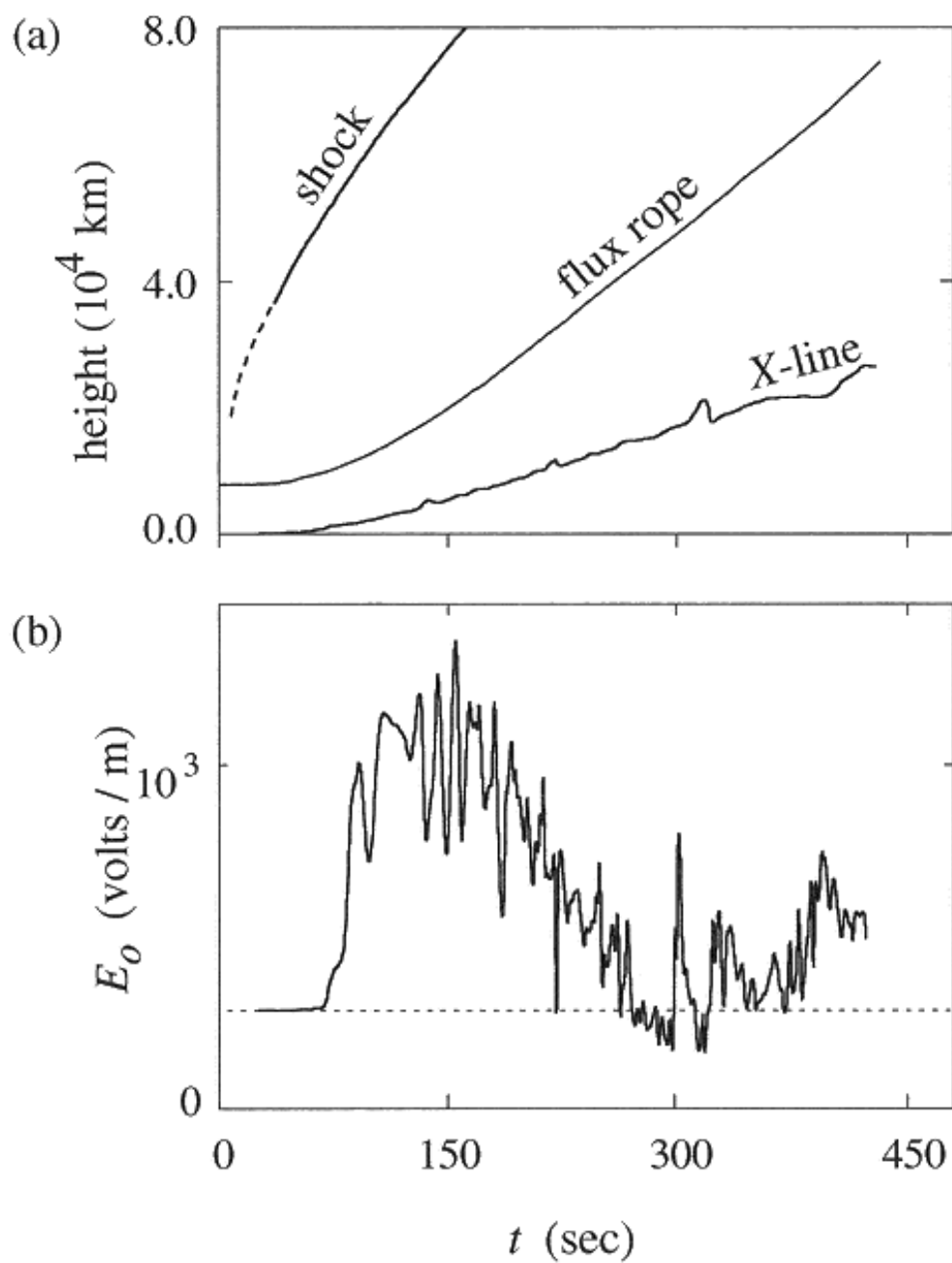


Fig. 10.8: (a) Trajectories of the shock, flux rope, and X-line for the simulation shown in the previous figure. (b) The electric field at the X-line as a function of time.

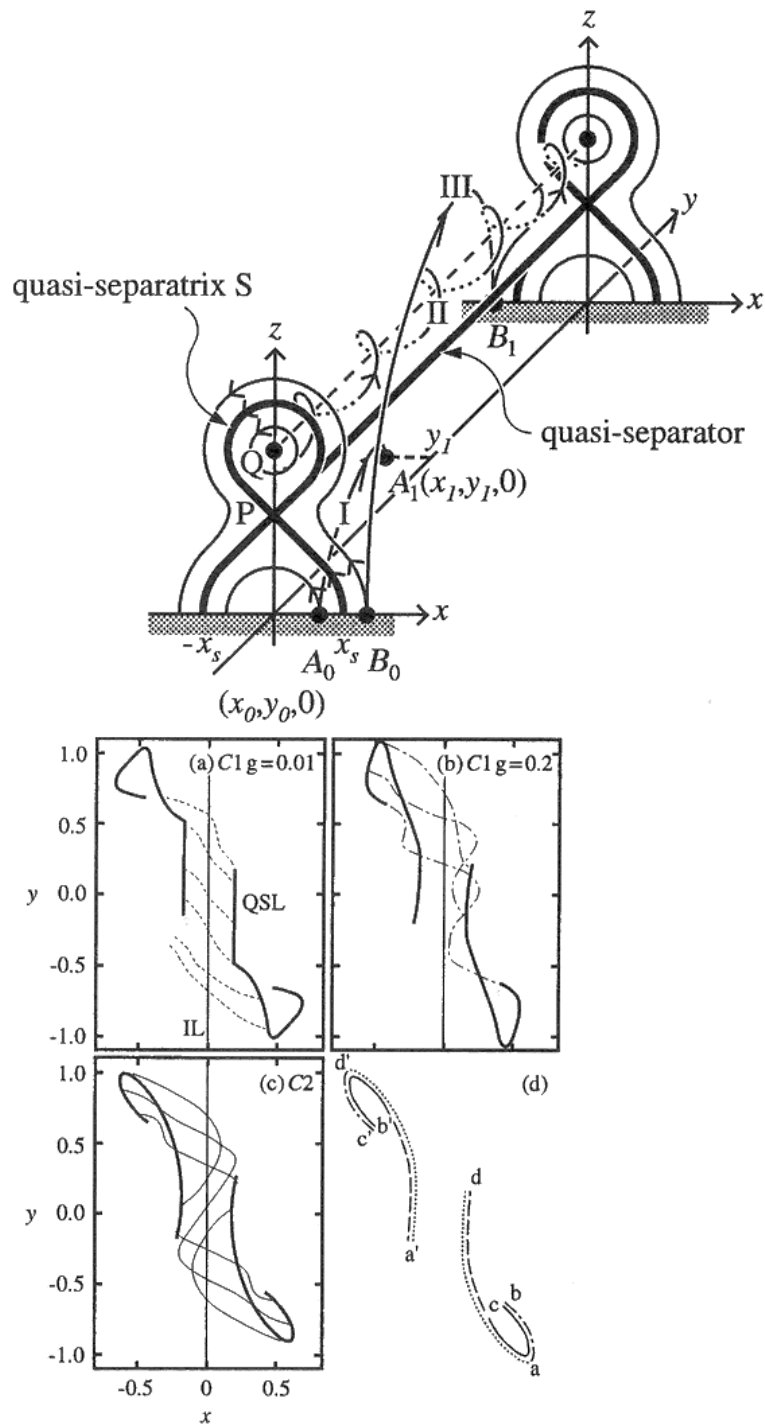


Fig. 10.9: (i) Twisted flux tube showing three types of field line I, II, and III. (ii) Quasi-separatrix layers viewed from above together with sample field lines of types (a) I (dotted curve), (b) III (dashed-dotted curve) and (c) II (solid curve) and (d) the connectivity of points on the quasi-separatrix layers.

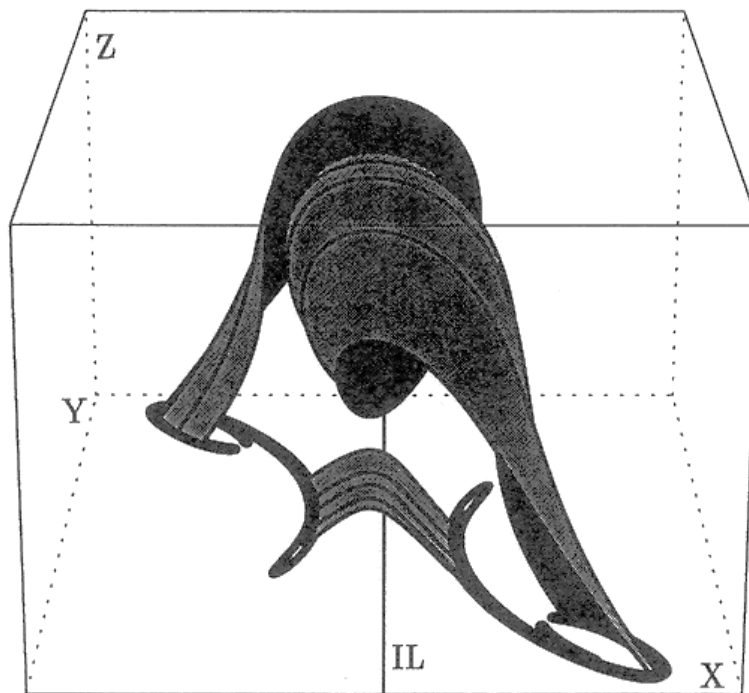


Fig. 10.10: Perspective view of a 3-D twisted configuration with a finite spatial extension and without nulls or field line tangent to the photosphere. Separatrices are no longer present, but there is a very thin volume (QSL) where the field line connectivity changes rapidly. The intersection of the QSL with the lower boundary (plane $z = 0$) is shown by an iso-contour of the function N (see chapter about connectivity). This intersection forms two elongated strips on both sides of the boundary inversion line (IL). From these strips the QLS extends above, following magnetic field lines (the complexity of this elongated volume precludes a clear drawing of it). Two representative sets of field lines have been included; they belong to the periphery of the twisted flux tube and to the lower arcade (Demoulin, 1997).

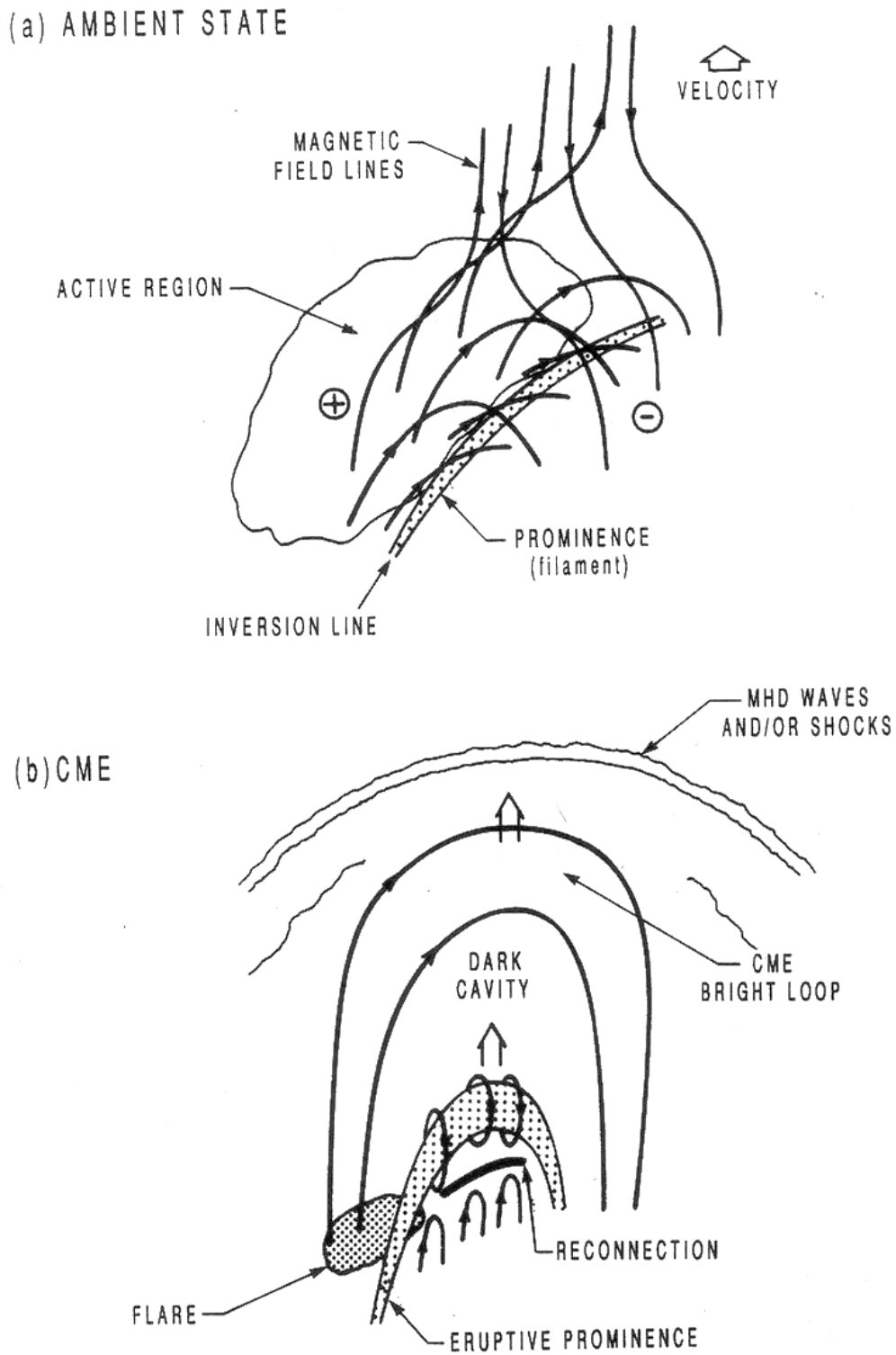


Fig. 10.11: A schematic representation of an ambient coronal streamer (a) in which a coronal mass ejection (b) originates.

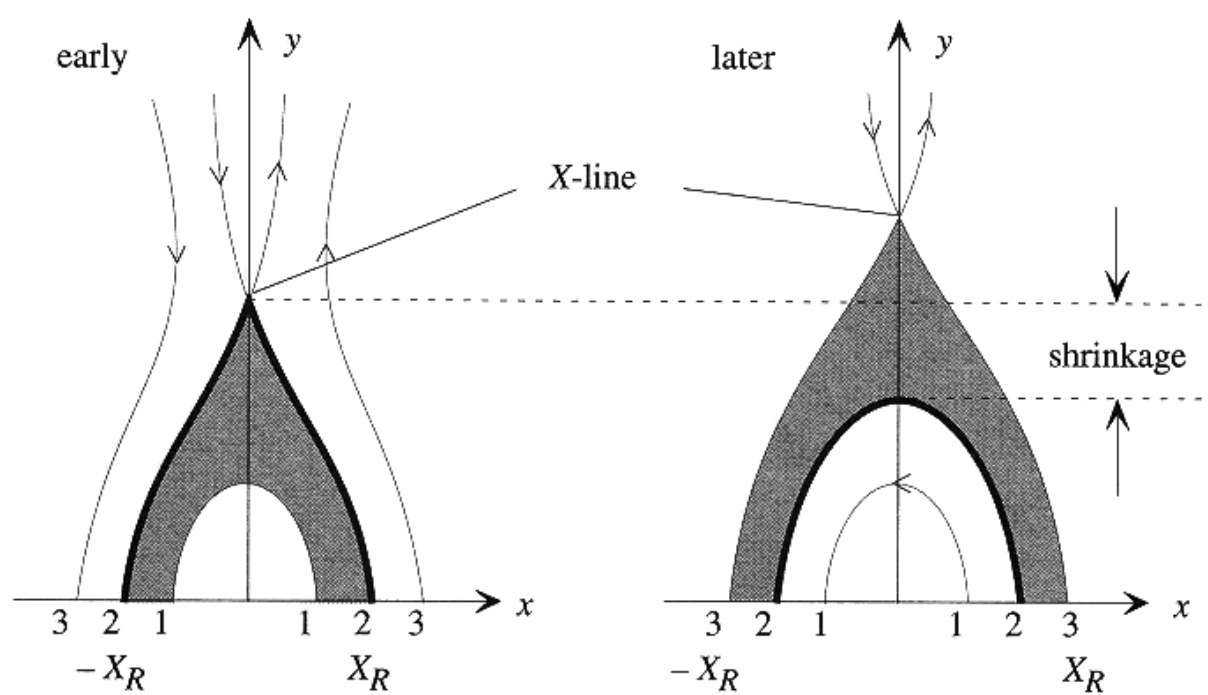


Fig. 10.12: How field line shrinkage is defined for flare loops. Shrinkage is simply a measure of the change in shape of a field line due to its closure by reconnection.

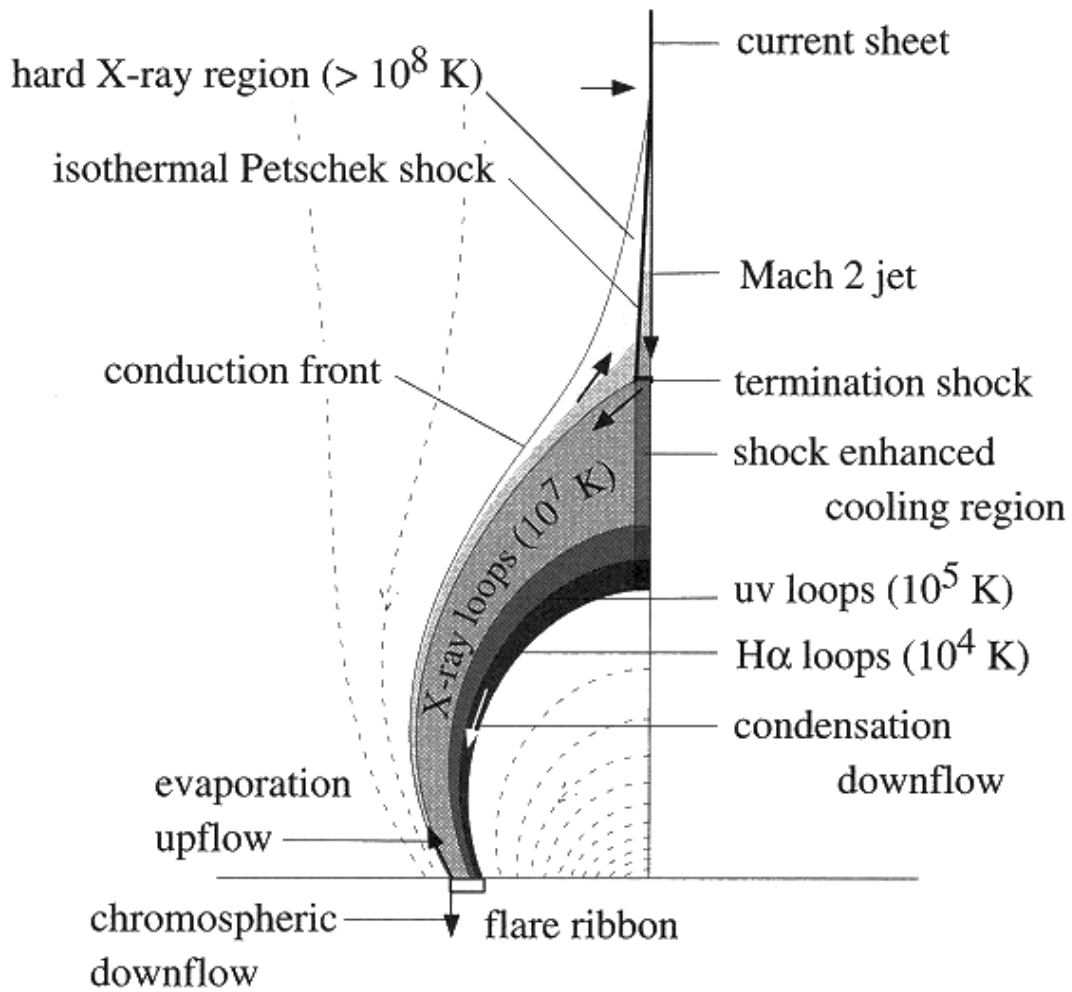


Fig. 10.13: Schematic diagram of a flare loop system formed by reconnection in the supermagnetosonic regime. This regime is most likely to occur in the early phase of a flare when the reconnecting fields are strong. It has both upward- and downward- directed jets, but only the region below the downward jet has high-density plasma, because in two-dimensional models chromospheric evaporation occurs on just those field lines that lie below the X-line. Solid curves indicate boundaries between various plasma regions, while dashed ones indicate magnetic field lines.

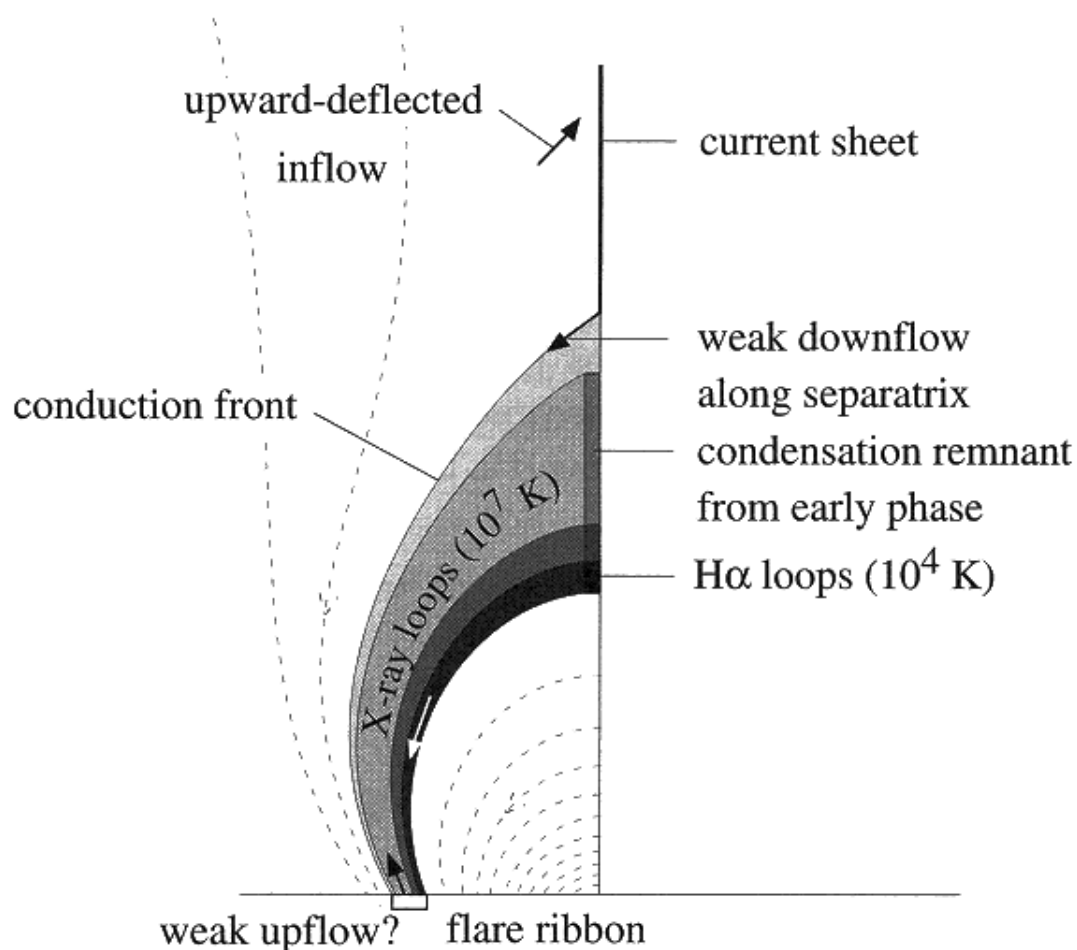


Fig. 10.14: Schematic diagram of a flare loop system formed by reconnection in the submagnetosonic regime. This regime is most likely to occur when the reconnection fields are weak. Here the downward jet of the previous figure is replaced by a weak bifurcated flow along the field lines mapping from tip of the current sheet to the chromosphere. Because of the weaker fields, the evaporation process is greatly reduced and the plasma density in the loops becomes too low to trigger a thermal condensation. However, condensation remnants may remain lower down as a result of an earlier supermagnetosonic phase.

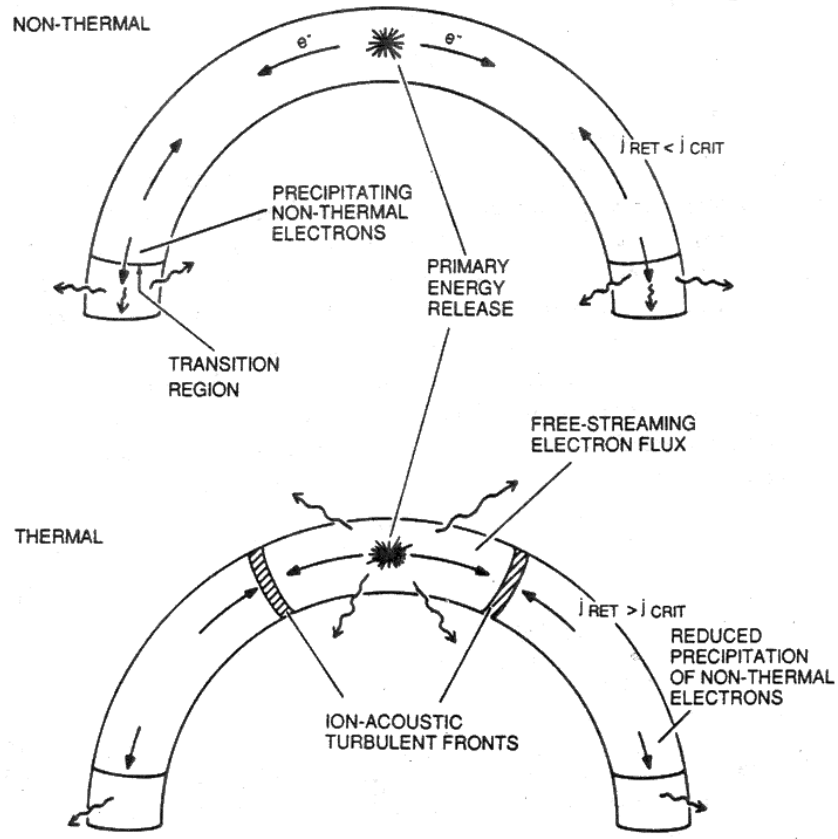


Fig. 10.15: Processes in flare loops.

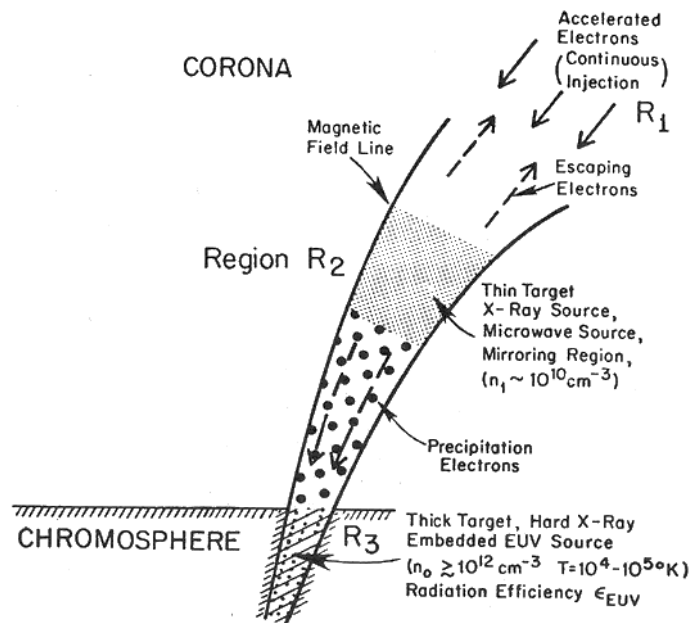


Fig. 10.16: Schematic model of impulsive hard X-ray, radio and EUV sources.

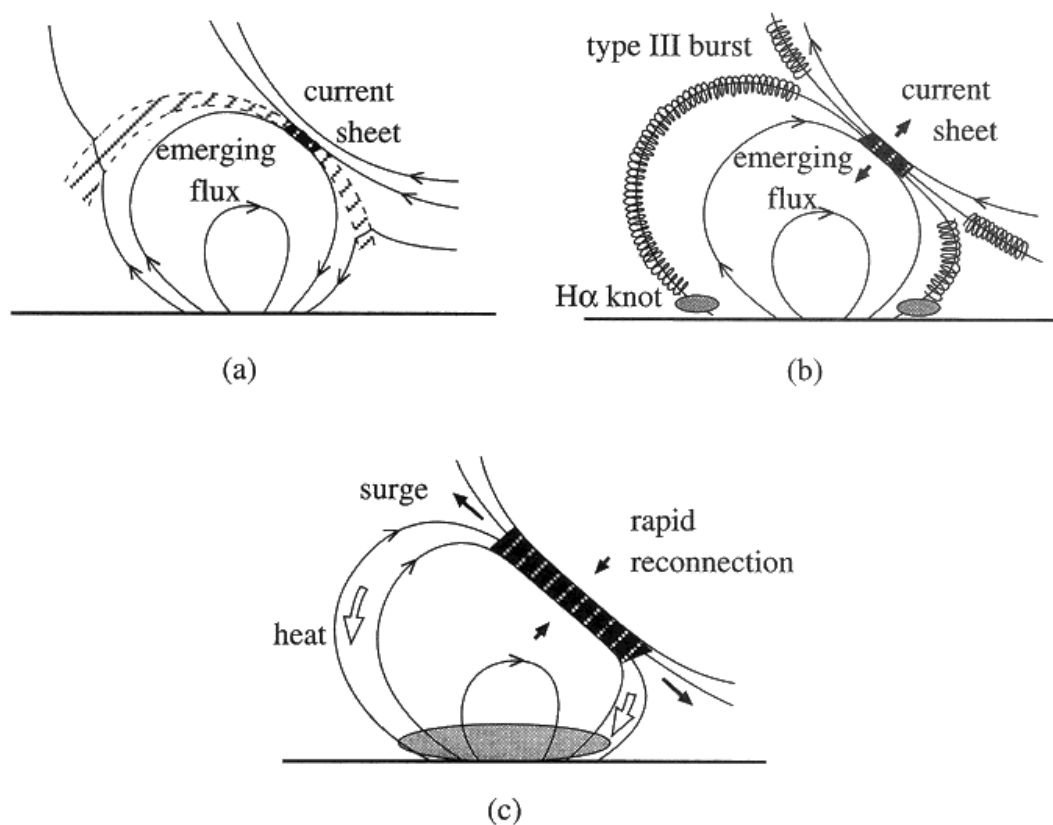


Fig. 10.17: The emerging flux model for a small flares. (a) The preflare phase when the emerging flux slowly reconnects with the over-lying field. Slow-mode shocks (dashed curves) radiate from a small current sheet and heat the plasma that passes through them (striped region). (b) The impulsive phase caused by the onset of turbulence and anomalous resistivity in the current sheet when it reaches a critical height. The electric field generated by the sudden enhancement in the reconnection rate accelerates the particles, which produce hard X-rays and type III radio bursts. In the main phase (c), quasi-steady reconnection leads to extensive heating.